Stem Cells International

Mesenchymal Stem Cells in Cancer, Drug Delivery, and Regenerative Medicine

Lead Guest Editor: Farid Menaa
Guest Editors: Somayeh Shahrokhi and Prasad Shastri

Mesenchymal Stem Cells in Cancer, Drug Delivery, and Regenerative Medicine

Stem Cells International

Mesenchymal Stem Cells in Cancer, Drug Delivery, and Regenerative Medicine

Lead Guest Editor: Farid Menaa
Guest Editors: Somayeh Shahrokhi and Prasad Shastri

Editorial Board

Contents

Hindawi
Stem Cells International
Volume 2018, Article ID 5023925, 3 pages
https://doi.org/10.1155/2018/5023925

Editorial

Impact and Challenges of Mesenchymal Stem Cells in Medicine: An Overview of the Current Knowledge

Farid Menaa,[1] **Somayeh Shahrokhi**,[2] **and Prasad Shastri**[3]

[1]*Department of Oncology, Stem Cells and Nanomedicine, California Innovations Corporation, La Jolla, San Diego, CA 92037, USA*
[2]*Department of Immunology, Lorestan University of Medical Sciences, Khorramabad, Iran*
[3]*Department of Cell Biology, University of Freiburg, Freiburg, Germany*

Correspondence should be addressed to Farid Menaa; dr.fmenaa@gmail.com

Received 7 December 2017; Accepted 8 December 2017; Published 17 December 2018

MSCs are multipotent adult SCs that exhibit the following main features [1–3]: (i) presence in almost any tissues (e.g., UBC, BM, WJ, skin, and dental); (ii) plastic adherence; (iii) capacity of self-renewing; (iv) ability of differentiating into multilineages (e.g., mesodermal (i.e., adipocytes, chondrocytes, and osteocytes) as well as ectodermal (e.g., neuronal cells) and endodermal (e.g., hepatocytes and pancreocytes)); (v) expression of specific set of cell surface markers according to the tissue origin (e.g., presence of CD73, CD90, and CD105 but absence of CD14, CD34, CD45, and HLA-DR); (vi) immunoregulatory properties (e.g., low alloreactivity and autoprotection from NKs due to low MHC I and lack of MHC II expressions along with costimulatory molecules such as CD80, CD40, and CD86; alleviation of disease response by favoring the conversion from Th2 (T helper cells) response to Th1 cellular immune response through modulation of IL-4 and IFN-γ levels in effector T-cells); (vii) homing capacity; and (viii) secretion of anti-inflammatory molecules (e.g., cytokines and receptors).

De facto, clinical applications of MSCs are tremendously promising in medicine (e.g., cell transplantation), pharmaceutical sciences (e.g., controlled drug delivery), and biological sciences (e.g., tissue engineering). They also provide greater advantages over other SCs (e.g., ESCs), which include [2, 4] (i) their relatively easy tissue isolation; (ii) the absence of obvious risk for the donor or ethical constraints; (iii) their capacity of migrating and homing to the injured site (e.g., tumor tropism) which can be tracked by noninvasive methods such as SPECT, BLI, or PET; (iv) their ability to expand for a relatively long period of time; (v) their ability to modify the host immune environment; (vi) their valuable immunomodulatory effects; and (vii) their higher *trans*differentiation potential as above specified.

Since the last 15 years, an increasing number of preclinical and clinical studies (>500) have been registered [5] using hMSCs as a valuable source in treatment of chronic diseases (e.g., autoimmune such as RA, inflammatory such as T1D, and CVD or degenerative diseases such as ALS, PD, and AD). Thereby, a number of studies [6, 7] pointed out the crucial role of MSCs in the improvement of RA, particularly at the onset of the disease, through a mechanism activating Treg cells and suppressing the production of inflammatory cytokines when injected into DBA/1 mice model. Also, transplantation of MSCs, when successfully differentiated into insulin-producing (beta) cells, was able to correct the hyperglycemia of STZ-induced diabetic rodents, enhance the survival rate of engrafted islets, and was found beneficial for treating non-insulin-dependent patients [8–10]. Besides, the transplantation of MSCs genetically modified to express GDNF improved the ALS phenotype and increased the number of neuromuscular connections [11]. In a pioneered study, MSCs delivered through nose to treat patients suffering from PD were found in different brain regions (e.g., hippocampus, olfactory lobe, and cortex) after 4.5 months of administration and could favorably modulate the expression of key enzymes (e.g., increased tyrosine hydroxylase and decreased toxin 6-hydroxydopamine levels) in the lesions of ipsilateral striatum and substantia nigra [12]. Moreover, MSCs were able to enhance the cell autophagy pathway, important in the amyloid plaque clearance,

activated Tregs which in turn regulated microglia activation, and increased the neuronal survival both *in vitro* and in AD mice model [13, 14]. Eventually, transplantation of MSCs into myocardial infarction animal model along with fibronectin-immobilized PCL nanofibers was very successful [15].

Nevertheless, many of these clinical applications are hindered by research barriers [1, 16–21]. Remaining challenges, related to safety and efficacy of MSCs, include (i) the establishment of a comprehensive procedure for MSC isolation (e.g., methods may include Ficoll density gradient, collagenase, and marrow filter device) and for characterization/quality control (e.g., specific expression of cell surface markers, cell viability, endotoxin assays, and oncogenic tests); (ii) a proper setup of *in vitro* MSC expansion. Indeed, depending upon the severity of disease, an optimal dose of multipotent MSCs is required. The difficulty to obtain a large amount of adequate cells is often explained by the senescence manifested by shortening telomere length, decline in differentiation potential, and morphological alterations during a long-term *in vitro* culture under certain conditions which besides present the advantage to not favor spontaneous malignant transformation at higher passages (e.g., expansion of MSCs in controlled oxygen concentration and in serum-free culture media rather than supplemented with serum and/or growth factors); (iii) the cryopreservation and large-scale banking of clinical grade MSCs lack optimization in terms of medium to be used, uniformity in temperature during freezing and thawing, and storage time in liquid nitrogen. Interestingly, recent studies suggest that MSCs cryopreserved in serum-free culture media supplemented with CPAs (e.g., mixture of glucose, sucrose, and ethylene glycol in PBS and polyvinylpyrrolidone) can be successful to prevent any freezing damage to cells and toxicities related to the routine use of DMSO; (iv) a specific administration time and route (e.g., intravenous, in situ/*local*, and nasal) remains to be decided in order to fully maintain the functional capacity of a larger number of MSCs. In this regard, it is thought that the most convenient and feasible way of MSC transplantation is local injection to the site of injury or near the site of injury; (v) the underlying mechanisms that regulate and modulate these MSCs should be better understood. For instance, homing of MSCs involves CXCR4 and SDF-1 alpha but the exact mechanism is still unclear to avoid off-target homing; (vi) the precise mechanism(s) by which MSCs regulate the immune response is/are also undefined.

From the overall studies published to date, it becomes thus clearer that the use of hMSCs for clinical applications, at least in regenerative medicine, will increase.

Abbreviations

AD: Alzheimer disease
ALS: Amyotrophic lateral sclerosis
BLI: Bioluminescence imaging
BM: Bone marrow
CD: Cluster of differentiation
CPAs: Cryoprotective agents
CVD: Cardiovascular diseases
DMSO: Dimethylsulfoxide
ESCs: Embryonic stem cells
GDNF: Glial cell line-derived neurotrophic factor
HLA: Human leukocyte antigen
IFN: Interferon
IL: Interleukin
MHC (I/II): Major histocompatibility complex (either class I or II)
MSCs: Mesenchymal stem cells
NKs: Natural killers
PBS: Phosphate-buffered saline
PCL: Polycaprolactone
PD: Parkinson disease
PET: Positron emission tomography
RA: Rheumatoid disease
SCs: Stem cells
SDF-1 alpha: Stromal cell-derived factor 1-alpha (or CXCL12)
SPECT: Single photon emission computed tomography
STZ: Streptozotocin
T1D: Type-1 diabetes
UCB: Umbilical cord blood
WJ: Wharton's jelly.

Acknowledgments

We sincerely thank this journal (MDPI) for providing us the opportunity to guest edit our successful special issue entitled "Mesenchymal Stem Cells in Cancer, Drug Delivery, and Regenerative Medicine" (https://www.hindawi.com/journals/sci/si/152812/cfp/).

Farid Menaa
Somayeh Shahrokhi
Prasad Shastri

References

[1] I. Ullah, R. B. Subbarao, and G. J. Rho, "Human mesenchymal stem cells - current trends and future prospective," *Bioscience Reports*, vol. 35, no. 2, pp. 1–18, 2015.

[2] S. Shahrokhi, S. Daneshmandi, and F. Menaa, "Tumor necrosis factor-α/CD40 ligand-engineered mesenchymal stem cells greatly enhanced the antitumor immune response and lifespan in mice," *Human Gene Therapy*, vol. 25, no. 3, pp. 240–253, 2014.

[3] International Society for Cellular Therapy (ISCT), http://www.celltherapysociety.org/.

[4] C. H. Ryu, S. A. Park, S. M. Kim et al., "Migration of human umbilical cord blood mesenchymal stem cells mediated by stromal cell-derived factor-1/CXCR4 axis via Akt, ERK, and p 38 signal transduction pathways," *Biochemical and Biophysical Research Communications*, vol. 398, no. 1, pp. 105–110, 2010.

[5] "ClinicalTrials.gov," https://clinicaltrials.gov/.

[6] A. Papadopoulou, M. Yiangou, E. Athanasiou et al., "Mesenchymal stem cells are conditionally therapeutic in preclinical models of rheumatoid arthritis," *Annals of the Rheumatic Diseases*, vol. 71, no. 10, pp. 1733–1740, 2012.

[7] A. Augello, R. Tasso, S. M. Negrini, R. Cancedda, and G. Pennesi, "Cell therapy using allogeneic bone marrow mesenchymal stem cells prevents tissue damage in collagen-induced arthritis," *Arthritis and Rheumatism*, vol. 56, no. 4, pp. 1175–1186, 2007.

[8] I. O. Unsal, Z. Ginis, F. A. Pinarli et al., "Comparison of therapeutic characteristics of islet cell transplantation simultaneous with pancreatic mesenchymal stem cell transplantation in rats with type 1 diabetes mellitus," *Stem Cell Reviews*, vol. 11, no. 3, pp. 526–532, 2015.

[9] M. M. Gabr, M. M. Zakaria, A. F. Refaie et al., "Insulin-producing cells from adult human bone marrow mesenchymal stem cells control streptozotocin-induced diabetes in nude mice," *Cell Transplantation*, vol. 22, no. 1, pp. 133–145, 2013.

[10] D. Q. Tang, Q. Wang, B. R. Burkhardt, S. A. Litherland, M. A. Atkinson, and L. J. Yang, "*In vitro* generation of functional insulin-producing cells from human bone marrow-derived stem cells, but long-term culture running risk of malignant transformation," *American Journal of Stem Cells*, vol. 1, no. 2, pp. 114–127, 2012.

[11] M. Suzuki, J. McHugh, C. Tork et al., "Direct muscle delivery of GDNF with human mesenchymal stem cells improves motor neuron survival and function in a rat model of familial ALS," *Molecular Therapy*, vol. 16, no. 12, pp. 2002–2010, 2008.

[12] L. Danielyan, S. Beer-Hammer, A. Stolzing et al., "Intranasal delivery of bone marrow-derived mesenchymal stem cells, macrophages, and microglia to the brain in mouse models of Alzheimer's and Parkinson's disease," *Cell Transplantation*, vol. 23, 1_Supplement, pp. 123–139, 2014.

[13] J. Y. Shin, H. J. Park, H. N. Kim et al., "Mesenchymal stem cells enhance autophagy and increase β-amyloid clearance in Alzheimer disease models," *Autophagy*, vol. 10, no. 1, pp. 32–44, 2014.

[14] H. Yang, H. Yang, Z. Xie, L. Wei, and J. Bi, "Systemic transplantation of human umbilical cord derived mesenchymal stem cells-educated T regulatory cells improved the impaired cognition in AβPPswe/PS1dE9 transgenic mice," *PLoS One*, vol. 8, no. 7, article e69129, 2013.

[15] B. J. Kang, H. Kim, S. K. Lee et al., "Umbilical-cord-blood-derived mesenchymal stem cells seeded onto fibronectin-immobilized polycaprolactone nanofiber improve cardiac function," *Acta Biomaterialia*, vol. 10, no. 7, pp. 3007–3017, 2014.

[16] B. W. Park, S. J. Jang, J. H. Byun et al., "Cryopreservation of human dental follicle tissue for use as a resource of autologous mesenchymal stem cells," *Journal of Tissue Engineering and Regenerative Medicine*, vol. 11, no. 2, pp. 489–500, 2017.

[17] G. Chen, A. Yue, Z. Ruan et al., "Monitoring the biology stability of human umbilical cord-derived mesenchymal stem cells during long-term culture in serum-free medium," *Cell and Tissue Banking*, vol. 15, no. 4, pp. 513–521, 2014.

[18] K. F. Baker and J. D. Isaacs, "Prospects for therapeutic tolerance in humans," *Current Opinion in Rheumatology*, vol. 26, no. 2, pp. 219–227, 2014.

[19] S. Shahrokhi, F. Menaa, K. Alimoghaddam, C. McGuckin, and M. Ebtekar, "Insights and hopes in umbilical cord blood stem cell transplantations," *Journal of Biomedicine and Biotechnology*, vol. 2012, Article ID 572821, 11 pages, 2012.

[20] S. Thirumala, J. M. Gimble, and R. V. Devireddy, "Cryopreservation of stromal vascular fraction of adipose tissue in a serum-free freezing medium," *Journal of Tissue Engineering and Regenerative Medicine*, vol. 4, no. 3, pp. 224–232, 2010.

[21] S. Thirumala, X. Wu, J. M. Gimble, and R. V. Devireddy, "Evaluation of polyvinylpyrrolidone as a cryoprotectant for adipose tissue-derived adult stem cells," *Tissue Engineering Part C*, vol. 16, no. 4, pp. 783–792, 2010.

Hindawi
Stem Cells International
Volume 2018, Article ID 6134787, 15 pages
https://doi.org/10.1155/2018/6134787

Research Article

Human Bone Marrow Contains Mesenchymal Stromal Stem Cells That Differentiate In Vitro into Contractile Myofibroblasts Controlling T Lymphocyte Proliferation

Yves Lecarpentier,[1] **Olivier Schussler**,[2] **Antonija Sakic**,[3] **José Maria Rincon-Garriz**,[4] **Priscilla Soulie**,[5] **Marie-Luce Bochaton-Piallat**,[3] **and Vincent Kindler**[4]

[1]*Centre de Recherche Clinique, Grand Hôpital de l'Est Francillien, 77104 Meaux, France*
[2]*Department of Cardiovascular Surgery, Research Laboratory, University Hospitals, Faculty of Medicine, Geneva, Switzerland*
[3]*Department of Pathology and Immunology, Centre Médical Universitaire Geneva Faculty of Medicine, Geneva, Switzerland*
[4]*Department of Specialties in Medicine, Hematology Service, Geneva University Hospitals, Faculty of Medicine, Geneva, Switzerland*
[5]*Department of Histology, Centre Médical Universitaire Geneva Faculty of Medicine, Geneva, Switzerland*

Correspondence should be addressed to Vincent Kindler; vincent.kindler@unige.ch

Received 23 November 2017; Revised 20 February 2018; Accepted 8 March 2018; Published 29 April 2018

Academic Editor: Somayeh Shahrokhi

Mesenchymal stromal stem cells (MSC) that reside in the bone marrow (BM) can be amplified in vitro. In 2-dimension (D) cultures, MSC exhibit a morphology similar to fibroblasts, are able to inhibit T lymphocyte and natural killer cell proliferation, and can be differentiated into adipocytes, chondrocytes, or osteoblasts if exposed to specific media. Here we show that medullar MSC cultured in 2D formed an adherent stroma of cells expressing well-organized microfilaments containing α-smooth muscle actin and nonmuscle myosin heavy chain IIA. MSC could be grown in 3D in collagen membranes generating a structure which, upon exposition to 50 mM KCl or to an alternating electric current, developed a contractile strength that averaged 34 and 45 μN/mm^2, respectively. Such mechanical tension was similar in intensity and in duration to that of human placenta and was annihilated by isosorbide dinitrate or 2,3-butanedione monoxime. Membranes devoid of MSC did not exhibit a significant contractility. Moreover, MSC nested in collagen membranes were able to control T lymphocyte proliferation, and differentiated into adipocytes, chondrocytes, or osteoblasts. Our observations show that BM-derived MSC cultured in collagen membranes spontaneously differentiate into contractile myofibroblasts exhibiting unexpected properties in terms of cell differentiation potential and of immunomodulatory function.

1. Introduction

Mesenchymal stromal stem cells (MSC) can be derived from almost any vascularized tissue of the organism after in vitro amplification with media supplemented with foetal calf serum, platelet-derived growth factor (PDGF), or human platelet lysate (HPL) [1–4]. The identification of the in vivo counterpart of MSC has been rather difficult to achieve because MSC precursors are scarce in vivo [5, 6]. For this reason in vitro amplification of MSC is generally required prior to any investigation. Since the mean doubling time of MSC derived from BM cultured with PDGF is 4 days [6], cells that are investigated at passages 2-3 (i.e., 20 days after seeding) have already achieved a significant number of mitosis in vitro and maybe biased compared to their in vivo counterpart. Nevertheless, there is now a growing consensus based on similarities in cell surface marker expression and in biological functions that MSC are derived from pericytes and/or adventitial cells that encircle the microvasculature of vascularized organs and tissues [7–9]. The media used to amplify MSC in vitro contain various biologically active factors including transforming growth factor-β (TGF-β),

PDGF, basal fibroblast growth factor, and insulin-like growth factor-1 which display proinflammatory features in specific situations. In particular TGF-β and PDGF that are released upon platelet activation participate to the migration of quiescent pericytes to inflammatory sites where they differentiate into myofibroblasts and provide a healing activity (for a review, see [10–12]). Although the environment required to achieve MSC amplification in vitro holds similarities with that observed in vivo when pericytes are activated after tissue injury, the hyperoxia produced by atmospheric oxygen, the artificial plastic surface lacking key adhesion molecules, and the repetitive thermic shocks and trypsinations may bias cell differentiation compared with the in vivo situation. The cells obtained after in vitro amplification are plastic adherent, prolong quiescent B and T lymphocyte survival, and differentiate into various mesenchymal lineages if exposed to the appropriate stimulus. Moreover, when exposed to an additional inflammatory stimulus such as γ-interferon (γ-IFN), MSC prevent T lymphocyte, B lymphocyte, or natural killer (NK) cell proliferation [13–15], thus demonstrating anti-inflammatory properties. Concerning human MSC, one of the major factors mediating T cell control is the enzyme indoleamine 2,3-dioxygenase (IDO), which degrades the essential amino acid L-tryptophan (tryp) in L-kynurenine (kyn) [16–19]. IDO is a holoenzyme containing a heme moiety that is functional only when the heme is reduced in the ferrous form by yet unidentified cofactors [20]. Consequently, the detection of either IDO mRNA or protein does not prove that the enzyme is functional; rather, the detection of the product metabolized by the enzyme (i.e., kyn) is required for such a claim. IDO is activated in MSC by various proinflammatory factors including γ-IFN, which is provided upon the course of an inflammatory process by the early activation of T lymphocytes and NK cells (see [18]). lDO can degrade tryp to such an extent that T lymphocyte, B lymphocyte, and NK cell proliferation, whose initiation and sustenance rely upon tryp concentration, is either prevented or arrested [16–19].

Myofibroblasts are contractile cells initially identified in the skin [21]. They express α-smooth muscle actin (αSMA) and the nonmuscle myosin heavy chain IIA (NMMHCIIA) that are both required to achieve cell contraction. Upon injury occurrence, myofibroblasts synthesize extracellular matrix proteins and retract, which favors healing and injury resolution [22]. Moreover, some myofibroblasts exhibit anti-inflammatory properties and may also favor injury resolution by shutting down inappropriate delayed immune response [23]. The ancestor of the myofibroblast is not fully identified yet. Fibrocytes, pericytes, and tissue resident fibroblasts have all been pointed out as possible progenitors of these cells [24, 25], and recently MSC derived from neonatal lungs have been shown to express a gene profile consistent with a myofibroblast progenitor phenotype [26], further emphasizing the similarities between MSC and myofibroblasts. It was therefore of interest to investigate whether myofibroblasts could be generated from a tissue such as bone marrow that is commonly used to generate MSC.

In order to do so, we designed a 3D culture system that allowed to maintain cells in a biocompatible scaffold for an extended period of time, and we developed specific devices to measure the mechanical strength generated by the cells immobilized in the scaffold. MSC were derived from BM, HPL was used as growth factor, and the scaffold consisted in 6 mm diameter patches of commercially available bovine collagen membranes.

We show here that under these culture conditions MSC express markers that are identical to that of 2D cultures including αSMA and NMMHCIIA, and that the cells contract and develop a sizable mechanical tension when exposed to relevant stimuli. Moreover, once resident in the membranes, MSC maintain their ability to differentiate into various mesenchymatous lineages and exert a strong control upon T cell proliferation. Thus MSC amplified in vitro exhibit features of both MSC and myofibroblasts, which allows wondering whether these cells are close parents.

2. Materials and Methods

2.1. Reactants

2.1.1. Cytokines and Chemicals. 1,4-Dithio-DL-threitol (DTT), 3-isobutyl-1-methylxanthine (IBMX), indomethacin (Indo), pyruvic acid, L-ascorbic acid 2-phosphate, dexamethasone, insulin, chondroitinase-ABC sodium β-glycerophosphate (βGP), and ascorbic acid (AsA) were from Sigma-Aldrich Chemie GmbH, Schnelldorf, Germany. L-Ascorbic acid-2-phosphate (AsAP) was purchased from Wako Pure Chemical Industries, Ltd. (Osaka, Japan), 1,25$(OH)_2$ vitamin D3 (vitaminD3) from BIOMOL (Plymouth Meeting, MA), and TRI Reagent from Molecular Research Center (Cincinnati, OH). ITS+ insulin, transferrin, selenious acid, bovine serum albumin, and linoleic acid premix (ITS) were from BD Biosciences, San Diego, CA. TGF-β was from R&D Systems. Hank's balanced salt solution (HBSS), Roswell Park Memorial Institute (RPMI) 1640 medium, Iscove's modified Dulbecco's medium (IMDM), and penicillin-streptomycin trypsin-EDTA solution were from Gibco BRL, Paisley, UK. 5(and 6)-carboxy fluorescein diacetate, succinimyl ester (CFSE) was from Molecular Probes Europe BV, Leiden, Netherlands. Collagenase type II and 4′,6-diamidino-2-phenylindole dihydrochloride (DAPI) were from Sigma-Aldrich. 3,3′-diamino-benzidine chromophore was from DakoCytomation, Glostrup, Denmark. Streptavidin-peroxydase kit (Vectastain, ABC kit, BA2000) was from Vector Laboratories, Burlingame, CA, and 3,3′-diaminobenzidine tetrahydrochloride dihydrate (DAB) from Fluka Chemie.

2.1.2. Antibodies

(1) FITC Labeled. Anti-CD54 (clone 15.2 mouse (m) IgG1) and anti-CD31 (clone 158-2B3 mIgG1) were from Ancell Corp., Bayport, MN, anti-CD45 (clone J33 mIgG1) was from Immunotech, Marseille, France, anti-CD90 (clone 5E10 mIgG1) was from BD Biosciences, San Diego, and anti-HLA-ABC (clone G46-2.6 mIgG1) was from BD Biosciences.

(2) RPE Labeled. Anti-CD3-RPE (clone UCHT-1, mIgG1) was from Ancell Corp., anti-CD34 (clone 8G12 mIgG1) was from BD Biosciences, anti-CD105 (clone SN6 mIgG1) was from AbD Serotec, Oxford, UK, anti-CD146 (clone P1H12 mIgG1) was from BioLegend, San Diego, CA, and anti-HLA-DR (clone 581 mIgG1) was from BD Biosciences.

(3) APC Labeled. Anti-CD44 (clone IM7 mIgG2b) was from eBioscience, anti-CD56 (clone AF12-7H3 mIgG1) was from Myltenyi Biotec, and anti-CD140b (clone 18A2 mIgG1) was from BioLegend.

(4) Unlabeled. Anti-αSMA (clone 1A4 mIgG1) was from [27].

(5) Monoclonal Isotype Controls. FITC, PE and biotin-labeled mIgG1, and biotin-labeled mIgG2b were from Dako, biotin-labeled mIgG2b was from Ancell, and unlabeled mIgG1 (clone MOPC-21) was from BioLegend.

(6) Polyclonal Antibodies. Anti-SMMHCs types 1 and 2 rabbit polyclonal IgG (BT-562) was from Biomedical Technologies Inc., Stoughton, MA, and anti-nonmuscle myosin heavy chain IIA (NMMHCIIA) rabbit polyclonal IgG (MYH9) was from Sigma-Aldrich.

(7) Secondary Antibodies. FITC-conjugated goat anti-mIgG2a and rhodamine-conjugated goat anti-rabbit IgG used as secondary antibodies were from Molecular Probes.

2.2. MSC Purification, Amplification, and In Vitro Differentiation

2.2.1. Purification. Cells were prepared and amplified in 2D cultures as previously reported [6]. Femoral heads were collected during hip replacement surgical interventions, according to the guidelines of the local ethics committee and after the patient's informed consent. Briefly, the fatty pulp of the femoral heads was released by scraping the bone with a spoon-shaped curette and deposited in a 50 ml Falcon tube containing Hank's balanced salt solution. The bone debris were allowed to settle for few minutes, and the cell suspension was transferred in a fresh tube. The sedimentation procedure was repeated once. Then a sample was collected, red cells were lysed with a hypotonic NH_4Cl solution, and nucleated cells were counted with a Neubauer hemocytometer. One million of live (trypan blue excluding) cells were distributed in 100 mm diameter Petri dishes containing 10 ml of RPMI medium complemented with 5% HPL and heparin. This led to final concentrations of 2.5–6 ng/ml of TGF-β, 0.5–1.5 ng/ml of PDGF, 4.5–9.5 pg/ml of basic fibroblast growth factor (βFGF, also known as FGF-2), and 5.3–6.5 ng/ml of insulin growth factor like (IGF) [3, 28]. After 48 hours, nonadherent cells were washed out and cultures were fed with the initial medium until subconfluency. Cells were then trypsinated (passage 1) and seeded at 10^5/100 mm diameter Petri dish (corresponding to 1.3×10^3 cells/cm^2) and grown until at half confluence (4×10^3/cm^2). Cultures up to passage 4 were used for the experiments.

2.2.2. MSC Seeding in Collagen Membranes. Small cylinders of Avitene™ Ultrafoam™ collagen hemostat (Bard Limited, Crawley, UK, ref. 1050050, 20–200 μm pore diameter, bovine dermal collagen of type I) were obtained by punching the commercially available membrane humidified with PBS with a sterile dermatologic biopsy punch of 6 mm diameter (Integra Miltex, Fisher Scientific). Each individual specimen, referred thereafter as a "membrane", was soaked for at least 24 hours in RPMI 5% HPL containing heparin. Membranes were then laid on a sterile gauze, and 10^5 MSC in 10 μl were delicately deposited on their upper surface. Cells were allowed to penetrate the patch for 1 hour at 37°C. The membranes were transferred in wells of a 24-well culture plate, containing 500 μl of medium. Medium was exchanged twice a week.

(1) Membrane Surface Measurement. Wet membranes loaded or not with MSC were laden on and photographed over a sterile petri dish whose basement was gridded with 4 mm^2 squares. Using the square grid, maximum and minimum diameters of each membrane were determined. These values were converted in mm, and one was multiplied by the other to obtain the approximate membrane surface.

(2) MSC Release. Membranes were removed from the culture vessel, transferred in Eppendorf conical tubes containing 1 ml of Hanks balanced salt solution (HBSS), and washed twice with HBSS. Digestion was undertaken in 1000 μl of a solution of HBSS supplemented with 3 mM $CaCl_2$ and 125 U/ml collagenase II, for 10 minutes at 37°C with strong vortexing at 5-minute intervals, or until full dissolution of the membrane. The cell suspensions were then centrifuged for 10 seconds at full speed on a Hettich table centrifuge and pellets were resuspended in 100 μl of RPMI 10% FCS prior to cell counting with the hemocytometer.

2.2.3. MSC In Vitro Differentiation

(1) Chondrogenic Differentiation. Chondrogenic differentiation was induced as previously described [29]. Four days after seeding, membranes were transferred in serum-free DMEM with 1% ITS+, 1 mM pyruvic acid, 37.5 μg/ml L-ascorbic acid-2 phosphate, 10^{-7} M dexamethasone, and 10 ng/ml TGF-β. Cells were cultured for 2 to 4 weeks, with medium changes every 3 days. Membranes were fixed in 4% paraformaldehyde, embedded in paraffin and cut into 5-micron thick sections. Sections were stained with Goldner's solution. Membranes from cultures in RPMI plus HPL were used as negative controls.

(2) Adipogenic Differentiation. Adipogenic differentiation was undertaken according to [5]. Briefly, 4 days after MSC seeding, membranes were incubated in the induction medium consisting of low glucose (1 g/l) DMEM, 10 μg/ml insulin, 10^{-6} M dexamethasone, 5×10^{-4} M IBMX, and 10^{-4} M indomethacin. After 48 hours, this medium was washed out and replaced by the maintenance medium consisting of high glucose (4.5 g/l) DMEM, 10% horse serum (HS), and 10^{-6} M dexamethasone for 48 hours. This cycle

was repeated 3 times. Membranes were then cultured in the maintenance medium until analysis. 2D cultures were established simultaneously as 3D cultures and submitted to the adipogenic differentiation procedure to determine the best time for adipocyte detection on the membranes. In general adipocytes were detectable in the 2D cultures 3 weeks after differentiation induction. Once the presence of adipocytes in the 2D cultures was confirmed, the corresponding membranes were then cryopreserved, sliced on a microtome, and stained with oil Red O.

(3) Osteoblastic Differentiation. Osteoblastic differentiation was achieved according to [30]. Four days after membrane seeding, medium was shifted to DMEM complemented with 10×10^{-7} M dexamethasone, 10^{-2} MβGP, and 5×10^{-5} M AsAP for 3 weeks. Membranes where then embedded in paraffin and cut into 5-micron thick sections prior to staining with Alizarin Red S.

2.3. Regulatory Activity of MSC upon Allogenic T Lymphocyte Proliferation. CD3+ T lymphocytes were obtained from peripheral blood of healthy donors after Ficoll-Paque gradient and negative selection (Dynal Biotech ASA, Oslo, Norway) and were labeled with 80 nM of CFSE [31] prior to coculture with allogenic MSC. MSC were seeded at 5×10^4 cells in 24-well plates in 500 μl of RPMI supplemented with 5% HPL and heparin 24–48 hours before the assays. Medium was replaced by fresh RPMI containing 10% FCS with 5×10^4 allogenic T lymphocytes per well. Alternatively MSC-laden or empty membranes were transferred into wells containing fresh RPMI, FCS, and 5×10^4 allogenic T lymphocytes. Cocultures were complemented with beads coated with anti-CD3 and anti-CD28 antibodies (a3-28) (Dynal Biotech) in a ratio of 0.5 beads per T lymphocyte seeded. Cell proliferation was assessed by flow cytometry after 5 days of coculture with MSC.

2.4. L-Tryptophan and L-Kynurenine Detection. Tryp and kyn concentrations were determined a described in [32, 33], respectively. Tryp was determined by fluorescence of the cleared culture supernatants after exposure to formaldehyde and $FeCl_3$ on a Twinkle LB 970 plate fluorimeter (Berthold Technologies, Regendsorf, Switzerland) with $\lambda_{ex} = 355$ nm and $\lambda_{em} = 460$ nm. Kyn was determined by absorbance of the culture supernatant at 490 nm on a Vmax ELISA plate reader (Molecular Devices Corporation, Menlo Park, CA) after precipitation with trichloroacetic acid and incubation with Ehrlich's reagent.

2.5. XTT Assay. The XTT assay was performed according to the manufacturer's instructions. Membranes recovered from the various incubations at 4°C were placed in 24-well plates containing 200 μl of fresh RPMI complemented with HPL and heparin. 100 μl of XTT (2,3-bis-(2-methoxy-4-nitro-5-sulfophenyl)-2H-tetrazolium-5-carboxanilide) was added to each well containing a membrane. After a 2-hour incubation at 37°C, 200 μl of supernatant was removed and the absorbance was measured at $\lambda = 450$ nm using an ELISA plate reader with a reference at $\lambda = 650$ nm. Membranes were then washed and photographed before resuming culture.

2.6. Immunofluorescence and Immunohistochemistry

2.6.1. Immunofluorescence. MSC were fixed for 20 minutes in RPMI 1% paraformaldehyde (PFA), 2% HEPES, rinsed in PBS, and incubated for 5 minutes at −20°C in methanol prior to staining with anti-αSMA [34]. Alternatively cells were fixed in ethanol for 30 seconds and stained with anti-SMMHCs or anti-NMMHCIIA. Whole membranes were fixed for 45 minutes in PBS 1% PFA, rinsed in PBS, and further incubated for 15 minutes at −20°C in methanol prior to staining with anti-αSMA. In some instances slides were fixed in ethanol for 1 minute and stained with anti-SMMHCs or anti-NMMHCIIA. Slides were mounted in buffered polyvinyl alcohol.

2.6.2. Immunohistochemistry. Membranes were fixed in 4% PFA, embedded in paraffin, and cut into 5-micron thick sections. Immunostaining for αSMA, SMMHCs, and NMMHCIIA were performed as described in [34, 35]. Sections were exposed to microwave radiation (750 W, 5 minutes) in citrate buffer (10 mM, pH 6.0) for αSMA and to a pressure cooker (3 minutes) in citrate buffer for SMMHCs and NMMHCIIA. Goat anti-mouse- or anti-rabbit-biotinylated IgGs were used as second antibodies. For visualization, the streptavidin-biotin peroxidase complex and 3,3′-diamino-benzidine chromophore was employed. Hemalun was used as counterstaining.

Double immunofluorescence staining of paraffin sections was also performed [34]. Slides were exposed to microwave radiation (250 W, 20 minutes) in Tris/EDTA (10 mM/1 mM, pH 9.1); specimens were then double stained with anti-αSMA and anti-SMMHCs or NMMHCIIA. FITC-conjugated goat anti-mIgG2a and rhodamine-conjugated goat anti-rabbit IgG were used as secondary antibodies. Nuclei were stained with DAPI. Slides were mounted in buffered polyvinyl alcohol. Images were recorded on an Axioskop 2 microscope (Carl Zeiss, Jena, Germany) equipped with a plan-Neofluar ×20/0.50 objective or an oil immersion plan-Neofluar ×40/1.4 objective and a high sensitivity, high-resolution digital color camera (Axiocam, Carl Zeiss). Whole membrane images were acquired using a confocal laser scan microscope (LSM800 Airyscan, Carl Zeiss) equipped with 2 lasers (excitation wavelengths at 488 and 561 nm) through an oil immersion Plan-Apochromat 63x/1.40 DIC f/ELYRA objective. Contrast and color adjustment of pictures, when required, were done using Adobe PhotoShop and applied across the integrality of the images. Similar levels of corrections were applied on the controls and the specimens labelled with the specific antibodies.

2.7. Electron Microscopy. MSC-seeded membranes were fixed with 1.5% glutaraldehyde in 0.1 M sodium cacodylate (Merck, Darmstadt, Germany) containing 1% sucrose for 3 hours. This was followed by fixation in 1% osmium tetroxide for 1 hour and subsequent dehydration and embedding in Epon. Semithin sections were stained with toluidine blue. Thin sections were treated with uranyl acetate and lead

citrate and examined in an electron microscope (Philips CM10 TEM; Philips, Eindhoven, the Netherlands).

2.8. Determination of the Contractility of MSC Seeded in Collagen Membranes. Settings for the monitoring of the mechanical study were performed as previously described [36]. Briefly, empty or MSC-laden membranes obtained after 19 days of culture that were cooled to 4°C for 48 to 72 hours before processing in the experiments were used (such a delay was unavoidable due to the shipment from the laboratory where MSC were grown to the location were contractibility experiments were undertaken). Twenty-five membranes laden with MSC and 23 empty membranes were studied. The membrane mechanical parameters were controlled by the software running on the recording PC. The lever displacement that mirrored membrane contraction was measured by means of an optoelectronic transducer. A small diaphragm on the lever modulated the light of a light-emitting diode (LED) falling on a photodiode. The transducer was constructed from a suitable d'Arsonval panel meter whereby the pointer was replaced by a thin L-shaped stainless steel tube acting as the lever.

2.8.1. Initial Settings. Under a binocular microscope, one end of the membrane was held by a small artery clip (S&T B-1 clamp) and fixed to a small linear micrometric translation stage. The opposite end of the membrane was then fixed to the tip of a homemade force-length transducer that was disposed in such a way that the membrane remained horizontal. Membranes were allowed to settle for 30 minutes at room temperature in a Krebs-Henseleit solution bubbled with 95% O_2-5% CO_2. The initial position for the displacement range was adjusted with a micrometer screw to a preload value of about 0.2 milliNewtons (mN). Basal resting tone (BT in mN/mm^2), which was the tension where neither spontaneous shortening nor lengthening of the matrix occurred, and initial length (Li) were recorded.

2.8.2. Membrane Passive Properties and Young's Modulus Computation. Membranes were then submitted to progressive elongation (in the absence of any other stimulus) to determine the Young modulus. The Young modulus (E) represents the slope of the stress/strain relationship. Stress (σ) is the force (F) per unit cross-sectional area (in m^2) (in Pascal (Pa) or N/m^2) imposed to the membrane and is expressed as

$$\sigma = \frac{F}{\mathrm{CSA}}. \quad (1)$$

Strain (ε) is the deformation of the membrane due to stress, that is, the elongation divided by the diameter of the membrane (L) at rest and is expressed as $\varepsilon = \mathrm{d}L/L$, where d L is the elongation of the membrane. The Young modulus E is expressed as E = stress/strain (expressed in Pascal; Pa).

$$E = \frac{F/\mathrm{CSA}}{\mathrm{d}L/L}. \quad (2)$$

Twenty-five membranes laden with MSC and 23 empty membranes were studied.

2.8.3. Induction of Contraction. All membranes (laden with or devoid of MSC) were exposed either to alternating electric tetanus (train period: 5 seconds; train duration: 2 seconds; stimulus frequency: 100 Hz) or to 50 mM KCl, until reaching a plateau corresponding to the maximum amplitude of isotonic shortening ($\Delta L_{\max}$). The membranes were then abruptly submitted to an isometric condition to measure the total isometric tension (TT). We measured the maximum amplitude of isotonic shortening ($\Delta L_{\max}$) and the total isometric tension. At the end of the experiment, membrane weight and diameter were measured to calculate their effective cross-sectional area (CSA in mm^2) using the ratio of the effective membrane weight (total weight/3) and the membrane diameter. The force observed (in mN) was normalized per CSA leading to tension (in mN/mm^2). The active tension was calculated as the total tension minus BT. Shortening length was normalized by Li (% Li).

2.9. Statistics. Mann–Whitney nonparametric rank test was used when 2 sets of data were compared and the Gaussian distribution could not be assessed. A value of $p < 0.05$ was considered as significant. For multiple comparisons, ANOVA with the Bonferroni correction was used after confirmation of the Gaussian distribution of the data. Means ± SDs are shown if not stated differently.

3. Results

3.1. MSC Amplified in 2D Cultures Express αSMA and Inhibit T Cell Proliferation. After 3–5 days of culture, BM cell suspensions formed discrete colonies of adherent cells. These colonies kept proliferating and formed a confluent cell layer, which for its vast majority stained positive for αSMA (Figure 1(a), top panel). High magnification micrographs showed that αSMA was organized in well-defined stress fibers throughout the cytoplasm (Figure 1(a), lower panel). Flow cytometry analysis undertaken on trypsinated cells showed that they expressed CD44, CD54, CD73, CD90, CD105, CD140b (also known as platelet-derived growth factor (PDGF) receptor-β), CD146, and αSMA, and were negative for HLA-DR, CD31, CD45, CD56 (Figure 1(b)), and CD34 (not shown). Flow cytometry analyses of MSC derived from 11 different donors allowed establishing that αSMA-positive cells represented on the mean 94 ± 7.7% of the cells recovered after trypsination of the stroma.

BM-derived MSC were exposed to 500 U/ml γ-interferon (γ-IFN). After 16 hours, kyn, which was undetectable in fresh medium was identified in MSC supernatants and its concentration increased up to day 5 (Figure 1(c), left panel).

The dependence of T cell proliferation upon the presence of tryp was assessed by stimulating lymphocytes with anti-CD3 and anti-CD28 antibodies immobilized on microbeads (a3-28) in media containing titrated concentrations of tryp. T lymphocytes exhibited a suboptimal proliferation when tryp concentration was <10 μM and could not proliferate in the absence of the amino acid (Figure 1(c), right panel).

The ability of MSC to degrade tryp in the presence of activated T lymphocytes and to inhibit their proliferation was assessed by coculturing lymphocytes stimulated with a3-28

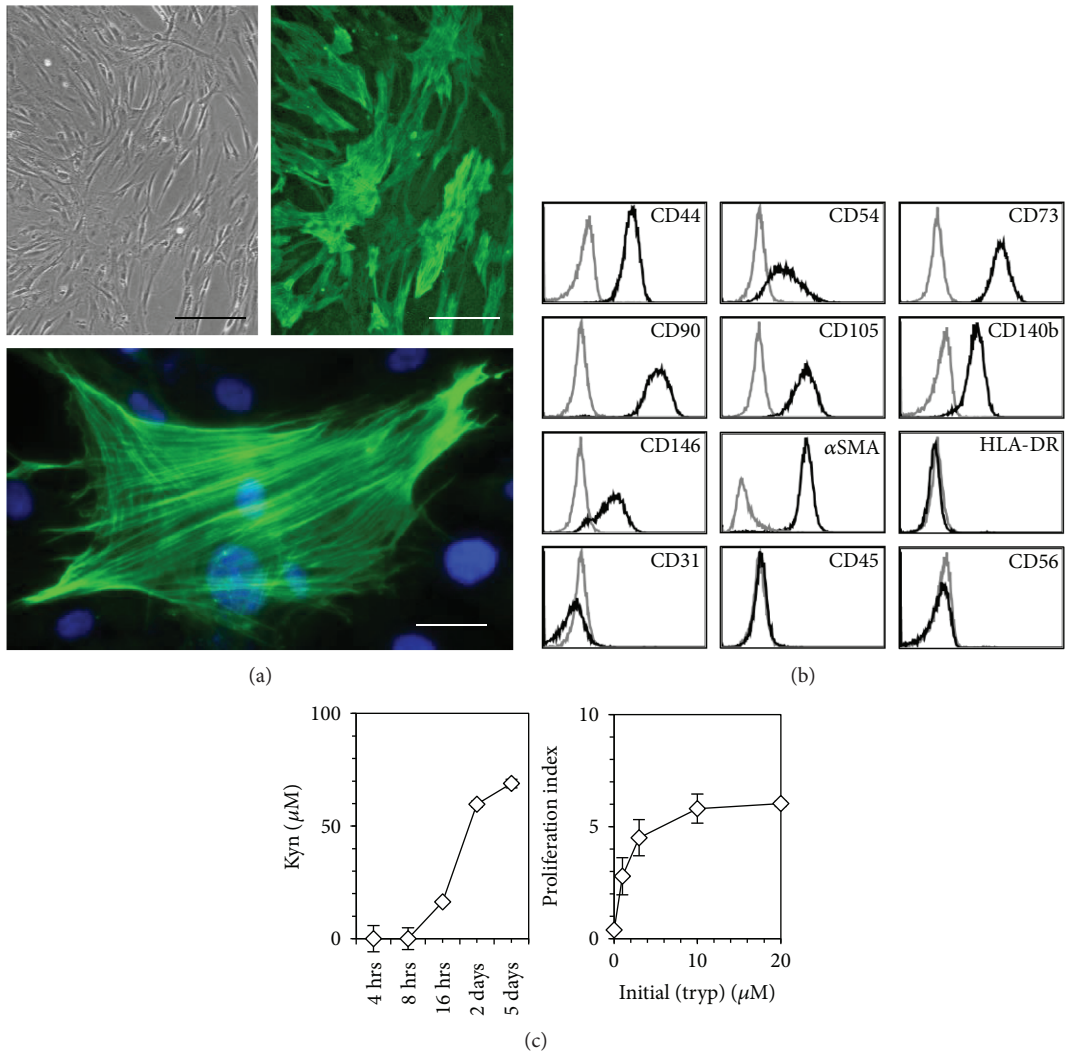

Figure 1: Biological characteristics of MSC cultured in 2D. (a) Amplified cells were fixed in the culture wells with 1% PFA in PBS, permeabilized with ice-cold absolute methanol, and labeled with anti-αSMA. *Left panel*: polarized light (scale bar is 150 μm), *right and lower panel*: fluorescence (scale bar is 100 and 20 μm, resp.). Original magnification 10x and 40x for top and lower panels, respectively. (b) Cultures were trypsinated before staining with various antibodies and flow cytometry analysis. Black profile: specific staining, gray profile: isotype control. Data for (a) and (b) are representative of 11 experiments. (c) *Left panel*: kinetics of kyn production by γ-IFN-stimulated MSC in IMDM medium (initial (tryp) 80 μM). One single add-on of 500 U/ml of γ-IFN was done on day 0. Supernatants were collected at the indicated time points and kyn titers were measured. Data of one experiment, representative of 3. *Right panel*: effect of tryp concentration upon T cell proliferation. Freshly purified, CFSE-labeled T lymphocytes were incubated with a3-28 for 5 days in tryp-free RPMI medium complemented with 0 to 20 μM of tryp, and proliferation was assessed by CFSE dilution. T lymphocyte proliferation is expressed as the inverse of the median CFSE fluorescence observed at the end of the cultures. Data of one experiment, representative of 2. Error bars are SD.

over a MSC stroma. By the end of the 5-day experiment, the titer of tryp averaged $2.5 \pm 1.5\,\mu$M ($n = 4$) in cocultures containing activated T lymphocytes and MSC, whereas it was $21 \pm 2.8\,\mu$M in cultures containing activated T lymphocytes exclusively, which is a titer similar to that of RPMI medium incubated for 5 days at 37°C without cells (21 μM of tryp). Kyn, which was undetectable in control medium and in cultures containing activated T lymphocytes exclusively averaged $10 \pm 2.9\,\mu$M in the cocultures of activated T lymphocytes and MSC. Consistent with the above observation (see Figure 1(c), right panel) and our previous data [18] showing that T lymphocyte proliferation is inhibited when tryp concentration is low, lymphocyte proliferation was efficiently inhibited in the presence of MSC (1.5 ± 1.9 versus 9.4 ± 3.7 CFSE arbitrary proliferation units in the presence and absence of MSC, resp.). Thus the early γ-IFN release by activated T lymphocytes was sufficient to activate IDO in MSC to such an extent that the depletion of tryp in the cultures ensuing IDO activation generated an environment that was inhibitory toward T lymphocyte proliferation.

3.2. MSC Colonize Collagen Membranes and Express Contractile Proteins. Four days after 3D culture initiation, the appearance of membranes seeded with MSC was

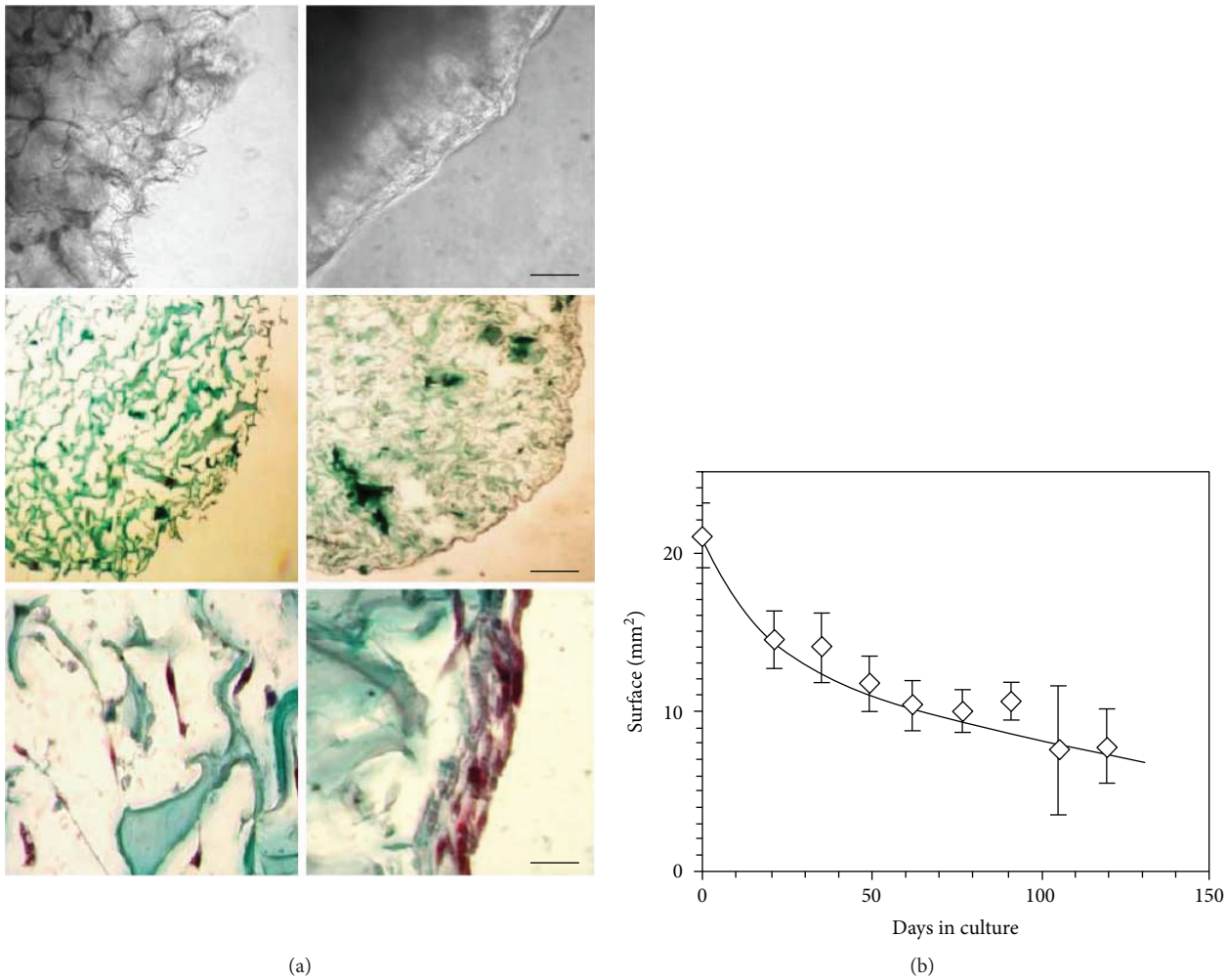

(a) (b)

Figure 2: Colonization of collagen membranes by MSC. Collagen membranes were seeded with MSC from passage 1 and maintained in RPMI medium supplemented with HPL for up to 119 days, with the medium changed every 2-3 days. (a) Membranes were observed by light microscopy in the culture vessels (upper panels, scale bar is 500 μm), or after fixation and staining with Goldner's stain (middle and lower panels, scale bars are 500 and 100 μm, resp.). *Upper left panel*: empty membrane; *upper right panel*: MSC-loaded membrane after 9 days of culture. *Middle left panel*: empty membrane section; *middle right panel*: MSC-laden membrane section cultured for 19 days. *Lower panels*: high magnification of a MSC-laden membrane section either in its center (left), or in the periphery (right). (b) Approximate membrane surface expressed in mm^2 in function of culture time. Data of (a) are of one experiment representative of 5 and data of (b) are the mean ± SD of 19 experiments until day 21 of culture, and of at least 3 experiments thereafter. Original magnifications of (a): higher panels 10x, middle panels 5x, and lower panels 20x.

modified: the extended ramifications of the collagen fibers visible by light microscopy prior to cell seeding were no longer detectable. A translucent coating filled the gaps between the fibers and smoothed the surface of the membranes (Figure 2(a), left and right upper panels). After 19 days of culture, membranes were fixed, sliced, and stained with Goldner's stain. This showed that the collagen scaffold of MSC-laden membranes was compressed compared to that of empty membranes (Figure 2(a), middle panels). Moreover, MSC had colonized the inner volume of the supports and had established a multicellular layer on their surface (Figure 2(a), lower panel). The membrane surface, which averaged 21 ± 2 mm^2 before seeding, decreased to 15 ± 2 mm^2 after 21 days of culture ($n = 19$ for both time points). Membranes kept decreasing in size thereafter until the end of the experiments (>100 days), albeit at lower pace (Figure 2(b)).

Staining membrane cross sections with anti-αSMA, anti-SMMHCs, and anti-NMMHCIIA antibodies showed that cells constituting the surface layer and those residing in the inner space of the membrane expressed αSMA and NMMHCIIA (Figure 3(a), upper left and right panels, resp.), but not SMMHCs (Figure 3(a) lower left panel). Confocal microscopy analysis demonstrated that αSMA and NMMHCIIA colocalized within the same stress fibers in the MSC grown in collagen membranes (Figure 3(b)). Electronic microscopy identified stress fibers within the cells (Figure 3(c)).

3.3. Biological Properties of MSC Cultured in 3-D Collagen Membranes. MSC-laden membranes prevented T lymphocyte proliferation whereas empty membranes did not (Figure 4(a)). Moreover, MSC seeded in scaffolds and

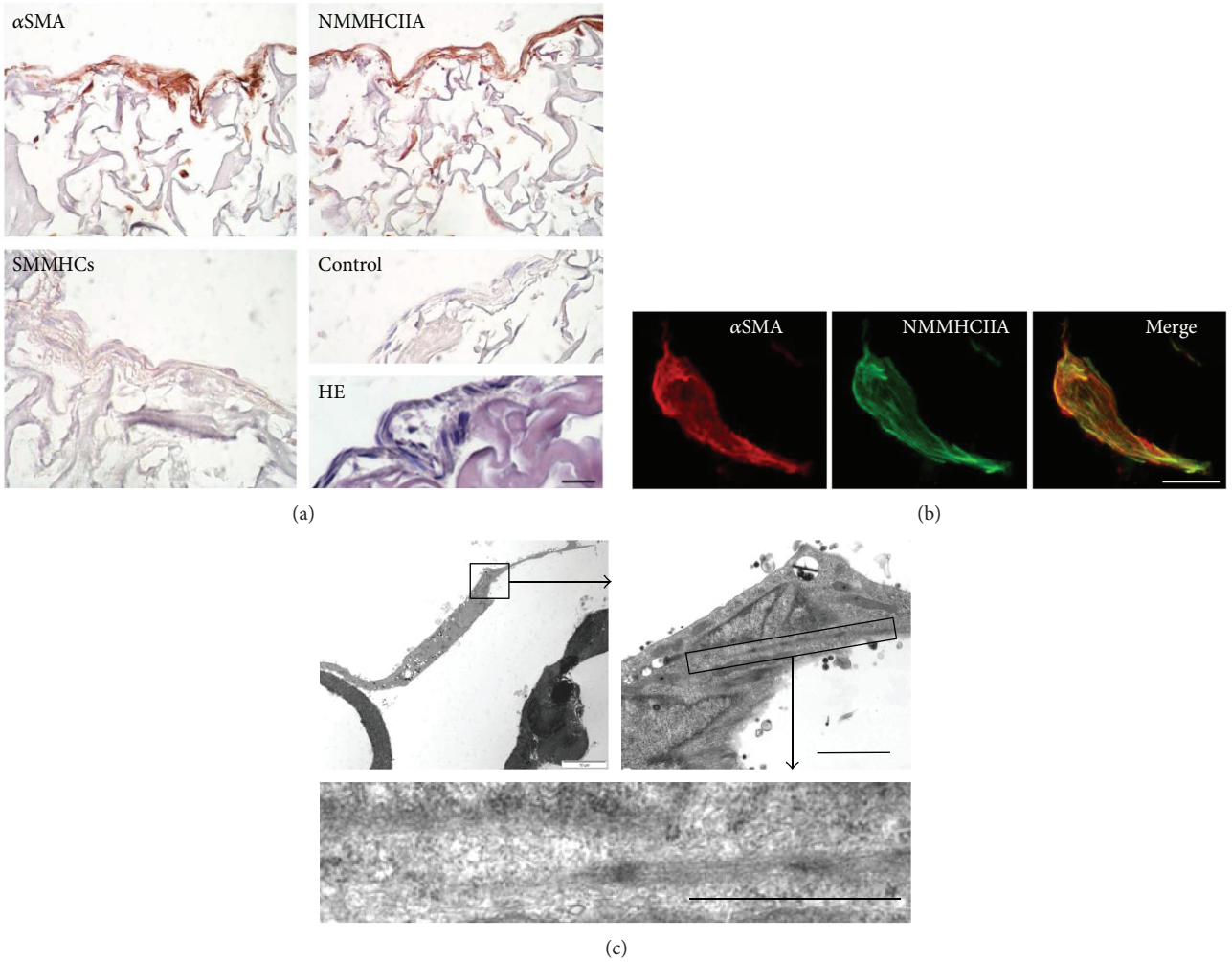

Figure 3: Expression of contractile proteins in MSC seeded in membranes. (a) Membrane sections stained either with anti-αSMA, anti-NMMHCIIA, anti-SMMHCs, and control antibody, or HE. (b) MSC-laden membrane stained with anti-NMMHCIIA (left panel), anti-αSMA (central panel), and merge picture (right panel) obtained after confocal laser scan microscopy of the paraffin section. Stress fibers positive for both NMMHCIIA and αSMA appear yellow on the merge picture. (c) Electronic micrographs with increasing magnification of one MSC located inside a collagen membrane, and cytoplasmic details. Scale bars are 100 μm (a), 10 μm (b), 2 μm, and 1 μm in the right and lower panels of (c), respectively. These data are from cultures harvested 19–21 days post membrane seeding, representative of 3 experiments for (a), 2 for (b), and 2 for (c).

exposed for 3 weeks to various media forcing differentiation toward either adipocytes, chondrocytes, or osteoblasts differentiated along these 3 pathways (Figure 4(b)).

MSC laden in membranes were stored for up to 5 days at 4°C. Their ability to reduce tetrazolium salts (XTT assay), to degrade tryp in the presence of activated T cells, and to prevent T lymphocyte proliferation were examined and compared with membranes that remained in regular cultures at 37°C. MSC-laden membranes stored at 4°C became orange when exposed to XTT, indicating that they were metabolically active, while empty membranes remained white (Figure 4(c), left). The formazan titers recovered in the culture supernatants of MSC-laden membranes that had been stored at 4°C prior to the XTT assay averaged 0.963 ± 0.064 (OD_{450}) (mean of day 1–5 of storage at 4°C, $n = 5$), which was similar to the value observed in supernatants of control cultures maintained at 37°C (0.972 (OD_{450})). Moreover, storage at 4°C did not impair the ability of MSC-laden membranes to metabolize tryp in the presence of activated T lymphocytes, and to decrease T cell proliferation (Figure 4(c), right).

Live MSC were released from the membranes by exposure to collagenase II. The number of cells recovered averaged $9.6 \pm 2.1 \times 10^4$ on day 7 ($n = 5$) and did not vary significantly with culture time (not shown). These cells expressed CD44, CD54, CD73, CD90, CD105, CD140b, and CD146, and were negative for HLA-DR, CD31, CD45, CD56 (Figure 4(d)), and CD34 (not shown). This phenotype was similar to that of MSC grown for the same duration in 2D cultures (see Figure 1(b)). Membrane-derived MSC could be seeded back in 2D cultures where they proliferated and expressed surface markers similar to cells continuously grown on plastic dishes (data not shown).

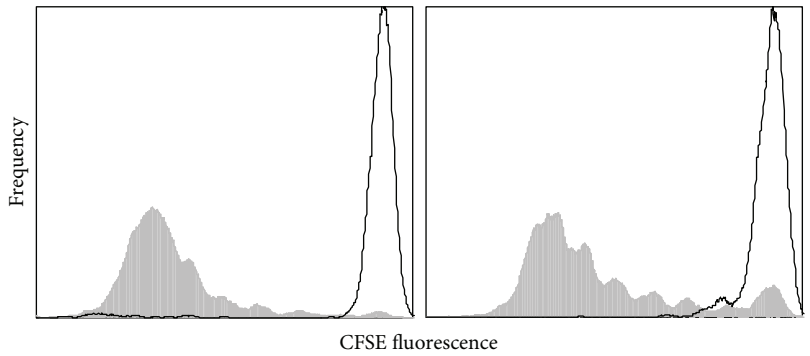

(a)

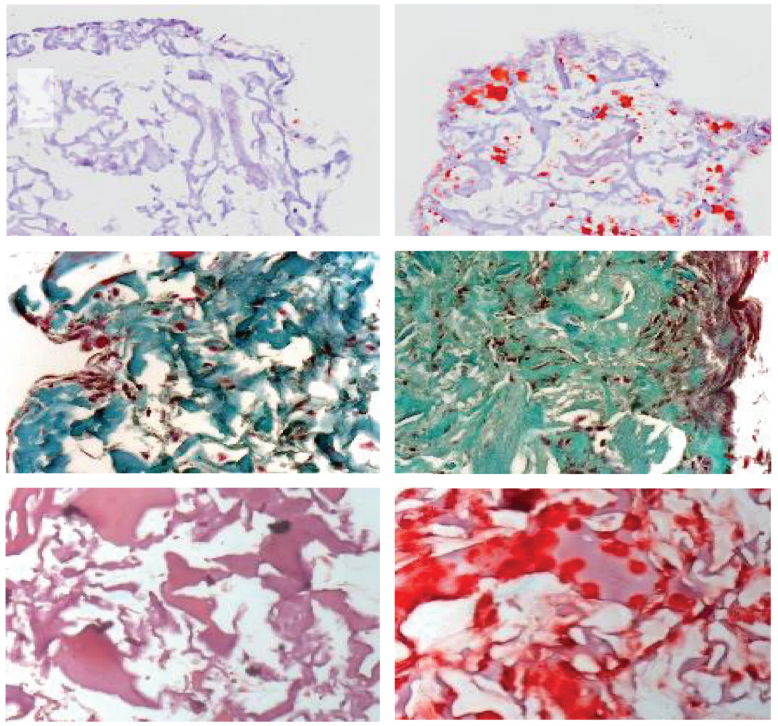

(b)

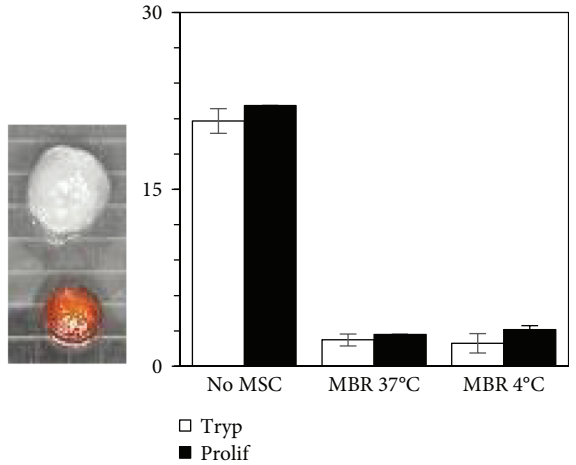

(c)

Figure 4: Continued.

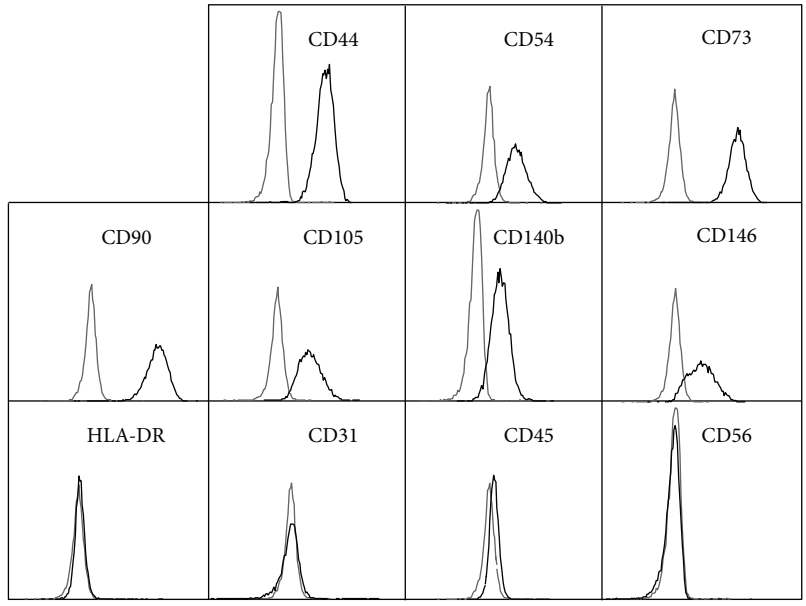

(d)

Figure 4: Biological properties of MSC cultured in 3D collagen membranes. (a) Regulation of T lymphocyte proliferation by MSC-laden membranes. T lymphocytes were labeled with CFSE prior to culture, and proliferation was assessed as CSFE fluorescence decrease. *Left panel*: T lymphocyte proliferation in the absence of a membrane and MSC: white profile: quiescent T lymphocytes; gray profile: T cells stimulated with a3-28. *Right panel*: proliferation of T cells stimulated with a3-28 in the presence of membranes: gray profile: empty membrane; white profile: membrane containing MSC. These data are representative of 5 experiments. (b) In vitro differentiation in collagen membranes: *left panels*: control cultures in the presence of HPL only; *upper right*: adipocytic (oil Red O stain); *median right*: chondrocytic (Goldner's stain); *lower right*: osteoblastic (Alizarin R stain) differentiation. Original magnifications are 10x, 20x, and 20x for adipocytic, chondrocytic, and osteoblastic differentiation, respectively. These data are representative of 3 experiments. (c) Biological activities of MSC-laden membranes after storage at 4°C for 0–5 days. *Left*: XTT reduction: an empty membrane (top) and a MSC-laden membrane (bottom) stored for 5 days at 4°C and subsequently exposed to XTT for 2 hours at 37°C are shown. The petri grid consists in 2×2 mm squares. *Right*: effect of MSC cocultured with activated T lymphocytes upon tryp degradation and T lymphocyte proliferation: "Tryp": residual tryp concentration in various supernatants, "Prolif": T lymphocyte proliferation. "No MSC": cultures of T cells stimulated with a3-28 in the absence of MSC; "MBR 37°C" and "MBR 4°C": cocultures of T lymphocytes and membranes seeded with MSC, without or with a previous storage of the latter at 4°C prior to the assay, respectively. The vertical axis refers either to the tryp concentration expressed in micromolar, or to the T cell proliferation expressed as the inverse of the median CFSE fluorescence. These data are representative of 2 experiments. (d) Flow cytometry analyses of surface molecules on MSC after membrane dissolution with collagenase II. The analyses are gated on 7AAD-negative live cells. Flow cytometry data are from one experiment, representative of 6.

3.4. Mechanical Properties of Collagen Membranes. The basic physical properties of membranes, that is, the properties observed without the application of electric or ionic stimulus are presented in Table 1. No significant differences were identified between the various groups in terms of membrane diameter, cross-sectional area (CSA), weight, and basal resting tone (BT). By contrast the mean Young modulus of the empty membranes (569 ± 270 Pascal (Pa)) was found to be significantly smaller to that of MSC-laden membranes (1508 ± 1409 Pa, mean $\pm$ SD of 23 and 25 measurements, respectively, $p = 2 \times 10^{-4}$) (Figures 5(a) and 5(b)).

Contraction and relaxation parameters are presented in Table 2. Membranes without MSC were exposed to electric tetanus because collagen holds converse piezoelectric properties. Piezoelectric effects can be either direct or converse. The direct effect consists in the internal generation of an electric charge resulting from the application of mechanical stress. The converse piezoelectric effect induces the generation of a mechanical strain once the material is exposed to an electric field. Both are observed in solid materials such as crystals, ceramics, collagen, bone, DNA, and various proteins [37, 38]. Applying an electric field to a membrane devoid of MSC induced both a weak shortening and a weak tension of the membrane, which characterizes the converse piezoelectric effect (Table 2(a)). Empty membranes were exposed to KCl because the solvation process could also induce a mechanical tension in collagen molecules. Solvation is a process of attraction and association of molecules of a solvent (here KCl) with molecules or ions of a solute (collagen). Solvation involves hydrogen bonding, ion-dipole, and dipole-dipole attractions or van der Waals forces and is induced when the ionic composition of the solvent is modified [39]. KCl, like tetanus, induced a weak shortening and a weak tension of the empty membranes (Table 2(a)). Once MSC-laden membranes were exposed to tetanus or KCl they shortened and developed an active tension after stimulation that were significantly higher compared with empty membranes (Table 2(a)) and which displayed a very slow kinetics (Figure 5(c)). Moreover, MSC-laden membranes stimulated with KCl relaxed after the addition of either isosorbide

Table 1: Basic physical properties of the membranes.

	Tetanus		KCl		
	No MSC ($n = 10$)	MSC ($n = 17$)	No MSC ($n = 10$)	MSC ($n = 9$)	p
Diameter (mm)	6.1 ± 0.7	5.4 ± 1.1	6.1 ± 0.2	5.8 ± 0.9	0.09
CSA (mm^2)	2.2 ± 0.6	2.4 ± 0.8	2.3 ± 1.1	2.3 ± 0.2	0.96
Weight (mg)	27.7 ± 10.1	22.5 ± 6.9	29.2 ± 14.9	25.3 ± 5.5	0.33
Basal tone (mN/mm^2)	0.037 ± 0.013	0.028 ± 0.013	0.033 ± 0.017	0.032 ± 0.005	0.51

Mean values ± SD of diameter, cross-sectional area of membranes (CSA), weight, and basal tone are shown. No MSC: empty collagen membrane; MSC: MSC-laden membrane; p: p value obtained from variance analysis performed on the 4 types of membranes. No significant difference is observed for the 4 parameters analyzed.

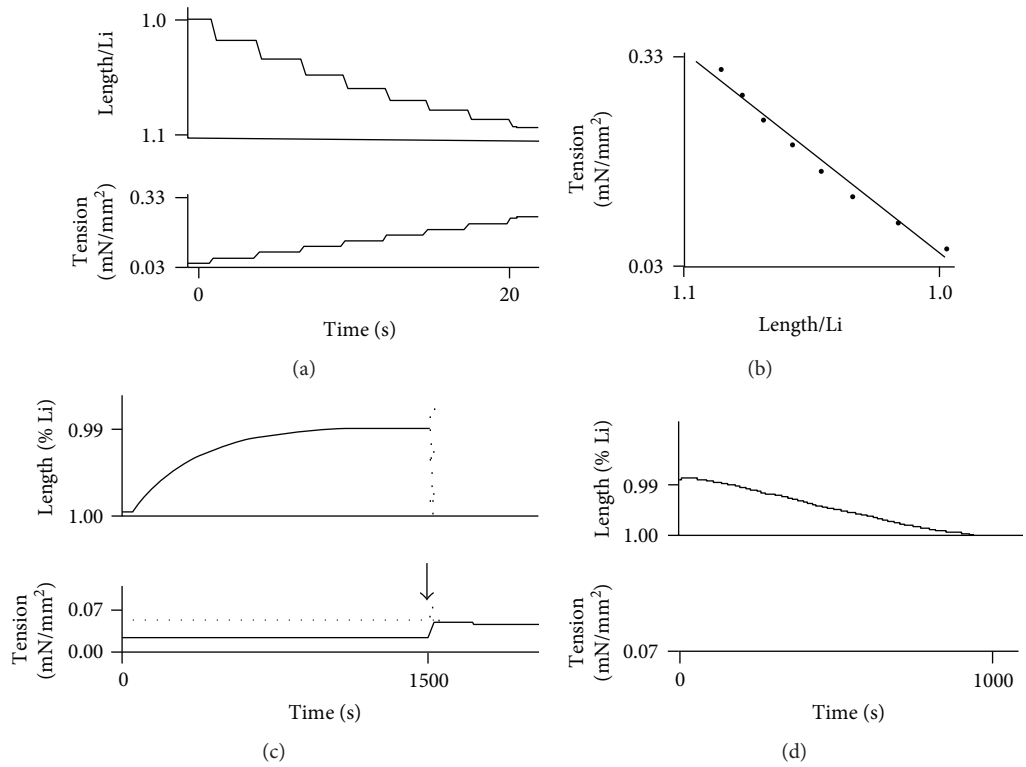

Figure 5: Row data of membrane contractility. Membrane tension is expressed in mN/mm^2; Li is the membrane length at resting basal tone; time is expressed in seconds (s). (a) Membrane length and tension variations are registered after successive increments by 0.1 mN loading steps, and are shown as a function of time. *Upper panel*: length increase (note that the scale is inverted in the vertical axis). *Lower panel*: tension increase. (b) Computation of the Young modulus using the data generated in (a). The membrane in this example is an empty membrane and its Young modulus is 450 Pa. (c) Effect of 50 mM KCl on a MSC-laden membrane. *Upper panel*: membrane shortening (note that the scale is inverted in the vertical axis on this plot: if membrane shortening increases, membrane length decreases). *Lower panel*: tension generation. The vertical arrow pointing downwards identifies the time point where tension was suddenly increased, shifting the system from isotonic mode to isometric mode. The active tension amplitude equals the total tension represented by the gray dotted line minus the basal tone, which is the lower solid black horizontal profile generated during the isotonic mode. (d) Relaxation of the membrane previously stimulated by KCl by ISDN (NO donor). *Upper panel*: membrane lengthening; *lower panel*: tension observed after the exposure to lSDN. Similar contractile parameters were observed with MSC-laden membranes stimulated by an electric tetanus. These data are representative of 23 experiments for empty membranes and 25 experiments for MSC-laden membranes for the Young modulus determination, 9 and 17 for KCl and tetanus stimulations, respectively, and 10 for ISDN relaxation and 9 for BDM relaxation (see Table 2).

dinitrate (ISDN) or 2,3-butanedione monoxime (BDM) (Figure 5(d)). Maximum isotonic lengthening (maxVr), negative peak isometric force derivative (−maxdF), and total duration of relaxation induced by both ISDN and BDM were of the same magnitude (Table 2(b)). MSC-laden membranes stimulated by an electric current spontaneously relaxed once the stimulus had stopped and were responsive again after a 10-minute rest. Consequently, the electric stimulation

Table 2: Contraction and relaxation parameters of the membranes.

(a) Contraction

	Tetanus			KCL		
	No MSC ($n = 12$)	MSC ($n = 17$)	p	No MSC ($n = 6$)	MSC ($n = 9$)	p
ΔLmax (%)	0.003 ± 0.003	0.013 ± 0.009	<0.001	0.003 ± 0.003	0.010 ± 0.003	<0.05
Active tension (mN/mm^2)	0.009 ± 0.009	0.045 ± 0.035	<0.001	0.007 ± 0.008	0.034 ± 0.014	<0.05

(b) Relaxation

	ISDN ($n = 10$)	BDM ($n = 9$)	p
Max Vr (mm/s)	0.048 ± 0.023	0.037 ± 0.023	0.35
Isot. relax. time (s)	980 ± 774	972 ± 433	0.98
−Max dF (mN/s)	0.48 ± 0.05	0.41 ± 0.30	0.64
Isom. relax. time (s)	1330 ± 877	1750 ± 901	0.45

(a) Maximum amplitude of isotonic shortening (ΔLmax) and p values comparing membranes with and without MSC exposed to either tetanus or KCl are shown. (b) Maximum relaxation velocity (Max Vr), time to isotonic relaxation (Isot. relax. time), negative peak of isometric relaxation (−max dF), and time to isometric relaxation (Isom. relax. time) are shown. No significant statistical differences were observed between ISDN and BDM for the 4 parameters of relaxation. (n) refers to the number of duplicates undertaken.

allowed the occurrence of several cycles of contraction-relaxation (data not shown).

4. Discussion

In this study we assessed whether the phenotype of MSC derived from human bone marrow was compatible with a pericyte origin, and because several studies reported that myofibroblasts may also originate from pericytes [11, 12], if MSC could differentiate into contractile myofibroblast in vitro. Our investigations comprised phenotypical flow cytometry analyses and various biological assays including cell differentiation assays, MSC-induced T lymphocyte inhibition, and the monitoring of MSC contractility. First, we showed that BM-derived MSC amplified in 2D cultures expressed CD44, CD76, CD90, CD105, CD140b/PDGF receptor-β, CD146, and αSMA, and were negative for CD45 and CD56 while exhibiting the ability to prevent T lymphocyte proliferation. Such a phenotype, as well as the potent inhibition of T lymphocyte proliferation, has been observed after in vitro amplification of pericytes derived from skeletal muscle [7, 8], thus strongly suggesting that our cells were derived from pericytes as well. Moreover, cell grown in 2D cultures expressed myofibroblast-associated markers such as NMMHCIIA and αSMA [40, 41]. One would expect that any cell simultaneously expressing NMMHCIIA and αSMA would be able to contract, but cell contractility could not be tested in 2D cultures due to the stiffness of the plastic supporting the stroma. Second, we showed that MSC survived for extended periods in collagen membranes and maintained a potent metabolic activity as documented by the XTT assay. However, the direct comparison of the metabolic activity developed by cells grown in 2D and 3D cultures could not be established using the XTT assay because the formazan salt released by the metabolizing cells was partially trapped in the membranes (coloring them in orange), and could not be quantitatively recovered for the densitometric analyses thus precluding an unbiased comparison with 2D cultures. Additional bioassays (see below) confirmed that MSC were fully functional while residing in the membranes, even after extended storage at 4°C. The array of biological markers expressed by the cells in 3D cultures, including NMMHCIIA and αSMA, was identical to that of the 2D cultures. Quite remarkably these contractile molecules were functional as evidenced by the fact that MSC-laden membranes exposed to the classical modes of sarcomeric and nonsarcomeric muscle stimulation readily contracted. Third, while the majority if not the totality of cells cultured with HPL expressed αSMA (see Figure 1(b)), our investigations showed that MSC laden in the membranes were simultaneously endowed with the ability to differentiate into chondrocytes, osteoblasts, or adipocytes, and prevented allogenic T lymphocyte proliferation. Thus, globally our data indicate that BM-derived MSC amplified with HPL most probably descended from pericytes, and spontaneously differentiate, when seeded in collagen membranes, into functional myofibroblasts while conserving phenotypic and functional features traditionally attributed to MSC.

If, in vivo, myofibroblasts exhibit the integrality of these features as well, not only would they help injury resolution via matrix synthesis and cellular contraction [22] but also by contributing directly to tissue reconstruction, and by preventing chronic inflammation via the silencing of delayed T cell activation. This hypothesis is consistent with the work of Pinchuk et al. [23], which showed that colonic myofibroblasts of human guts efficiently inhibit T cell proliferation and may play a prominent role in the establishment and

sustenance of mucosal intestinal tolerance. Thus it may be interesting to reassess the overall contribution of myofibroblasts upon systemic immune tolerance.

Some studies have indirectly assessed the retractile properties of MSC differentiated into myofibroblasts (for review see [22]). BM-derived MSC expressing αSMA have been reported to retract in collagen gels as determined by comparing gel size before and after incubation with TGF-β or PDGF using photographs [42] or a microscope micrometer [43]. However in order to claim that a tissue is contractile one has to show that it can contract under the action of a stimulus that is generally electric or (bio)chemical, and that it can relax when exposed to appropriate drugs, such as BDM that targets actin-myosin bridges or ISDN that decreases intracellular calcium. This dual process of contraction-relaxation has to be reversible, that is, it can be applied several times to the same preparation. Moreover, one has to provide data concerning the strength/tension developed by the preparation during the exposition to the stimulus using transducers monitoring the entire process in real time. Although the studies quoted above [42, 43] demonstrated that cells retracted, they did not quantify the cell mechanical power developed during the process of contraction, as measured in the present work.

Other studies quantified the force developed by myofibroblasts (but not MSC) trapped in gels, or used substrates of defined compliance to establish the correlation between support stiffness and myofibroblast maturation [44–47], but none measured the Young modulus of matrices before and after cell colonization, nor assessed the impact of classic modes of sarcomeric and nonsarcomeric muscle stimulation such as electric tetanus and KCl upon MSC/myofibroblast contraction.

In this study, we showed that the Young modulus of collagen membranes significantly increased when the structures were infiltrated with MSC. This indicates that cells firmly bound to the collagen membranes, as confirmed by the necessity to use collagenase to release them from the scaffold. TGF-β, present in biologically active concentrations in HPL [3] and known to enhance cell attachment to collagen [28, 48, 49], is certainly involved in this process. Moreover, the significant decrease of membrane size observed during culture (see Figure 2(b)) may be provoked together by TGF-β and the increase of membrane stiffness associated with membrane colonization. Both are known to favor myofibroblast contraction [44–46].

To validate our study, we had to identify the active mechanical properties of the membranes devoid of MSC. These are the converse piezoelectricity and solvation, which can occur when empty membranes are submitted to an electric field, or are soaked in high salt concentration, respectively [37, 38]. Hopefully enough, the mechanical tension induced on empty membranes by an electric field or a solvation process were significantly lower than those observed when MSC-loaded membranes were exposed to the stimuli. These findings, plus the observation that BDM and ISDN induced membrane relaxation, further confirmed that MSC-laden membrane contractions were produced by cells that were metabolically active and did not result from chemical or physical artifacts.

The fine mechanics of nonmuscular contractile biological systems has been investigated in the human placenta [36, 50, 51]. Placental myofibroblasts are located in the stem villi [52], exhibit a low isometric tension [49–51], and have a slow shortening velocity. They also exhibit a low myosin ATPase activity [53–55]. This is coherent with the observation that the dominant molecular motor in placental myofibroblasts is the nonmuscle myosin IIA [40, 41] whose molecular kinetics are dramatically slow [36, 55]. MSC-laden membrane stimulation lead to a similarly slow shortening velocity, which is consistent with the observation that nonmuscle myosin IIA, but not smooth muscle myosin, was detectable in the cells laden in membranes.

5. Conclusion

This work showed that MSC derived from human BM and cultured in collagen membranes supplemented with HPL expressed a phenotype that is compatible with a pericyte origin. Moreover, MSC spontaneously differentiated in the collagen scaffold into contractile myofibroblasts, which were simultaneously able to control T lymphocyte proliferation and to differentiate further into various mesenchymatous lineages. Our data suggest that myofibroblasts are not exclusively involved in tissue healing as initially sought, but also participates to inflammation shutdown and perhaps, due to their broad distribution within the body, to systemic self-tolerance as well. In addition MSC-laden collagen membranes, due to the extended survival of MSC in these structures, can be shipped to distant destinations without altering the biological potency of the cells, therefore representing a versatile and promising therapeutic tool to control local inflammation or favor the reconstruction of various tissues after injury.

Conflicts of Interest

All coauthors declare no conflict of interest regarding the publication of this article.

Authors' Contributions

Marie-Luce Bochaton-Piallat and Vincent Kindler contributed equally to this work.

Acknowledgments

This work has been supported in part by the Dr. Dubois-Ferrière Dinu Lipatti Foundation, the Ligue Genevoise Contre le Cancer, the CANSEARCH Foundation, and the Swiss National Science Foundation Grant no. 310030_166357/1 (MLBP), Switzerland. The excellent technical work of Mrs. N. Brouwers and of Mr. Ph. Henchoz is largely acknowledged. Special thanks go to Dr. D. Hochstrasser, without whom this work would not have been completed. The authors also thank Dr. Ch. Locher, President of the "Fédération de la Recherche Clinique du Grand Hôpital de l'Est Francilien".

References

[1] L. da Silva Meirelles, "Mesenchymal stem cells reside in virtually all post-natal organs and tissues," *Journal of Cell Science*, vol. 119, no. 11, pp. 2204–2213, 2006.

[2] A. J. Friedenstein, "Osteogenetic activity of transplanted transitional epithelium," *Cells Tissues Organs*, vol. 45, no. 1-2, pp. 31–59, 1961.

[3] C. Doucet, I. Ernou, Y. Zhang et al., "Platelet lysates promote mesenchymal stem cell expansion: a safety substitute for animal serum in cell-based therapy applications," *Journal of Cellular Physiology*, vol. 205, no. 2, pp. 228–236, 2005.

[4] A. Klimczak and U. Kozlowska, "Mesenchymal stromal cells and tissue-specific progenitor cells: their role in tissue homeostasis," *Stem Cells International*, vol. 2016, Article ID 4285215, 11 pages, 2016.

[5] M. F. Pittenger, A. M. Mackay, S. C. Beck et al., "Multilineage potential of adult human mesenchymal stem cells," *Science*, vol. 284, no. 5411, pp. 143–147, 1999.

[6] D. Suva, G. Garavaglia, J. Menetrey et al., "Non-hematopoietic human bone marrow contains long-lasting, pluripotential mesenchymal stem cells," *Journal of Cellular Physiology*, vol. 198, no. 1, pp. 110–118, 2004.

[7] M. Crisan, S. Yap, L. Casteilla et al., "A perivascular origin for mesenchymal stem cells in multiple human organs," *Cell Stem Cell*, vol. 3, no. 3, pp. 301–313, 2008.

[8] M. Corselli, C. W. Chen, M. Crisan, L. Lazzari, and B. Peault, "Perivascular ancestors of adult multipotent stem cells," *Arteriosclerosis, Thrombosis, and Vascular Biology*, vol. 30, no. 6, pp. 1104–1109, 2010.

[9] I. R. Murray, C. C. West, W. R. Hardy et al., "Natural history of mesenchymal stem cells, from vessel walls to culture vessels," *Cellular and Molecular Life Sciences*, vol. 71, no. 8, pp. 1353–1374, 2014.

[10] A. I. Caplan and D. Correa, "The MSC: an injury drugstore," *Cell Stem Cell*, vol. 9, no. 1, pp. 11–15, 2011.

[11] S. N. Greenhalgh, K. P. Conroy, and N. C. Henderson, "Healing scars: targeting pericytes to treat fibrosis," *QJM*, vol. 108, no. 1, pp. 3–7, 2015.

[12] C. Schrimpf, O. E. Teebken, M. Wilhelmi, and J. S. Duffield, "The role of pericyte detachment in vascular rarefaction," *Journal of Vascular Research*, vol. 51, no. 4, pp. 247–258, 2014.

[13] M. Krampera, S. Glennie, J. Dyson et al., "Bone marrow mesenchymal stem cells inhibit the response of naive and memory antigen-specific T cells to their cognate peptide," *Blood*, vol. 101, no. 9, pp. 3722–3729, 2003.

[14] A. Pradier, J. Passweg, J. Villard, and V. Kindler, "Human bone marrow stromal cells and skin fibroblasts inhibit natural killer cell proliferation and cytotoxic activity," *Cell Transplantation*, vol. 20, no. 5, pp. 681–691, 2011.

[15] G. M. Spaggiari, A. Capobianco, S. Becchetti, M. C. Mingari, and L. Moretta, "Mesenchymal stem cell-natural killer cell interactions: evidence that activated NK cells are capable of killing MSCs, whereas MSCs can inhibit IL-2-induced NK-cell proliferation," *Blood*, vol. 107, no. 4, pp. 1484–1490, 2006.

[16] D. H. Munn, E. Shafizadeh, J. T. Attwood, I. Bondarev, A. Pashine, and A. L. Mellor, "Inhibition of T cell proliferation by macrophage tryptophan catabolism," *The Journal of Experimental Medicine*, vol. 189, no. 9, pp. 1363–1372, 1999.

[17] R. Meisel, A. Zibert, M. Laryea, U. Göbel, W. Däubener, and D. Dilloo, "Human bone marrow stromal cells inhibit allogeneic T-cell responses by indoleamine 2,3-dioxygenase-mediated tryptophan degradation," *Blood*, vol. 103, no. 12, pp. 4619–4621, 2004.

[18] D. Suva, J. Passweg, S. Arnaudeau, P. Hoffmeyer, and V. Kindler, "In vitro activated human T lymphocytes very efficiently attach to allogenic multipotent mesenchymal stromal cells and transmigrate under them," *Journal of Cellular Physiology*, vol. 214, no. 3, pp. 588–594, 2008.

[19] E. O. Stenger, R. Chinnadurai, S. Yuan et al., "Bone marrow-derived mesenchymal stromal cells from patients with sickle cell disease display intact functionality," *Biology of Blood and Marrow Transplantation*, vol. 23, no. 5, pp. 736–745, 2017.

[20] S. R. Thomas and R. Stocker, "Redox reactions related to indoleamine 2,3-dioxygenase and tryptophan metabolism along the kynurenine pathway," *Redox Report*, vol. 4, no. 5, pp. 199–220, 1999.

[21] G. Gabbiani, G. B. Ryan, and G. Majno, "Presence of modified fibroblasts in granulation tissue and their possible role in wound contraction," *Experientia*, vol. 27, no. 5, pp. 549-550, 1971.

[22] M. L. Bochaton-Piallat, G. Gabbiani, and B. Hinz, "The myofibroblast in wound healing and fibrosis: answered and unanswered questions," *F1000Research*, vol. 5, 2016.

[23] I. V. Pinchuk, J. I. Saada, E. J. Beswick et al., "PD-1 ligand expression by human colonic myofibroblasts/fibroblasts regulates CD4+ T-cell activity," *Gastroenterology*, vol. 135, no. 4, pp. 1228–1237.e2, 2008.

[24] B. M. Dulmovits and I. M. Herman, "Microvascular remodeling and wound healing: a role for pericytes," *The International Journal of Biochemistry & Cell Biology*, vol. 44, no. 11, pp. 1800–1812, 2012.

[25] B. Hinz, "Formation and function of the myofibroblast during tissue repair," *Journal of Investigative Dermatology*, vol. 127, no. 3, pp. 526–537, 2007.

[26] A. P. Popova, P. D. Bozyk, A. M. Goldsmith et al., "Autocrine production of TGF-beta1 promotes myofibroblastic differentiation of neonatal lung mesenchymal stem cells," *American Journal of Physiology-Lung Cellular and Molecular Physiology*, vol. 298, no. 6, pp. L735–L743, 2010.

[27] M. Coen, G. Marchetti, P. M. Palagi et al., "Calmodulin expression distinguishes the smooth muscle cell population of human carotid plaque," *The American Journal of Pathology*, vol. 183, no. 3, pp. 996–1009, 2013.

[28] R. Crespo-Diaz, A. Behfar, G. W. Butler et al., "Platelet lysate consisting of a natural repair proteome supports human mesenchymal stem cell proliferation and chromosomal stability," *Cell Transplantation*, vol. 20, no. 6, pp. 797–812, 2011.

[29] A. M. Mackay, S. C. Beck, J. M. Murphy, F. P. Barry, C. O. Chichester, and M. F. Pittenger, "Chondrogenic differentiation of cultured human mesenchymal stem cells from marrow," *Tissue Engineering*, vol. 4, no. 4, pp. 415–428, 1998.

[30] N. Jaiswal, S. E. Haynesworth, A. I. Caplan, and S. P. Bruder, "Osteogenic differentiation of purified, culture-expanded human mesenchymal stem cells in vitro," *Journal of Cellular Biochemistry*, vol. 64, no. 2, pp. 295–312, 1997.

[31] A. B. Lyons and C. R. Parish, "Determination of lymphocyte division by flow cytometry," *Journal of Immunological Methods*, vol. 171, no. 1, pp. 131–137, 1994.

[32] D. L. Bloxam and W. H. Warren, "Error in the determination of tryptophan by the method of Denkla and Dewey. A revised procedure," *Analytical Biochemistry*, vol. 60, no. 2, pp. 621–625, 1974.

[33] Y. Kudo and C. A. R. Boyd, "Human placental indoleamine 2,3-dioxygenase: cellular localization and characterization of an enzyme preventing fetal rejection," *Biochimica et Biophysica Acta (BBA) - Molecular Basis of Disease*, vol. 1500, no. 1, pp. 119–124, 2000.

[34] M. Coen, K. Burkhardt, P. Bijlenga et al., "Smooth muscle cells of human intracranial aneurysms assume phenotypic features similar to those of the atherosclerotic plaque," *Cardiovascular Pathology*, vol. 22, no. 5, pp. 339–344, 2013.

[35] H. Hao, G. Gabbiani, E. Camenzind, M. Bacchetta, R. Virmani, and M.-L. Bochaton-Piallat, "Phenotypic modulation of intima and media smooth muscle cells in fatal cases of coronary artery lesion," *Arteriosclerosis, Thrombosis, and Vascular Biology*, vol. 26, no. 2, pp. 326–332, 2006.

[36] Y. Lecarpentier, V. Claes, E. Lecarpentier et al., "Ultraslow myosin molecular motors of placental contractile stem villi in humans," *PLoS One*, vol. 9, no. 9, article e108814, 2014.

[37] E. Fukada, H. Ueda, and R. Rinaldi, "Piezoelectric and related properties of hydrated collagen," *Biophysical Journal*, vol. 16, no. 8, pp. 911–918, 1976.

[38] D. Denning, M. T. Abu-Rub, D. I. Zeugolis et al., "Electromechanical properties of dried tendon and isoelectrically focused collagen hydrogels," *Acta Biomaterialia*, vol. 8, no. 8, pp. 3073–3079, 2012.

[39] I. Streeter and N. H. de Leeuw, "A molecular dynamics study of the interprotein interactions in collagen fibrils," *Soft Matter*, vol. 7, no. 7, pp. 3373–3382, 2011.

[40] S. Matsumura, K. Sakurai, T. Shinomiya et al., "Biochemical and immunohistochemical characterization of the isoforms of myosin and actin in human placenta," *Placenta*, vol. 32, no. 5, pp. 347–355, 2011.

[41] I. Komatsu, J. Bond, A. Selim, J. J. Tomasek, L. S. Levin, and H. Levinson, "Dupuytren's fibroblast contractility by sphingosine-1-phosphate is mediated through non-muscle myosin II," *The Journal of Hand Surgery*, vol. 35, no. 10, pp. 1580–1588, 2010.

[42] M. A. Ngo, A. Müller, Y. Li et al., "Human mesenchymal stem cells express a myofibroblastic phenotype in vitro: comparison to human cardiac myofibroblasts," *Molecular and Cellular Biochemistry*, vol. 392, no. 1-2, pp. 187–204, 2014.

[43] V. A. Farias, J. L. Linares-Fernández, J. L. Peñalver et al., "Human umbilical cord stromal stem cell express CD10 and exert contractile properties," *Placenta*, vol. 32, no. 1, pp. 86–95, 2011.

[44] B. Hinz, G. Celetta, J. J. Tomasek, G. Gabbiani, and C. Chaponnier, "Alpha-smooth muscle actin expression upregulates fibroblast contractile activity," *Molecular Biology of the Cell*, vol. 12, no. 9, pp. 2730–2741, 2001.

[45] N. P. Talele, J. Fradette, J. E. Davies, A. Kapus, and B. Hinz, "Expression of α-smooth muscle actin determines the fate of mesenchymal stromal cells," *Stem Cell Reports*, vol. 4, no. 6, pp. 1016–1030, 2015.

[46] P. D. Arora, N. Narani, and C. A. G. McCulloch, "The compliance of collagen gels regulates transforming growth factor-beta induction of alpha-smooth muscle actin in fibroblasts," *The American Journal of Pathology*, vol. 154, no. 3, pp. 871–882, 1999.

[47] M. Eastwood, D. Mcgrouther, and R. Brown, "A culture force monitor for measurement of contraction forces generated in human dermal fibroblast cultures: evidence for cell-matrix mechanical signalling," *Biochimica et Biophysica Acta (BBA) - General Subjects*, vol. 1201, no. 2, pp. 186–192, 1994.

[48] R. Montesano and L. Orci, "Transforming growth factor beta stimulates collagen-matrix contraction by fibroblasts: implications for wound healing," *Proceedings of the National Academy of Sciences of the United States of America*, vol. 85, no. 13, pp. 4894–4897, 1988.

[49] R. A. Brown, K. K. Sethi, I. Gwanmesia, D. Raemdonck, M. Eastwood, and V. Mudera, "Enhanced fibroblast contraction of 3D collagen lattices and integrin expression by TGF-β1 and -β3: mechanoregulatory growth factors?," *Experimental Cell Research*, vol. 274, no. 2, pp. 310–322, 2002.

[50] E. Lecarpentier, V. Claes, O. Timbely et al., "Role of both actin-myosin cross bridges and NO-cGMP pathway modulators in the contraction and relaxation of human placental stem villi," *Placenta*, vol. 34, no. 12, pp. 1163–1169, 2013.

[51] A. E. Farley, C. H. Graham, and G. N. Smith, "Contractile properties of human placental anchoring villi," *American Journal of Physiology-Regulatory, Integrative and Comparative Physiology*, vol. 287, no. 3, pp. R680–R685, 2004.

[52] A. C. Feller, H. Schneider, D. Schmidt, and M. R. Parwaresch, "Myofibroblast as a major cellular constituent of villous stroma in human placenta," *Placenta*, vol. 6, no. 5, pp. 405–415, 1985.

[53] T. M. King and U. Gröschel-Stewart, "Placental contractile protein," *American Journal of Obstetrics and Gynecology*, vol. 93, no. 2, pp. 253–258, 1965.

[54] G. Huszar and P. Bailey, "Isolation and characterization of myosin in the human term placenta," *American Journal of Obstetrics and Gynecology*, vol. 135, no. 6, pp. 707–712, 1979.

[55] M. Kovács, F. Wang, A. Hu, Y. Zhang, and J. R. Sellers, "Functional divergence of human cytoplasmic myosin II: kinetic characterization of the non-muscle IIA isoform," *Journal of Biological Chemistry*, vol. 278, no. 40, pp. 38132–38140, 2003.

Hindawi
Stem Cells International
Volume 2018, Article ID 4809673, 15 pages
https://doi.org/10.1155/2018/4809673

Research Article

Developmental Pathways Pervade Stem Cell Responses to Evolving Extracellular Matrices of 3D Bioprinted Microenvironments

Quyen A. Tran,[1] Visar Ajeti,[1] Brian T. Freeman,[2] Paul J. Campagnola,[1] and Brenda M. Ogle[2,3,4,5]

[1]*Department of Biomedical Engineering, University of Wisconsin, Madison, WI 53706, USA*
[2]*Department of Biomedical Engineering, University of Minnesota-Twin Cities, Minneapolis, MN 55455, USA*
[3]*Stem Cell Institute, University of Minnesota-Twin Cities, Minneapolis, MN 55455, USA*
[4]*Lillehei Heart Institute, University of Minnesota-Twin Cities, Minneapolis, MN 55455, USA*
[5]*Institute of Engineering in Medicine, University of Minnesota-Twin Cities, Minneapolis, MN 55455, USA*

Correspondence should be addressed to Paul J. Campagnola; pcampagnola@wisc.edu and Brenda M. Ogle; ogle@umn.edu

Received 17 August 2017; Revised 10 November 2017; Accepted 10 December 2017; Published 28 March 2018

Academic Editor: Farid Menaa

Developmental studies and 3D *in vitro* model systems show that the production and engagement of extracellular matrix (ECM) often precede stem cell differentiation. Yet, unclear is how the ECM triggers signaling events in sequence to accommodate multistep process characteristic of differentiation. Here, we employ transcriptome profiling and advanced imaging to delineate the specificity of ECM engagement to particular differentiation pathways and to determine whether specificity in this context is a function of long-term ECM remodeling. To this end, human mesenchymal stem cells (hMSCs) were cultured in 3D bioprinted prisms created from ECM proteins and associated controls. We found that exogenous ECM provided in 3D microenvironments at early time points impacts on the composition of microenvironments at later time points and that each evolving 3D microenvironment is uniquely poised to promote stem cell differentiation. Moreover, 2D cultures undergo minimal ECM remodeling and are ill-equipped to stimulate pathways associated with development.

1. Introduction

Although soluble factors supportive of differentiation of stem cells are well studied, our understanding of how extracellular matrix proteins (ECM) regulate differentiation is incomplete. Knowing the mechanistic contribution of the ECM to the dynamics of stem cell state is relevant for *in vitro* platforms for drug screening, toxicity testing, and disease modeling and is critical for *in vivo* therapeutic strategies involving tissue and whole-organ regeneration where ECM exposure is inevitable. A growing body of literature supports an association between exposure of stem cells to particular ECM types and specific differentiation outcomes. For example, Linsley et al. observed that hMSCs grown on two-dimensional type I collagen and fibronectin-coated surfaces differentiated towards the osteogenic lineage [1]. In addition, work by Lu et al. showed that acellular ECM generated by MSCs or chondrocytes was capable of inducing chondrogenic differentiation [2]. Similar studies have been extended to 3D environments [3, 4], where Jung et al. showed a complementary, but augmented, differentiation effect with 3D ECM exposure relative to that of 2D ECM [5, 6]. Similarly, Becerra-Bayona et al. examined mouse mesenchymal stem cell (mMSC) behavior in poly(ethylene glycol) (PEG) hydrogels conjugated with fibronectin, fibrinogen, and laminin and noted an increase in osteogenic differentiation in PEG hydrogels containing the latter two proteins [7]. Taken one step further, our lab has shown that ECM formulations can be optimized by using a "design of experiments" statistical approach to promote differentiation of particular cell types [8].

The impact of ECM on stem cell differentiation *in vitro* is perhaps not surprising given that *in vivo* developmental studies long ago demonstrated that the production and engagement of ECM often precedes differentiation events. For example, fibronectin has been shown essential for mesodermal, neuronal, and vascular development [9, 10]. Similarly, mass and clonal cultures of mouse cephalic and quail trunk neural crest were analyzed and it was found that fibronectin promotes differentiation of smooth muscle cells [11]. The effect was quite specific as differentiation of associated glia, neurons, and melanocytes was observed. In addition, the effect was not related to massive cell death or proliferation of smooth muscle cells [11]. But what is surprising is that most differentiation "programs" (whether of pluripotent or of multipotent cells) require multiple signals in sequence to achieve full maturation [12–14]. Does this mean ECM provides a first, middle, or end signal and requires additional soluble factor or cell-cell signaling to complete the sequence? *Or alternatively, can the ECM remodel or "evolve" to provide the stimulation sequence necessary for differentiation?* The latter scenario would require the stem cell or a supportive stromal cell type to institute the remodeling. This is important as the remodeling of the ECM and the subsequent change in cell activity have been shown to be important in processes such as vasculature and skeletal development, wound healing, and cancer development and progression [15, 16] as well as cell differentiation.

To determine whether the ECM evolves in association with differentiation, we devised an *in vitro* 3D model wherein multiphoton-excited (MPE) photochemistry was used to print 3D rectangular prisms composed of full-length type I collagen (Col1), fibronectin (FN), or laminin-111 (LN) proteins and containing human mesenchymal stem cells. Fabrication of the prisms occurs without addition of synthetic polymers, additional collagen type I, or other bioactive materials often added to support FN and LN which do not form spontaneous hydrogels ex vivo. The fabrication method is analogous to multiphoton laser scanning microscopy (MPLSM) in that the excitation, and thus, the photochemistry is restricted to the focal volume [17]. We demonstrated that MPE fabrication technology can crosslink soluble and structural proteins, layer by layer, into 3D protein matrices and fiber patterns with spatial fidelity of >85% [18]. We have characterized many of the material properties of the scaffold as well as examined stem cell-ECM interactions [19]. We have further shown that the cells adhere, migrate, and express focal adhesions on multiphoton excitation- (MPE-) crosslinked ECM scaffolds. Here, we used this 3D model system to study mechanistic underpinnings associating ECM engagement and remodeling with stem cell differentiation. (An earlier version of this work was presented as an abstract at the Biomedical Engineering Society Annual Meeting, 2017.)

2. Materials and Methods

2.1. Fabrication Instrument and Photochemistry. The multiphoton fabrication instrument has been described in detail previously and is only described here briefly [18]. A ti:sapphire femtosecond laser is coupled to an upright microscope stand (Axioskop 2, Zeiss, Thornewood, NY), and scanning is performed through a combination of laser scanning galvos (Cambridge Technologies, Bedford, MA) and a motorized stage (x-y-z, Ludl Electronic Products Ltd., Hawthorne, NY) under LabVIEW control with a field-programmable gate array (FPGA) board (Virtex-II PCI-7831R, National Instruments, Austin, TX) functioning as a data acquisition element (DAQ) [18]. Fabrication parameters such as power, scanning area, scan rate of galvos, and repetition of scanning pattern (#scans/layer) are set within the graphical user interface (GUI).

An FPGA was incorporated in the fabrication system to exploit parallelism of command executions (80 MHz clock rate) and to avoid bottlenecks in communications between the central processing unit (CPU) and hardware through four of the first-in, first-out (FIFO) channels. The first two FIFO channels relay information from the main LabVIEW program to the FPGA to control the galvo mirrors and fast electrooptic modulator (EOM) shutter, while the other two record information from the photomultiplier tube (PMT) to create a live image of the fabrication making the communication between the CPU and hardware near real time. The source code of the instrument control software is freely available at: http://campagnola.molbio.wisc.edu/.

The two-photon excitation of the Rose Bengal photoactivator is induced by a femtosecond titanium sapphire laser (Mira, Coherent, Santa Clara, CA) operating at 780 nm. The photochemistry proceeds through the generation of singlet oxygen which then attacks residues containing aromatic groups and free amines [20]. The resulting radical protein then links to a second protein molecule, generating a covalent bond. A 20x, 0.75 numerical aperture objective lens was used.

2.2. Structure Fabrication. Three-dimensional scaffolds were fabricated from solutions containing pure BSA (Sigma-Aldrich, St. Louis, MO), BSA and murine laminin-111 (LN) (isolated from Engelbreth-Holm-Swarm mouse sarcoma, EMD Millipore, Darmstadt, Germany), BSA and fibronectin (FN) (isolated from bovine plasma, Sigma), or BSA and collagen type I (Col1) (isolated via acetic acid digest from rat tail, Sigma), where the concentrations of BSA was 50 mg/mL for all scaffolds and for scaffolds with ECM added, the ECM concentration was 0.5 mg/mL for each individual ECM protein. BSA was used alone as a negative control for ECM exposure and also in the samples containing ECM protein, to provide enhanced structural stability [19]. Scaffold dimensions were set at $350 \times 350 \times 100$ μm to ensure the complete encapsulation of MSCs and to maintain structure integrity.

Scaffolds were linked to a nonspecific BSA self-assembled monolayer (SAM) linked to another organosilane SAM on a glass slide. The slides were prepared by (i) plasma cleaning, immersion in octadecyltrichlorosilane (OTDS) (Gelest Inc., Morrisville, PA), (ii) washing with anhydrous toluene to remove any residual ODTS, (iii) drying with N_2, and (iv) heating for 30 min at 120°C to complete the formation of the $Si^{-}O$ bonds of the self-assembled organosilane monolayer. The silanized slides were then soaked in a 10 mg/mL

solution of BSA to form the background self-assembled monolayer and then rinsed.

The protein solution and Rose Bengal photoactivator (2 mM) were confined in a small circular rubber chamber (Grace Bio-Labs, SA8R-0.5) seated on top of the BSA monolayer. Fabrication parameters such as structure size, laser power, size of axial steps, and scanning rate were optimized for maximum crosslinking without photodamage. After fabrication, scaffolds were exposed to high laser power to photobleach the residual Rose Bengal to ensure cell viability with prolonged imaging. Slides were then immersed in 1X PBS pH 7.4 (GIBCO) containing 400 μg/mL penicillin and 400 μg/mL streptomycin under sterile conditions and kept hydrated for cell plating.

2.3. Fluorescence Lifetime Imaging Microscopy. Fluorescence lifetime imaging microscopy (FLIM) was used to image MSCs inside the 3D structures where the respective contrasts were DAPI staining of the cell nucleus and residual entrapped Rose Bengal. The FLIM images were acquired on a custom-built, multiphoton microscope located at the Laboratory for Optical and Computational Instrumentation (LOCI) using time-correlated single photon counting (TCSPC; SPC830, Becker and Hickl, Berlin, Germany). Images were taken with a 40 Å~1.15 NA water immersion objective, where each optical section had a field of 512 Å~512 pixels and 64 time bins per pixel and required 60 s for acquisition. A z stack was comprised of 100 optical sections with a 1 μm axial step size. All FLIM measurements used two-photon excitation at 890 nm, and the DAPI emission was collected with a 520/35 nm filter (Chroma Technology, Rockingham, VT), whereas Rose Bengal fluorescence was collected with a 620/35 nm filter (Chroma Technology). FLIM images were fitted using the hardware-bundled analysis software (SPCImage, Becker-Hickl) to a single exponential decay model. Analyzed images were color mapped according to the fluorescence lifetime, exported, and reconstructed in 3D using Imaris software (Bitplane, Zurich, Switzerland).

2.4. Physical Characterization of BSA, BSA/FN, BSA/Col1, and BSA/LN Scaffolds

2.4.1. Determination of Volumetric Swelling Ratio. To characterize the relative crosslinking of the structure, the volumetric swelling ratios were measured, where this is defined as the ratio of the hydrated to the dehydrated volume [19]. The former was determined by obtaining two photon-excited fluorescence (TPEF) images (890 nm excitation) of the structure in physiologic medium at 1 μm axial step sizes with an 0.8 NA objective lens, where the contrast was from residual entrapped Rose Bengal. The structures were dehydrated by immersion in 100% ethanol and then dried completely and imaged under the same conditions as the hydrated case. The areas and heights (and resulting volumes) were determined using the freely available FIJI image analysis software (http://fiji.sc/wiki/index.php/Fiji).

2.5. Fractal Dimension Determination. Scanning electron microscopy (SEM) was used to determine the structural assembly at higher resolution than by optical microscopy, where we specifically determine the fractal dimension, rather than pore sizes or their distribution. Prior to scanning, structures were fixed overnight (4°C) using a 0.1 M phosphate buffer containing 1.5% glutaraldehyde and 1% tannic acid and then dehydrated using a series of ethanol washes and a critical point drying step (Samdri 780 critical point drier, Tousimis, Research Corp., Rockville, MD). Lastly, gold/palladium (60 : 40) was deposited onto the structures, with a thickness of 30 nm, using a DC sputter coater (Auto Conductavac IV, Seevac Inc., Pittsburgh, PA). SEM images were acquired using the Hitachi S-570 microscope (Hitachi, Tokyo, Japan). The mean fractal dimension was computed using the FIJI FracLac plugin.

2.6. Cell Culture. Embryonic stem cell-derived mesenchymal stem cells [21, 22] were cultured in αMEM, 10% fetal bovine serum, 1% L-glutamine, 1% nonessential amino acid, and 1% penicillin/streptomycin. hMSCs were plated at 10,000 cells/mm^2 with daily media changes for 28 days. hMSCs used for scaffold modification analysis were seeded at a concentration of 5000 cells/cm^2 and cultured for 14 days. hMSCs used for MMP, integrin, and ECM analysis were seeded at 10,000 cells/cm^2 and cultured for 28 days.

2.7. Tracking of BSA, BSA/FN, BSA/FN, and BSA/LN Physical Structure Modifications. To track physical modification of the structures, phase contrast images of the structures were taken daily for 14 days. Images were obtained on an Axiovert 40C microscope (Zeiss) using a 10x objective with a 0.25 NA. Structure size was measured using the freely available Fiji software (http://fiji.sc/wiki/index.php/Fiji, Supplemental Table 1).

2.8. Gene Expression Analysis Using RNA Sequencing. hMSCs specifically within the structures were excised and RNA was extracted according to the RNeasy Mini Kit (Qiagen, Germantown, MD). cDNA was generated using the SMARTer Ultra Low RNA kit (Clontech, Mountain View, CA). mRNA library was produced according to the Illumina Nextera XT preparation kit's manufacture protocol (Illumina, San Diego, CA). RNA was sequenced using the Illumina MiSeq sequencher with paired end reads, a length of 75 bp, and a depth 20 million reads. This work, except RNA extraction, was performed at the University of Minnesota Genomics Center.

Gene expression was analyzed using the Galaxy software (Minnesota Supercomputing Institute (MSI), University of Minnesota, MN), and all generated data can be found on the GEO database, accession number GSE102737, reviewer token OGLE30. RNA sequencing reads were aligned to the human genome (hg19.fa and hg19_genes_2012–03-09.gtf) using the TopHat software (version 2.0.09, open source software, http://ccb.jhu.edu/software/tophat/index.shtml). TopHat results were further analyzed using Cufflinks (version 2.2.1, open source software, http://cole-trapnell-lab.github.io/cufflinks/) software to assemble the gene transcripts and estimate gene abundance. Read counts were normalized to obtain FPKM (fragment per kilobase of transcript per million mapped reads, Supplemental Table 1). Differential gene

expression was determined using the single-cell differential expression (SCDE) toolset [23, 24]. Genes with a q value less than 0.05 were considered "differentially expressed." Gene-annotation enrichment analysis was performed with the Database for Annotation, Visualization and Integrated Discovery (DAVID) informatics resources 6.7 of the National Institute of Allergy and Infectious Diseases (NIAID) and of the National Institutes of Health (NIH) (Supplemental Tables 3 and 4).

2.9. Quantitative Polymerase Chain Reaction. The cDNA for RNA sequencing verification was amplified from cDNA used for RNA sequencing. Primers for COL1, SGPL1, and MAGED2 were purchased from Qiagen, and GAPDH (forward: TTAAAAGCAGCCCTGGTGAC reverse: CTCTGC TCCTCCTGTTCGAC) was used as an internal control. Quantitative polymerase chain reaction (PCR) was performed using SYBR Green Master Reagent (Thermo Fisher Scientific, Waltham, MA) and ran on an Applied Biosystems StepOne Plus machine. Gene fold change was determined using the $\Delta\Delta C_t$ method with each gene normalized to GAPDH and 3D/FN normalized to BSA structures.

2.10. Statistical Analysis. Volumetric swelling ratio, mean fractal dimension, and changes in ECM, integrin, and MMP expression were analyzed for statistical significance using ANOVA with Tukey post hoc analyses using JMP software (SAS, Cary, NC). Hierarchical clustering and principal component analyses were conducted using R software.

3. Results

3.1. Physical Characterization of 3D ECM-Based Bioprinted Prisms. To track the interplay between 3D ECM exposure and hMSC differentiation, we selected ECM proteins for our 3D *in vitro* model representing the primary classes of ECM found in stromal environments, namely, fibrillar collagens, basement membrane, and small adaptor proteins. Thus, 3D bioprinted prisms were fabricated from ECM protein collagen type I (Col1), laminin-111 (LN), or fibronectin (FN) supplemented with bovine serum albumin (BSA) to improve crosslinking efficiency and subsequently seeded with hMSCs. 3D bioprinting was accomplished via multiphoton excitation-based fabrication and was utilized here so that hMSCs could be exposed to ECM proteins in 3D, even ECM proteins that do not spontaneously form hydrogels outside the body (Figures 1(a) and 1(b)). Bioprinted prisms containing different ECM proteins were physically characterized in terms of pore size and relative crosslinking density. We found that the ECM type slightly affected the topography of the structure in terms of fractal dimension but the associated crosslinking density remained consistent between structures (Figures 1(c) and 1(d)). For this reason, altered differentiation outcomes following culture in the 3D bioprinted prisms will largely reflect biochemical differences of the prisms, but also nuances in topography. hMSCs were seeded on 3D bioprinted prisms, and soon after seeding, hMSCs infiltrated the prisms and maintained viability in the prisms for several weeks [19] (Figure 1(e)).

3.2. Transcriptional Profile of hMSCs in 3D ECM-Based Bioprinted Prisms. Given the myriad of differentiation outcomes of hMSCs, we decided to employ RNAseq of hMSCs to ensure global assessment of transcriptional outcomes of ECM exposure in our 3D *in vitro* model. Thus, after 28 days of culture, RNAseq was conducted on hMSCs of 3D bioprinted prisms (termed 3D/Col1, 3D/LN, and 3D/FN) as well as controls including hMSCs just prior to matrix seeding (2D/D0), hMSCs cultured for 28 days on tissue culture polystyrene (2D/D28), and hMSCs infiltrating 3D printed prisms composed of bovine serum albumin (3D/BSA) for 28 days. 3D/BSA was used to control for BSA added for structural stability of the bioprinted prisms with ECM and to distinguish outcomes associated with engagement of the integrin family of receptors since BSA does not bind integrins. Overall gene expression profiles were analyzed via hierarchical clustering and principal component analysis (PCA) to determine the extent of similarity/dissimilarity between experimental groups based on overall mRNA expression profiles for each sample. Hierarchical clustering group samples were based on mRNA expression profiles over a variety of scales by creating a cluster tree or dendogram where clusters of samples at one level are joined as clusters at the next level, allowing one of determine the scale of clustering or association for the cell populations exposed to disparate ECM in 3D. PCA uses an orthogonal transformation to convert the set of mRNA expression data for each sample that may be correlated into a set of linearly uncorrelated variables called principal components. The transformation is defined such that the first principal component represents the largest possible variance and the second principal component has the highest variance possible under the constraint that it is orthogonal to principal component 1. The resulting vectors are an uncorrelated orthogonal basis set which, when plotted on an x-y grid, can reveal unbiased associations between mRNA expression levels of two or multiple samples (in this case, cell populations exposed to disparate ECM in 3D scaffolds) based on proximity on the plot. The hierarchical clustering and PCA analyses included all genes of each sample with an FPKM value greater than 1. Analysis showed that the initial hMSC population (2D/D0, $n = 3$ populations from three independent experiments, but same passage) and hMSCs after 28 days in standard 2D culture (2D/D28, $n = 6$ populations from three independent experiments, but same passage) cluster far from each other (Figures 2(a) and 2(c)) suggesting that the extended duration in culture without passaging alters the transcriptome, which is consistent with previous reports [25]. hMSCs cultured in 3D bioprinted prisms ($n > 5$ prisms for each ECM type from three independent experiments, but same passage) cluster away from those in 2D at 28 days, suggesting that the transition from 2D to 3D culture also has a substantial effect on the hMSC transcriptome. Clustering differences between 3D prisms of different ECM composition are more subtle and easier to visualize when compared, independent of the 2D controls. When viewed in this way, we observed a separation between 3D/BSA and 3D/LN or 3D/FN indicating that the presence of FN and LN substantially altered the gene expression of hMSCs after 28 days of 3D culture (Figures 2(d)–2(f)). However, PCA analysis

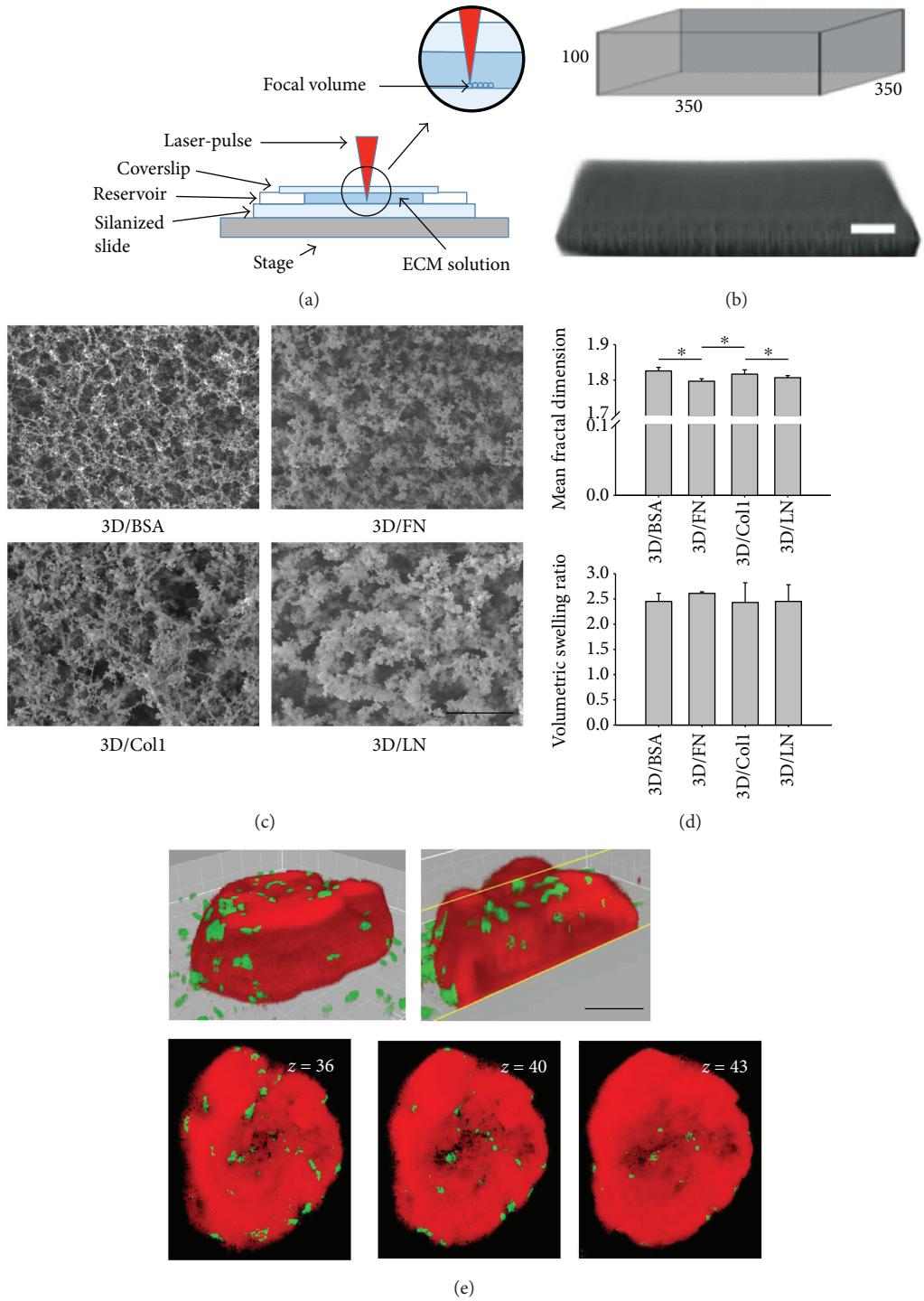

Figure 1: Fabrication of 3D ECM-based, bioprinted prisms. (a) Fabrication Schematic. Multiphoton excitation was used to polymerize a focal volume containing individual ECM proteins (e.g., FN, Col1, and LN) and associated photocrosslinking agent. 3D printing of this type was used so that a three-dimensional construct, in this case a rectangular prism, could be generated even with ECM types that do not form hydrogels spontaneously ex vivo. (b) Geometric template (above; dimensions of micron scale) and associated bioprinted ECM-based rectangular prism containing BSA and LN (BSA/LN; below). Scale bar = 50 μm. (c) Representative SEM images of prisms fabricated with BSA, FN, Col1, and LN. Scale bar = 10 μm. (d) Average fractal dimension of each ECM-based, 3D bioprinted prism (above); volumetric swelling ratio of each ECM-based bioprinted prism (below). Error bars depict standard deviation (SD), $^*P < 0.05$, $n = 3$ experimental replicates. (e) Multiphoton imaging to show interaction of hMSCs with bioprinted prism containing BSA only after 3 days of seeding. 3D reconstruction (left) and cut-away view (right) show cellular infiltration (e, upper panels). Also, in support of hMSC infiltration are shown multiple cross sections at various z depths (e, lower panels). Green (CD90) indicates MSCs; red indicates the bioprinted matrix. Scale bar = 100 μm.

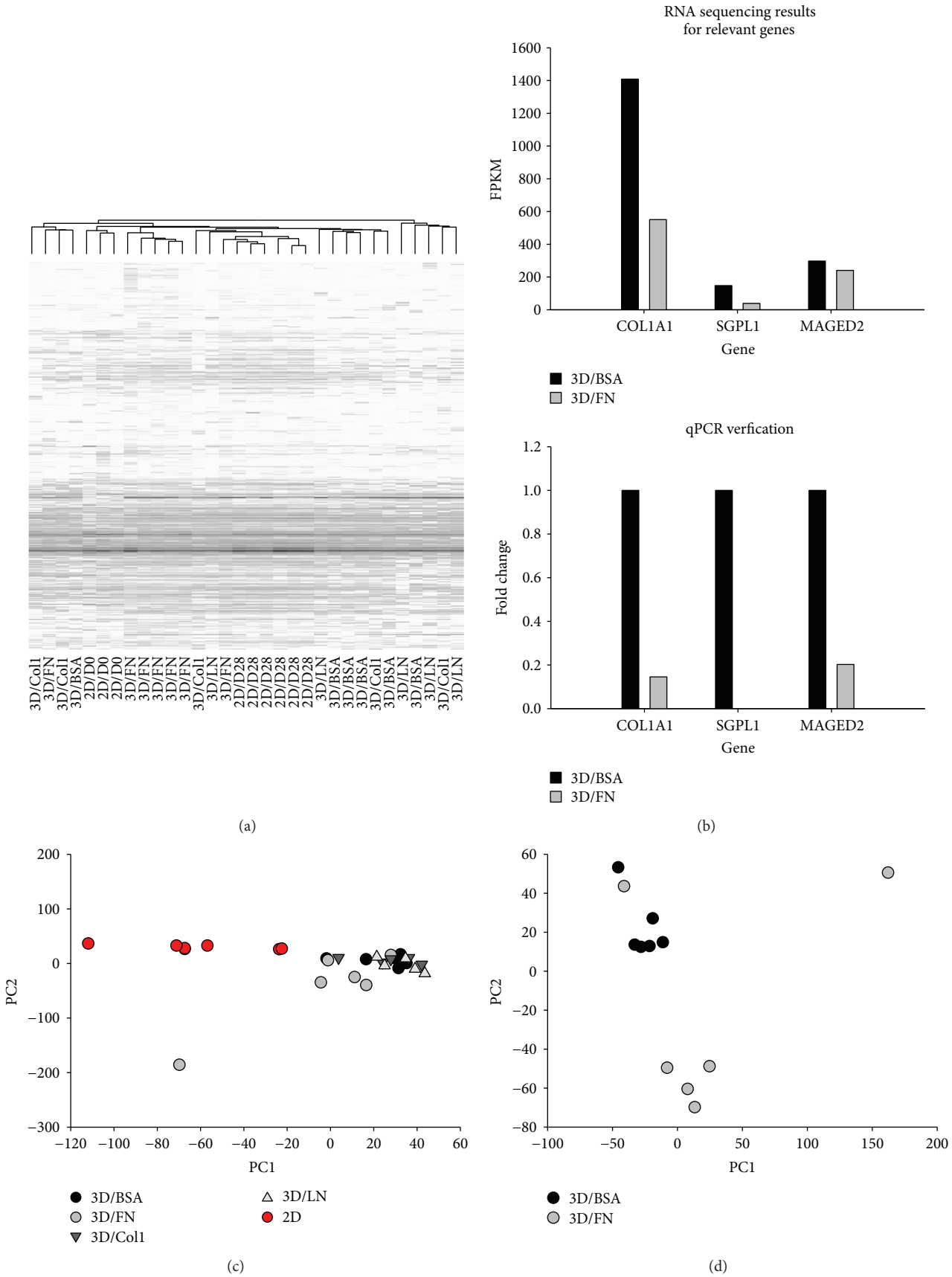

Figure 2: Continued.

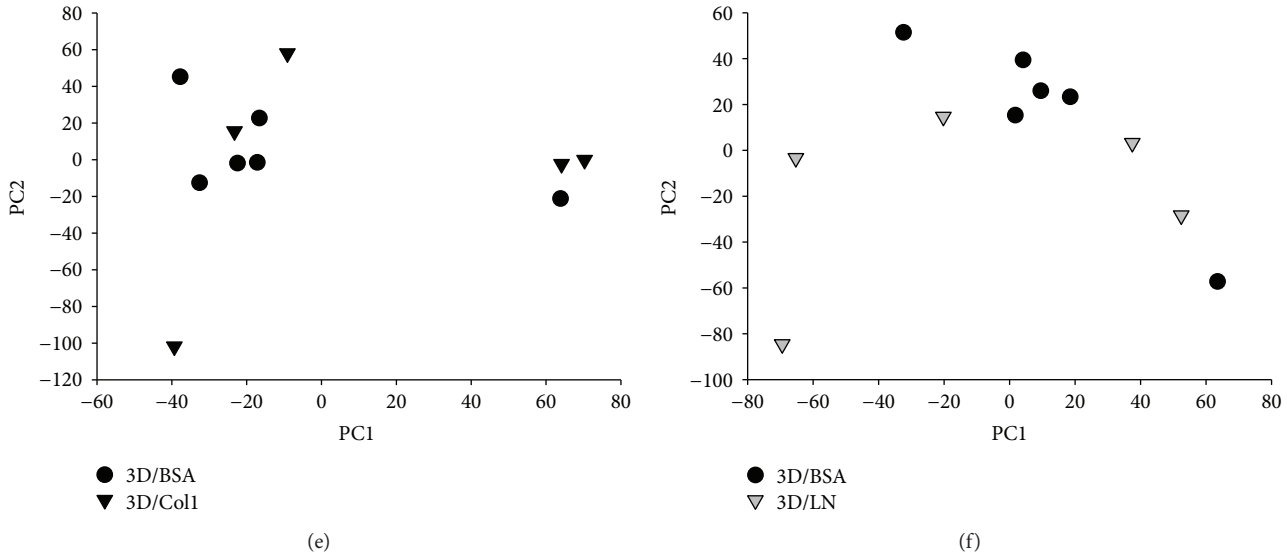

Figure 2: RNA sequencing analysis of hMSCs in 3D bioprinted prisms at 0 and 28 days. (a) Hierarchical clustering of all genes with FPKM > 1 for 3D bioprinted prisms containing either BSA alone (3D/BSA), 3D/FN, 3D/Col1, or 3D/LN at day 28 and associated 2D control cultures at day 28. (b) qPCR validation of gene expression of a subset of genes. These genes were selected as they represent families of ECM proteins and differentiation markers associated with hMSC progeny. (c) PCA analysis of all genes with FPKM > 1. (d–f) Comparison of individual 3D bioprinted prisms containing ECM to bioprinted prisms with BSA only.

revealed that 3D/Col1 structures did not vary from BSA, suggesting that provision of exogenous, full-length collagen type I did not augment or change hMSC transcript expression relative to the 3D albumin base. RNA sequencing data was verified using quantitative PCR, and indeed, the trend in the FPKM levels of COL1A1 (alpha 1 chain of type I collagen), SGPL1 (sphingosine-1-phosphate lyase 1), and MAGED2 (MAGE family member D2) genes matched quantitative PCR results (Figure 2(b)). Thus, gene expression profiles of hMSCs between 2D standard culture and 3D structures vary substantially, with significant but more subtle differences emerging between 3D structures fabricated from distinct ECM protein types.

3.3. Protein Degradation, Differentiation, and Development Pathways Altered in Association with Specific ECM Proteins. Gene ontology (GO) analysis was performed on differentially expressed genes to identify pathways significantly altered by 3D culture and varied exogenous ECM of 3D prisms. The two pathways most significantly altered by 3D culture were (1) protein degradation and (2) development and differentiation (Supplementary Table 2). These processes even exceeded proliferation, migration, and cytoskeletal activation, indicating that the environment generated at this time point (28 days) was conducive to matrix remodeling and cell specification. We therefore began by exploring the effect that the cells exerted to remodel the 3D bioprinted environments.

3.4. Quantification of Matrix Remodeling. In order to understand how hMSCs remodel their external environment, we initially examined the physical modifications that the cells exerted on the 3D bioprinted prisms. hMSCs were introduced to 3D/BSA, 3D/FN, 3D/Col1, and 3D/LN prisms and cultured for two weeks. Physical modifications to the prisms were tracked by examining changes in structure for the duration of the experiment. Representative phase contrast microscope images for the four different prisms at days 1, 7, and 14 are shown in Figure 3(a), and the quantitative temporal evolution is shown in Figures 3(b) and 3(c). hMSCs associated with BSA prisms migrated into and around the entire structure without large modifications to the structure during the first week. The second week of culture resulted in reduced matrix size to varying degrees (loss of 10–80%). The cells of the BSA/FN prisms rapidly modified the structure, which continued to decrease in size during the 2-week duration. Cells of the BSA/Col1 prisms did not greatly alter the structure dimensions in the first week. However, the cells rapidly degraded the prisms during the second week resulting in complete destruction of the structures. BSA/LN structures retained the original features in the first week but were reduced in size by the hMSCs during the second week. The final size of the structures relative to the initial condition is shown in Figures 3(b) and 3(c). Overall, hMSCs physically manipulated the structures with varying kinetic, and to different degrees, the order is from highest to lowest in terms of final size: 3D/Col1 < 3D/FN < 3D/BSA < 3D/LN.

3.5. Kinetics of Integrin, Matrix Metalloproteinase, and Extracellular Matrix Expression in Bioprinted Prisms. The varying kinetics and degree of modification to the prisms may reflect the initial state of the hMSCs, particularly the expression of integrin family members. Integrins are potent ECM adhesion and contraction molecules where each family member harbors specificity for particular ECM proteins. Thus, we examined the initial expression level of the common α and β subunits by hMSCs via the RNAseq data (Figure 3(d)). We found that MSCs expressed the integrin α

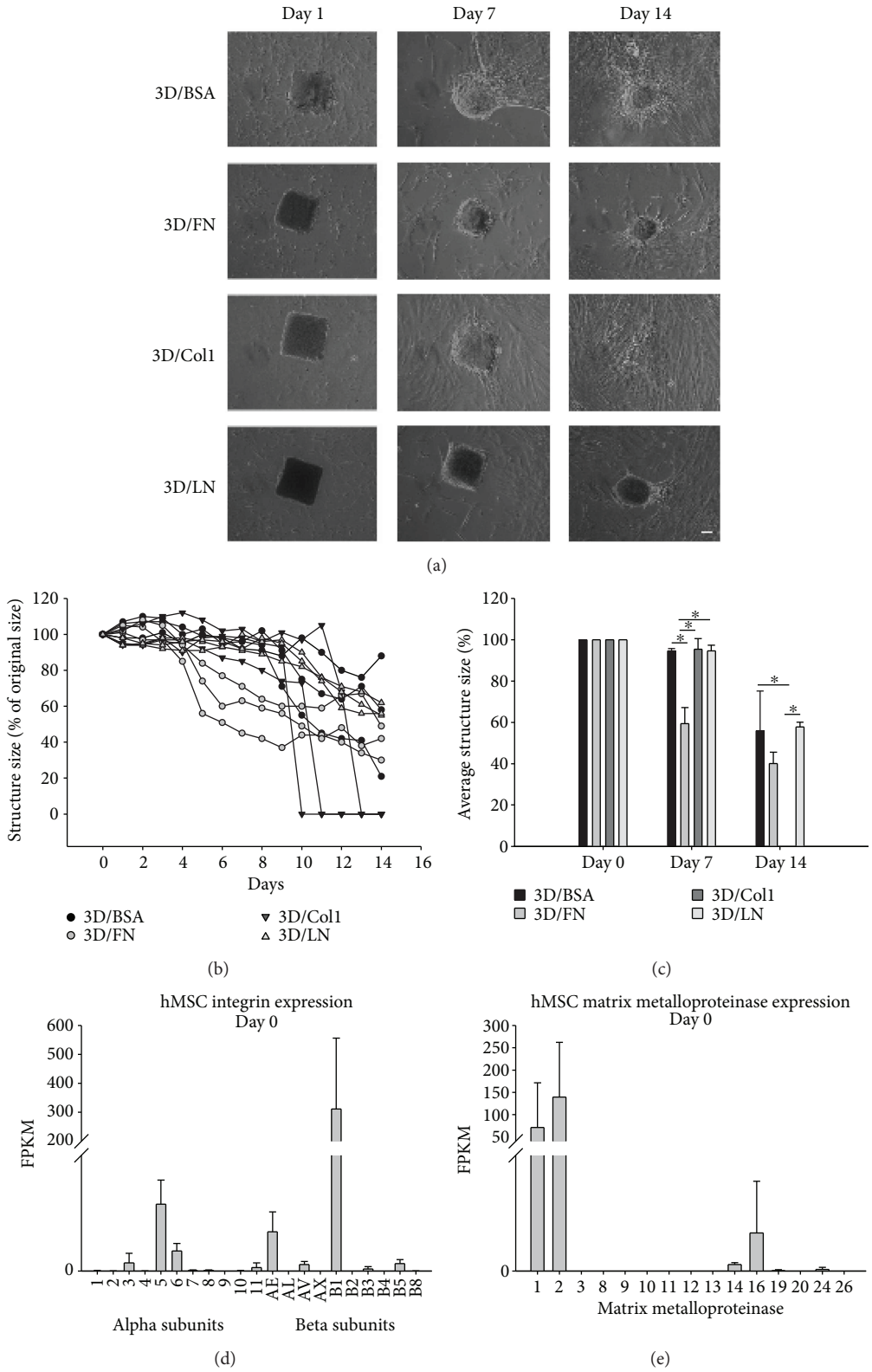

Figure 3: Physical modification of three-dimensional structures composed of 3D/BSA, 3D/FN, 3D/Col1, and 3D/LN by hMSCs. (a) Representative phase contrast images of 3D/BSA, 3D/FN, 3D/Col1, and 3D/LN structures on day 1, 7, and 14. Scale bar = 50 μm. (b) Line graph showing changes in 3D/BSA, 3D/FN, 3D/Col1, and 3D/LN structure size over a two-week period. (c) Bar graph showing the average structure size after 14 days in culture. Error bars depict SD associated with $n = 2$ experimental replicates with at least 3 different prisms analyzed per experimental replicate. $^*P < 0.05$. (d, e) Expression levels of integrins and matrix metalloproteinases in day 0 hMSC population. (d) Bar graph showing the expression of α3, α5, α6, α11, αE, αV, β1, β3, and β5 integrin subunits in day 0 cells. (e) Bar graph showing the expression of MMP1, 2, 14, 16, 19, and 24 in day 0 hMSCs.

and β subunits associated with fibronectin (α5, αV, and β1), laminin (α3, α6, and β1), and collagen type I (α11, β1) [26, 27]. However, these integrin subunits were detected at different levels and can be ranked from highest to lowest according to ECM affinity as follows: FN > LN > collagen type I (Figure 3(d)). This level of expression complements the kinetics of remodeling such that those prisms with high levels of integrins with binding capacity (3D/FN) were restructured more quickly than those with lower levels of integrins with binding capacity. This could also account for the mild and sporadic degradation of the 3D/BSA prisms, which lack a direct interface to the powerful actin cytoskeleton afforded by integrin engagement.

The integrins typically associated with Col1 binding ($\alpha1\beta1$ and $\alpha2\beta1$) were not well expressed by the hMSCs, which may account for the lag in remodeling kinetics. However, the 3D/Col1 structures are completely degraded at 2 weeks. Therefore, we examined the initial expression of matrix metalloproteinases (MMPs), enzymes that degrade specific ECM proteins dependent on the MMP family member. We observed highest expression of MMP1 and MMP2, which are both capable of collagen type I degradation (Figure 3(e)). Thus, the initial expression of these specific MMPs may have allowed MSCs to slowly but substantially degrade the 3D/Col1 structures. Notably, MMP1 does not significantly degrade FN [28] or LN [29], while MMP2 can degrade FN, but not LN. Of the other four MMPs expressed at moderate levels in hMSCs at day 0 (MMP14, MMP16, MMP19, and MMP24), only MMP14 can degrade collagen type I, FN, and LN [30–32]. Taken together, the speed with which ECM prisms were remodeled reflects initial integrin expression, while the extent of degradation is likely tied more closely with MMP expression.

Since complete degradation of prisms appeared to accelerate in the second week for all prisms except 3D/FN, we examined changes in MSC genes associated with matrix remodeling, including endogenous ECM (Table 1), integrins (Table 2), and MMPs (Table 3), *after 28* days with a focus on those genes significantly altered between prism type. Interestingly, we note that expression levels of most integrins were not significantly altered between most 3D conditions and relative to 2D controls (Table 2, Figure 3(d)). We next examined differential expression of MMPs between 3D bioprinted prisms at day 28 (Table 3). MMP16 was upregulated in 3D/Col1 bioprinted prisms. MMP16 is a membrane-type metalloproteinase shown to cleave and thereby activate MMP2, which is known to cleave collagens. In addition, MMP13 was upregulated in 3D/Col1 and is known to degrade type I collagen, though with a preference for type II collagen. Augmented expression of MMP13 and MMP16, together with sustained expression of MMP1 and MMP2, supports the rapid and complete degradation of 3D/Col1 prisms in week 2. The incomplete degradation of 3D/FN and 3D/LN structures may reflect the low or lack of expression of MMPs specific for these ECM proteins, namely, MMP7, MMP10, MMP11, MMP14, and MMP15 for LN and MMP7, MMP10, MMP11, MMP12, MMP14, and MMP15 for FN. In addition, cells cultured in 3D/LN exhibited high levels of tissue inhibitor of metalloproteinases (TIMP) 3.

Ignored in the analyses thus far are newly deposited ECM proteins that likely to also contribute to remodeling kinetics of ECM prisms. Table 1 shows most dramatic changes in transcript expression of fibronectin, syndecan4, versican, and tenascin C between ECM prism types. Of course, transcript expression is not necessarily indicative of deposition and this snapshot is sure to miss ECM that may have been deposited at intermediate time points. However, differential expression of ECM between prisms further supports the premise that exposure to different ECM proteins at early time points results in the specific evolution of microenvironments supportive of distinct behaviors.

3.6. Development and Differentiation Behaviors Prevalent in Evolving ECM Environments. Development and differentiation pathways were also prevalent in cells of 3D prisms, even exceeding proliferation, migration, and cytoskeletal activation, indicating that the environment generated at this time point (28 days) was conducive to cell specification. Upon closer examination of the development and differentiation pathways, we noted that a larger number of developmental pathways compared to differentiation pathways were significantly affected. Interestingly, many of these developmental pathways are not typically associated with MSCs, such as lung and gland development. In addition, the developmental or differentiation pathways triggered were ECM specific in some cases (Figures 4(a) and 4(b)). In particular, skeletal development was associated with 3D/BSA and 3D/LN structures; muscle development and gland development were altered by 3D/LN structures; neural development was linked with 3D/Col1 structures; lung development and overall differentiation pathways were associated with 3D/LN and 3D/Col1 structures. Vasculature development was connected to all ECM-based prisms with 3D/FN structures well-surpassing the others. Interestingly, 3D/FN was only associated with vasculature development, indicating the utility of this ECM protein in 3D tissue engineering efforts that seek to include a functioning vasculature.

3.7. Vasculature and Blood Vessel Development in 3D/FN Structures. We further probed vascular development in the 3D/FN structures given the need in the tissue engineering field to generate functioning and integrated vascular networks for thick tissues. In particular, we inspected the expression of key endothelial and smooth muscle cell markers, as these cells are important in the development of a functioning vasculature network. hMSCs cultured in 3D/FN structures for 28 days expressed both endothelial cell (MCAM, VCAM) and smooth muscle cell markers (ACTA2, TAGLN) indicating that exogenous, full-length fibronectin protein presented in 3D can trigger differentiation of hMSCs into these two cell types (Figures 4(c) and 4(d)). We also probed for spingosine-1-phosphate (S1P), a sphingolipid that has been shown to play a role in vasculature development and is irreversibly degraded by SGPL1 [33–35]. We noted a significant reduction in sphingosine phosphate lyase (SGPL1) in cells cultured in 3D/FN structures specifically (Figure 4(e)). Thus, while functional maturation of vascular cell types in 3D/FN

Table 1: Expression levels of ECM proteins in hMSCs cultured for 28 days in 2D standard and 3D ECM-based structure conditions.

Gene	Average FPKM					Significance
	2D/D28	3D/BSA	3D/FN	3D/Col1	3D/LN	
COL1A1	1694.69	**1408.85**	**550.58**	*1796.03*	**656.82**	
COL1A2	1437.28	**967.59**	**596.87**	**1363.82**	**1391.45**	
COL3A1	331.77	*582.23*	*363.92*	*549.25*	*694.15*	
COL4A1	39.19	**16.04**	**16.18**	**27.23**	**3.37**	
COL4A5	3.16	*8.90*	*8.37*	*10.34*	0.00	
COL5A1	34.22	**27.83**	**21.03**	**20.68**	**15.59**	
COL5A2	30.84	*42.84*	**29.80**	*55.98*	**28.19**	
COL6A1	22.61	*68.66*	*72.65*	*61.24*	*47.19*	
COL6A3	102.42	*196.03*	*139.69*	*173.26*	*177.62*	
COL8A1	24.32	*52.07*	*61.73*	*76.64*	*100.51*	
COL8A2	7.88	*12.63*	**5.02**	*8.64*	**2.20**	
COL10A1	5.34	*6.97*	**4.53**	*9.20*	*11.18*	
COL11A1	10.60	*58.77*	*16.37*	*59.43*	*39.83*	
COL12A1	3.44	*13.00*	*8.38*	*11.41*	*10.26*	
COL14A1	0.53	*4.33*	*10.65*	*7.61*	*6.84*	
FN1	2206.39	*3823.51*	**2129.52**	*4017.30*	*5628.25*	d, h
LAMA4	15.13	*36.67*	*30.44*	*30.82*	*46.42*	
LAMB1	67.78	*107.45*	**65.75**	111.18	**67.06**	
LAMB2	11.67	**4.08**	**7.36**	**8.31**	*14.50*	
LAMC1	28.32	*65.12*	*31.50*	*61.57*	*39.43*	
LAMC2	7.05	*11.45*	*9.53*	*15.77*	**0.33**	
CD44	96.64	*120.43*	*132.88*	*179.45*	*168.33*	
ELN	16.18	**2.01**	0.97	**1.65**	0.15	
FBN1	30.03	*84.49*	*54.72*	*85.81*	*86.47*	
FBLN1	80.54	*170.48*	*126.57*	*131.39*	*215.67*	
FBLN5	95.26	*118.34*	**52.77**	**75.25**	**77.58**	
SDC2	16.83	**14.14**	**13.80**	**12.82**	**12.50**	
SDC4	18.49	**2.18**	**11.96**	**8.78**	**5.02**	a, c, d, f
TNC	38.44	*179.79*	*83.47*	*168.76*	*465.74*	d, h
THBS1	299.96	*696.28*	**239.23**	*538.79*	*819.96*	
THBS2	45.80	*68.03*	*61.96*	*97.85*	*94.65*	
THBS3	33.11	**19.98**	**10.57**	**17.22**	**23.76**	
VCAN	98.11	*279.02*	*188.23*	*237.38*	*334.81*	a, c, d, h
HAS2	234.75	*307.97*	**100.67**	*401.46*	*505.58*	

Bold: reduction in expression, compared to 2D standard. Italic: increase in expression, compared to 2D standard. Underlined: FPKM < 1. a: 2D versus BSA; b: 2D versus 3D/FN; c: 2D versus 3D/Col1; d: 2D versus 3D/LN; e: BSA versus 3D/I; f: BSA versus 3D/LN; g: 3D/FN versus 3D/Col1; h: 3D/FN versus 3D/LN.

remains to be seen, initiation of these differentiation pathways is strongly supported.

4. Discussion

In this work, we examined the global influence on transcription of full-length type I collagen, fibronectin, and laminin-111 individually on hMSC behavior after 28 days of 3D culture. Predominant outcomes reflected changes in protein degradation, differentiation, and development pathways. Interestingly, we observed no statistical difference in the differentiation of MSCs towards the adipogenic and chondrogenic lineages; however, alternate developmental pathways including lung, neural, vascular, and muscle development were activated and such activation was related to the original composition of the 3D ECM-based microenvironment. The ECM composition of the microenvironments changed substantially during the four-week-study duration supporting the notion that evolving ECM may provide temporal cues required for differentiation to multiple different lineages.

Among the most striking differentiation outcomes was vascular differentiation associated with fibronectin. The differentiation of stem cells into endothelial cells in connection with fibronectin has previously been demonstrated [36]. In particular, studies by Battista et al. examined the differentiation of mESCs in the presence of LN or FN in a collagen I

Table 2: Expression levels of integrins in hMSCs cultured for 28 days in 2D standard and 3D ECM-based structure conditions.

Gene	Average FPKM					Significance
	2D/D28	3D/BSA	3D/FN	3D/Col1	3D/LN	
ITGA1	1.28	*5.34*	*2.93*	*5.12*	*7.34*	
ITGA2	2.18	*9.54*	*4.37*	*4.18*	*11.33*	
ITGA3	1.40	0.55	0.31	0.72	0.39	
ITGA4	0.68	*15.22*	*3.15*	*2.55*	**0.63**	a
ITGA5	62.99	**36.35**	**24.16**	**25.63**	**55.23**	
ITGAE	19.68	**16.17**	**17.53**	**11.81**	**16.99**	
ITGAV	3.89	*17.92*	*13.74*	*33.58*	*18.13*	c, g
ITGA6	0.60	*2.49*	*7.93*	*3.76*	0.96	
ITGA7	0.15	*2.82*	0.23	0.18	**0.00**	
ITGA8	1.81	0.00	0.38	**1.74**	**1.79**	
ITGA10	3.98	*20.99*	*19.55*	*27.72*	*50.63*	d
ITGA11	33.87	**25.68**	**18.59**	*46.22*	*50.06*	
ITGB1	280.32	*547.67*	*456.69*	*572.81*	*551.84*	
ITGB2	0.16	0.00	0.59	*6.30*	0.00	
ITGB4	0.00	0.00	0.50	*2.84*	0.00	
ITGB5	37.11	**27.88**	**25.67**	**29.49**	**22.85**	
ITGB8	0.68	12.44	4.52	11.86	6.27	

Bold: reduction in expression, compared to 2D standard. Italic: increase in expression, compared to 2D standard. Underlined: FPKM < 1. a: 2D versus BSA; b: 2D versus 3D/FN; c: 2D versus 3D/Col1; d: 2D versus 3D/LN; e: BSA versus 3D/I; f: BSA versus 3D/LN; g: 3D/FN versus 3D/Col1; h: 3D/FN versus 3D/LN.

Table 3: Expression levels of MMPS, ADAMS, and TIMPs in hMSCs cultured for 28 days in 2D standard and 3D ECM-based structure conditions.

Gene	Average FPKM					Significance
	2D/D28	3D/BSA	3D/FN	3D/Col1	3D/LN	
MMP1	48.12	*822.48*	*283.69*	*640.14*	*1395.91*	d
MMP2	689.96	**598.60**	**601.51**	*830.16*	*1332.27*	
MMP3	8.08	*10.23*	**3.77**	**8.00**	*19.02*	
MMP8	0.00	*10.62*	0.26	0.00	*7.48*	
MMP11	5.08	**1.71**	**1.71**	0.00	0.00	
MMP13	9.76	*40.09*	*111.21*	*76.32*	*224.58*	d, f
MMP14	2.43	*3.87*	**1.02**	**1.41**	0.81	
MMP16	3.62	*4.69*	*4.40*	*26.89*	*6.98*	c, e, g
MMP19	14.86	**12.39**	**7.18**	*29.18*	**10.34**	
MMP24	1.65	0.45	0.37	**1.34**	0.17	
ADAM1	0.00	0.00	0.27	0.31	2.18	
ADAM9	29.28	*39.54*	*40.17*	*30.69*	*42.11*	
ADAM10	9.86	*15.55*	*15.02*	*22.07*	*49.41*	d, f, h
ADAM12	20.52	*67.73*	*26.70*	*46.95*	*49.82*	a, b
ADAM15	0.19	0.00	0.25	*2.97*	*1.08*	
ADAM17	7.86	*15.32*	*14.24*	*12.09*	*14.60*	
ADAM19	31.25	**6.38**	**3.71**	**6.91**	**4.20**	a, b, c, d
ADAM21	0.00	*1.72*	0.02	0.00	0.00	
ADAM23	2.55	0.39	0.18	**1.20**	*2.91*	
ADAM33	0.26	0.00	*2.07*	0.94	0.00	
TIMP1	18055.04	**2719.30**	**5834.20**	**2490.98**	**3835.62**	a, c, d
TIMP2	68.19	*160.04*	*127.25*	*143.54*	*154.66*	
TIMP3	1321.25	*2670.46*	**879.00**	*2115.14*	*3145.51*	h

Bold: reduction in expression, compared to 2D standard. Italic: increase in expression, compared to 2D standard. Underlined: FPKM < 1. a: 2D versus BSA; b: 2D versus 3D/FN; c: 2D versus 3D/Col1; d; 2D versus 3D/LN; e: BSA versus 3D/I; f: BSA versus 3D/LN; g: D/FN versus 3D/Col1; h: 3D/FN versus 3D/LN.

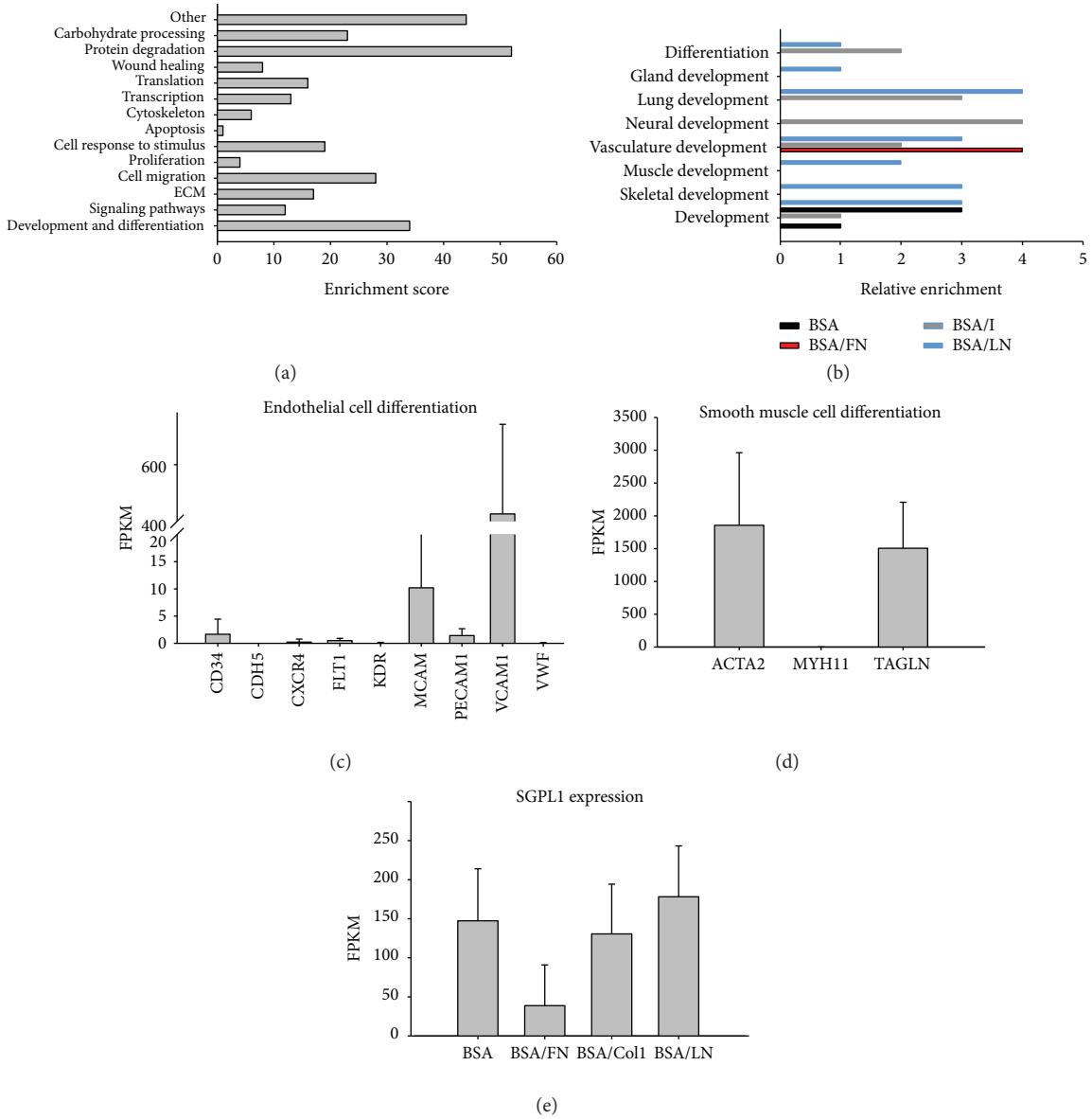

Figure 4: GO analysis of hMSCs in 3D bioprinted prisms, especially related to the differentiation state. (a) Counts of GO terms associated with commonly examined stem cell responses. Protein degradation, development, and differentiation are the most significantly expressed pathways. (b) Development and differentiation pathways separated by 3D ECM structures. Most influential 3D structures rank from 3D/LN > 3D/Col1 > 3D/BSA > 3D/FN, with 3D/FN structures predominantly influencing vasculature development. Expression of endothelial cell markers (c), smooth muscle cell markers (d), and sphingosine phosphate lyase (e) in hMSCs cultured in 3D/FN structures. Error bars depict SD associated with $n = 3$ experimental replicates with at least 2 different prisms analyzed per experimental replicate. hMSCs cultured in 3D/FN structures expressed markers for both endothelial and smooth muscle cells and had a reduction in SGPL1 expression.

hydrogel and observed that fibronectin stimulated EC differentiation and vascularization while LN stimulated cardiomyogenic differentiation [37]. Additionally, studies like those by Clark et al. indicated a close association between fibronectin and endothelial cell activity [38]. But this is the first study to show that the dominant response of MSCs to fibronectin exposure is vascular differentiation and it is one of the most potent ECM-stimulated responses that we observed in the context of our 3D model system. It should be noted that our 3D model system includes a crosslinking regime that could hide critical cell binding or soluble factor sequestration sites and thereby complicate comparison to native tissue or other 3D model systems that do not include exogenous crosslinking of this type. Even so, these studies suggest inclusion of full-length fibronectin in engineered tissue, especially that thick tissues with a vascular requirement may be advantageous.

As evidence builds supporting the notion that the extracellular matrix is a potent signaling molecule, it is now time to address what happens following integrin engagement and before transcription of proteins associated with a maturing cell type. The design of this study was not crafted to be able to address this question effectively since we can only access beginning and end events in the kinetics of pathway

activation with ECM-guided differentiation. Future studies might benefit from an altered design wherein signaling dynamics could be captured. There are a few recent publications that begin to probe these dynamics. For example, peptide activation of $\alpha5\beta1$ can drive osteogenic differentiation of mesenchymal stem cells via the Wnt/β-catenin pathway activated via PI3K/Akt signaling [39]. In addition, engagement of fibroblast-derived ECM via $\beta1$, $\alpha2$, and $\alpha3$ integrins in human embryonic stem cells has been shown to activate the Wnt/β-catenin pathway via the MEK-ERK pathway, which drives endoderm differentiation [40]. Finally, we have preliminary evidence to suggest that activation of integrin-linked kinase (ILK) of focal adhesions couples β-catenin activation via GSK3β to enable cardiomyocyte differentiation. Missing in these studies is consideration of the multistep process inherent in any differentiation outcome. Thus, while provision of exogenous ECM might provide a potent "signal 1," the source of subsequent signals is unknown and could arise from stimulation of endogenous ECM, degradation of ECM, soluble factor synthesis, or soluble factor sequestration. Discerning the source of signals 2, 3, and so on for ECM-guided differentiation and manipulation of associated intracellular signaling pathways like those described above will be useful in the context of ECM-based *in vitro* platforms for drug screening, toxicity testing, and disease modeling and will *be critical* for stem cell-based therapeutic strategies where ECM exposure is inevitable.

Abbreviations

ECM: Extracellular matrix
hMSC: Human mesenchymal stem cells
PEG: Polyethylene glycol
FN: Fibronectin
COLI: Type I collagen
LN: Laminin-111
FPKM: Fragments per kilobase pair per million mapped reads
COL1A1: Alpha 1 chain of type I collagen
SGPL1: Sphingosine-1-phosphate lyase 1
MAGED2: MAGE family member D2
GO: Gene ontology
MMP: Matrix metalloproteinase
VCAM: Vascular cell adhesion molecule
MCAM: Melanoma cell adhesion molecule
ACTA2: Smooth muscle aortic alpha-actin
TAGLN: Transgelin
mESC: Mouse embryonic stem cell
MEK: Mitogen-activated protein kinase kinase
ERK: Extracellular signal-regulated kinase
FPGA: Field-programmable gate array
FIFO: First-in, first-out
PMT: Photomultiplier tube
GUI: Graphical user interface
BSA: Bovine serum albumin
OTDS: Octadecyltrichlorosilane
FLIM: Fluorescence lifetime imaging microscopy
NA: Numerical aperture
SEM: Scanning electron microscopy
SCDE: Single-cell differential expression
DAVID: Database for Annotation, Visualization and Integrated Discovery
ANOVA: Analysis of variance.

Conflicts of Interest

The authors declare that they have no conflicts of interest.

Authors' Contributions

The manuscript was written through contributions of all authors. All authors have given approval to the final version of the manuscript.

Acknowledgments

The authors thank Jerry Daniels, University of Minnesota Genomics Center, for careful processing of RNA samples via RNAseq. The authors acknowledge Alison Berman and Thomas Houghland for the technical assistance. The authors also thank Peiman Hematti, University of Wisconsin-Madison, for providing mesenchymal stem cells. Funding for this work was provided by the NSF Graduate Research Fellowship to Quyen A. Tran. NSF BME Award, 1445650. NIH R01 HL137204. NIH R01 HL131017.

Supplementary Materials

Supplementary 1. Supplemental Table 1: contains raw data related to the tracking of physical structure modification.

Supplementary 2. Supplemental Table 2: contains FPKM data for all transcripts of all samples.

Supplementary 3. Supplemental Table 3: contains differentially expressed genes between sample types.

Supplementary 4. Supplemental Table 4: contains gene ontology analyses.

References

[1] C. Linsley, B. Wu, and B. Tawil, "The effect of fibrinogen, collagen type I, and fibronectin on mesenchymal stem cell growth and differentiation into osteoblasts," *Tissue Engineering. Part A*, vol. 19, no. 11-12, pp. 1416–1423, 2013.

[2] H. Lu, T. Hoshiba, N. Kawazoe, I. Koda, M. Song, and G. Chen, "Cultured cell-derived extracellular matrix scaffolds for tissue engineering," *Biomaterials*, vol. 32, no. 36, pp. 9658–9666, 2011.

[3] E. Cukierman, R. Pankov, and K. M. Yamada, "Cell interactions with three-dimensional matrices," *Current Opinion in Cell Biology*, vol. 14, no. 5, pp. 633–640, 2002.

[4] J. P. Stegemann and R. M. Nerem, "Altered response of vascular smooth muscle cells to exogenous biochemical stimulation in two- and three-dimensional culture," *Experimental Cell Research*, vol. 283, no. 2, pp. 146–155, 2003.

[5] J. P. Jung, A. J. Sprangers, J. R. Byce et al., "ECM-incorporated hydrogels cross-linked via native chemical ligation to engineer stem cell microenvironments," *Biomacromolecules*, vol. 14, no. 9, pp. 3102–3111, 2013.

[6] J. P. Jung, M. K. Bache-Wiig, P. P. Provenzano, and B. M. Ogle, "Heterogeneous differentiation of human mesenchymal stem cells in 3D extracellular matrix composites," *BioResearch Open Access*, vol. 5, no. 1, pp. 37–48, 2016.

[7] S. Becerra-Bayona, V. Guiza-Arguello, X. Qu, D. J. Munoz-Pinto, and M. S. Hahn, "Influence of select extracellular matrix proteins on mesenchymal stem cell osteogenic commitment in three-dimensional contexts," *Acta Biomaterialia*, vol. 8, no. 12, pp. 4397–4404, 2012.

[8] J. P. Jung, D. Hu, I. J. Domian, and B. M. Ogle, "An integrated statistical model for enhanced murine cardiomyocyte differentiation via optimized engagement of 3D extracellular matrices," *Scientific Reports*, vol. 5, no. 1, article 18705, 2016.

[9] S. Astrof, D. Crowley, and R. O. Hynes, "Multiple cardiovascular defects caused by the absence of alternatively spliced segments of fibronectin," *Developmental Biology*, vol. 311, no. 1, pp. 11–24, 2007.

[10] E. L. George, E. N. Georges-Labouesse, R. S. Patel-King, H. Rayburn, and R. O. Hynes, "Defects in mesoderm, neural tube and vascular development in mouse embryos lacking fibronectin," *Development*, vol. 119, no. 4, pp. 1079–1091, 1993.

[11] B. Costa-Silva, M. C. da Costa, F. R. Melo et al., "Fibronectin promotes differentiation of neural crest progenitors endowed with smooth muscle cell potential," *Experimental Cell Research*, vol. 315, no. 6, pp. 955–967, 2009.

[12] C. L. Mummery, J. Zhang, E. S. Ng, D. A. Elliott, A. G. Elefanty, and T. J. Kamp, "Differentiation of human embryonic stem cells and induced pluripotent stem cells to cardiomyocytes: a methods overview," *Circulation Research*, vol. 111, no. 3, pp. 344–358, 2012.

[13] S. Abolpour Mofrad, K. Kuenzel, O. Friedrich, and D. F. Gilbert, "Optimizing neuronal differentiation of human pluripotent NT2 stem cells in monolayer cultures," *Development, Growth & Differentiation*, vol. 58, no. 8, pp. 664–676, 2016.

[14] X. Zhang, M. P. Bendeck, C. A. Simmons, and J. P. Santerre, "Deriving vascular smooth muscle cells from mesenchymal stromal cells: evolving differentiation strategies and current understanding of their mechanisms," *Biomaterials*, vol. 145, pp. 9–22, 2017.

[15] P. Lu, K. Takai, V. M. Weaver, and Z. Werb, "Extracellular matrix degradation and remodeling in development and disease," *Cold Spring Harbor Perspectives in Biology*, vol. 3, no. 12, 2011.

[16] G. E. Davis and D. R. Senger, "Endothelial extracellular matrix: biosynthesis, remodeling, and functions during vascular morphogenesis and neovessel stabilization," *Circulation Research*, vol. 97, no. 11, pp. 1093–1107, 2005.

[17] L. P. Cunningham, M. P. Veilleux, and P. J. Campagnola, "Freeform multiphoton excited microfabrication for biological applications using a rapid prototyping CAD-based approach," *Optics Express*, vol. 14, no. 19, pp. 8613–8621, 2006.

[18] V. Ajeti, C. H. Lien, S. J. Chen et al., "Image-inspired 3D multiphoton excited fabrication of extracellular matrix structures by modulated raster scanning," *Optics Express*, vol. 21, no. 21, pp. 25346–25355, 2013.

[19] P. J. Su, Q. A. Tran, J. J. Fong, K. W. Eliceiri, B. M. Ogle, and P. J. Campagnola, "Mesenchymal stem cell interactions with 3D ECM modules fabricated via multiphoton excited photochemistry," *Biomacromolecules*, vol. 13, no. 9, pp. 2917–2925, 2012.

[20] D. Balasubramanian, X. Du, and J. S. Zigler Jr., "The reaction of singlet oxygen with proteins, with special reference to crystallins," *Photochemistry and Photobiology*, vol. 52, no. 4, pp. 761–768, 1990.

[21] P. Trivedi and P. Hematti, "Simultaneous generation of $CD34^+$ primitive hematopoietic cells and $CD73^+$ mesenchymal stem cells from human embryonic stem cells cocultured with murine OP9 stromal cells," *Experimental Hematology*, vol. 35, no. 1, pp. 146–154, 2007.

[22] P. Trivedi and P. Hematti, "Derivation and immunological characterization of mesenchymal stromal cells from human embryonic stem cells," *Experimental Hematology*, vol. 36, no. 3, pp. 350–359, 2008.

[23] P. V. Kharchenko, L. Silberstein, and D. T. Scadden, "Bayesian approach to single-cell differential expression analysis," *Nature Methods*, vol. 11, no. 7, pp. 740–742, 2014.

[24] B. T. Freeman, J. P. Jung, and B. M. Ogle, "Single-cell RNA-seq reveals activation of unique gene groups as a consequence of stem cell-parenchymal cell fusion," *Scientific Reports*, vol. 6, no. 1, article 23270, 2016.

[25] J. A. Santiago, R. Pogemiller, and B. M. Ogle, "Heterogeneous differentiation of human mesenchymal stem cells in response to extended culture in extracellular matrices," *Tissue Engineering. Part A*, vol. 15, no. 12, pp. 3911–3922, 2009.

[26] C. Zeltz, N. Lu, and D. Gullberg, "Integrin $\alpha 11\beta 1$: a major collagen receptor on fibroblastic cells," *Advances in Experimental Medicine and Biology*, vol. 819, pp. 73–83, 2014.

[27] X. Zhang, J. E. Groopman, and J. F. Wang, "Extracellular matrix regulates endothelial functions through interaction of VEGFR-3 and integrin $\alpha_5\beta_1$," *Journal of Cellular Physiology*, vol. 202, no. 1, pp. 205–214, 2005.

[28] P. A. Torzilli, M. Bhargava, and C. T. Chen, "Mechanical loading of articular cartilage reduces IL-1-induced enzyme expression," *Cartilage*, vol. 2, no. 4, pp. 364–373, 2011.

[29] A. Pardo and M. Selman, "MMP-1: the elder of the family," *The International Journal of Biochemistry & Cell Biology*, vol. 37, no. 2, pp. 283–288, 2005.

[30] H. Birkedal-Hansen, W. G. Moore, M. K. Bodden et al., "Matrix metalloproteinases: a review," *Critical Reviews in Oral Biology & Medicine*, vol. 4, no. 2, pp. 197–250, 1993.

[31] S. Chandler, K. M. Miller, J. M. Clements et al., "Matrix metalloproteinases, tumor necrosis factor and multiple sclerosis: an overview," *Journal of Neuroimmunology*, vol. 72, no. 2, pp. 155–161, 1997.

[32] V. M. Kahari and U. Saarialho-Kere, "Matrix metalloproteinases in skin," *Experimental Dermatology*, vol. 6, no. 5, pp. 199–213, 1997.

[33] B. Y. Binder, P. A. Williams, E. A. Silva, and J. K. Leach, "Lysophosphatidic acid and sphingosine-1-phosphate: a concise review of biological function and applications for tissue engineering," *Tissue Engineering. Part B, Reviews*, vol. 21, no. 6, pp. 531–542, 2015.

[34] A. Skoura, T. Sanchez, K. Claffey, S. M. Mandala, R. L. Proia, and T. Hla, "Essential role of sphingosine 1-phosphate receptor 2 in pathological angiogenesis of the mouse retina," *The Journal of Clinical Investigation*, vol. 117, no. 9, pp. 2506–2516, 2007.

[35] M. Kono, Y. Mi, Y. Liu et al., "The sphingosine-1-phosphate receptors $S1P_1$, $S1P_2$, and $S1P_3$ function coordinately during embryonic angiogenesis," *The Journal of Biological Chemistry*, vol. 279, no. 28, pp. 29367–29373, 2004.

[36] E. S. Wijelath, S. Rahman, J. Murray, Y. Patel, G. Savidge, and M. Sobel, "Fibronectin promotes VEGF-induced CD34$^+$ cell differentiation into endothelial cells," *Journal of Vascular Surgery*, vol. 39, no. 3, pp. 655–660, 2004.

[37] S. Battista, D. Guarnieri, C. Borselli et al., "The effect of matrix composition of 3D constructs on embryonic stem cell differentiation," *Biomaterials*, vol. 26, no. 31, pp. 6194–6207, 2005.

[38] R. A. Clark, P. DellaPelle, E. Manseau, J. M. Lanigan, H. F. Dvorak, and R. B. Colvin, "Blood vessel fibronectin increases in conjunction with endothelial cell proliferation and capillary ingrowth during wound healing," *The Journal of Investigative Dermatology*, vol. 79, no. 5, pp. 269–276, 1982.

[39] Z. Saidak, C. Le Henaff, S. Azzi et al., "Wnt/β-catenin signaling mediates osteoblast differentiation triggered by peptide-induced $\alpha5\beta1$ integrin priming in mesenchymal skeletal cells," *The Journal of Biological Chemistry*, vol. 290, no. 11, pp. 6903–6912, 2015.

[40] K. Dzobo, M. Vogelsang, and M. I. Parker, "Wnt/β-catenin and MEK-ERK signaling are required for fibroblast-derived extracellular matrix-mediated endoderm differentiation of embryonic stem cells," *Stem Cell Reviews and Reports*, vol. 11, no. 5, pp. 761–773, 2015.

Hindawi
Stem Cells International
Volume 2017, Article ID 9843120, 10 pages
https://doi.org/10.1155/2017/9843120

Research Article

Mesenchymal Stem Cells Protect Nucleus Pulposus Cells from Compression-Induced Apoptosis by Inhibiting the Mitochondrial Pathway

Sheng Chen, Lei Zhao, Xiangyu Deng, Deyao Shi, Fashuai Wu, Hang Liang, Donghua Huang, and Zengwu Shao

Department of Orthopaedic Surgery, Union Hospital, Tongji Medical College, Huazhong University of Science and Technology, Wuhan 430022, China

Correspondence should be addressed to Zengwu Shao; szwpro@163.com

Received 25 July 2017; Revised 21 October 2017; Accepted 9 November 2017; Published 14 December 2017

Academic Editor: Farid Menaa

Objective. Excessive apoptosis of nucleus pulposus cells (NPCs) induced by various stresses, including compression, contributes to the development of intervertebral disc degeneration (IVDD). Mesenchymal stem cells (MSCs) can benefit the regeneration of NPCs and delay IVDD, but the underlying molecular mechanism is poorly understood. This study aimed to evaluate the antiapoptosis effects of bone marrow-derived MSC (BMSC) on rat NPCs exposed to compression and investigate whether the mitochondrial pathway was involved. *Methods*. BMSCs and NPCs were cocultured in the compression apparatus at 1.0 MPa for 36 h. Cell viability, apoptosis, mitochondrial function, and the expression of apoptosis-related proteins were evaluated. *Results*. The results showed that coculturing with BMSCs increased the cell viability and reduced apoptosis of NPCs exposed to compression. Meanwhile, BMSCs could relieve the compression-induced mitochondrial damage of NPCs by decreasing reactive oxygen species level and maintaining mitochondrial membrane potential as well as mitochondrial integrity. Furthermore, coculturing with BMSCs suppressed the activated caspase-3 and activated caspase-9, decreased the expressions of cytosolic cytochrome *c* and Bax, and increased the expression of Bcl-2. *Conclusions*. Our results suggest that BMSCs can protect against compression-induced apoptosis of NPCs by inhibiting the mitochondrial pathway and thus enhance our understanding on the MSC-based therapy for IVDD.

1. Introduction

Intervertebral disc degeneration (IVDD) is the main cause of low back pain (LBP) with high prevalence, which leads to disability and creates heavy financial burden globally [1–3]. The intervertebral disc (IVD) is composed of three parts: nucleus pulposus (NP), annulus fibrous (AF), and cartilaginous endplates. The centrally situated NP consists of NP cells (NPCs) and extracellular matrix (ECM), and the outer AF is mainly made of collagen fibers. Evidences show that the IVD progressively degenerates with the number of NPC loss, ECM reduction, and type I collagen synthesis increase [4]. And recently, many studies in vitro and in vivo have indicated that excessive apoptosis of NPCs induced by various stresses, including compression, hypoxia or reactive oxygen species (ROS), plays an essential role in the progression of IVDD [5–7].

The IVD functions as a shock absorber, and external forces on the spine lead to intense stresses that act on the IVD. From a mechanical point of view, disc cells embedded in the different areas are exposed to wide ranges of mechanical loads [8, 9]. Inappropriate or excessive compressive force stimulus applied to intervertebral discs (IVDs) is an important contributing factor in causing disc degeneration. Previous studies have suggested that excessive loading affects the synthesis of ECM and promotes the secretion of inflammatory factors in NPCs [10, 11]. We have reported that apoptosis could be induced by compression at a magnitude of 1 MPa via mitochondrial or intrinsic pathways in rabbit NPCs previously [12]. However, there are few researches to study

how to reverse the apoptosis of NPCs induced by compression and thus the repair of IVDD.

Mesenchymal stem cells (MSCs), especially bone marrow-derived MSC- (BMSC-) based therapies, have been commonly used in IVDD repair and have shown exciting perspectives [13, 14]. A great number of studies have discussed the interaction between MSCs and NPCs under different conditions. It was reported that coculture of MSCs and NPCs facilitated MSC differentiation towards the NP cell phenotype [15, 16] and promoted the synthesis of ECM in degenerated NPCs [15, 17]. However, limited studies demonstrated the antiapoptosis effect of MSCs on NPCs and the specific mechanisms under compression condition. Therefore, this study aimed to evaluate the antiapoptosis effect of BMSCs on rat NPCs under compression and investigate whether the mitochondrial pathway was involved.

2. Methods

2.1. BMSCs and NPCs Culture. The experimental procedures were approved by the Institutional Animal Care and Use Committee of Tongji Medical College of Huazhong University of Science and Technology. The NPCs were isolated from Sprague-Dawley rats (male, 3 months and 250–300 g) as described previously [18]. The obtained cells were suspended and cultured in Dulbecco's Modified Eagle's Medium/Ham's F-12 (DMEM/F-12, Gibco, USA) containing 10% fetal bovine serum (FBS, Gibco, USA) supplemented with 1% penicillin-streptomycin (Sigma) at 37°C with 5% CO_2. The media were changed every two days, and the primary culture was 1 : 2 subcultured when cells reached confluence over 80%. The second generation NP cells were used in this study.

We used the same rats to isolate and obtain bone marrow MSCs simultaneously, as previously described [19]. The MSCs were maintained in DMEM/F-12 (Gibco, USA) containing 10% FBS (Gibco, USA) supplemented with 1% penicillin-streptomycin (Sigma) at 37°C with 5% CO_2. NPCs and BMSCs were from the same source at each coculture system.

2.2. Indirect Cocultures and Application of a Compression Apparatus. The indirect cocultures were conducted in 6-well plates with 0.4 μm pore-size transwell inserts. Passage 2 NPCs and passage 3 BMSCs were used. BMSCs were seeded into transwell inserts, whereas NPCs were plated into the lower chamber. Cells were seeded at ratios of 50 : 50 (10×10^4 per well). Cocultured cells were maintained in 10% DMEM/F-12 at 37°C with 5% CO_2.

To determine the antiapoptosis effect of BMSCs on NPCs exposed to static compression, cocultured cells were cultured in a custom-made compression apparatus as previously described [12, 18]. The coculture system was subjected to 1 MPa compression load (CL) for 36 h. The groups of the experiment were as follows: (i) NPC alone as control; (ii) NPC + BMSC; (iii) NPC + BMSC + CL; and (iv) NPC + CL.

2.3. Cell Viability Measurement. Cell viability was measured by CCK-8 (Dojindo, Japan) with modifications. CCK-8 working solution was made by mixing CCK-8 solution and 10% DMEM/F-12 medium at 1 : 9 (*v*/*v*). After different treatments, the culture inserts as well as original culture medium were removed and 2 mL CCK-8 working solution was added. The plates were incubated at 37°C with 5% CO_2 for 2 h. Then, 100 μL of reacted solution was transferred to a 96-well plate. The surviving cell counts were determined by absorbance detection at 450 nm with a spectrophotometer (BioTek, USA).

2.4. Detection of Apoptosis by Flow Cytometry. Apoptosis rate was detected by Annexin V-FITC/PI Apoptosis Detection Kit (KeyGen Biotech, China). In brief, the cells were collected and washed with PBS and then resuspended in 500 μL binding buffer. 5 μL Annexin V-FITC and PI were added and the specimens were incubated in the dark at room temperature for 15 min. The labeled cells were detected via flow cytometry (BD LSR II, Becton Dickinson), and the data were analyzed by FACSDiva Software (Becton Dickinson, USA).

2.5. Observation of Cell Morphology. After treatment with compressive stress, cells were observed by inverted microscopy (Olympus, Japan). To further observe the apoptotic features, Hoechst 33258 staining was used. The collected cells were washed with PBS and then stained with Hoechst 33258 (Sigma, USA) for 15 min in the dark according to the manufacturer's instructions. Thereafter, morphologic changes of NPCs were observed and imaged under the inverted fluorescence microscope (Olympus, Japan).

2.6. TUNEL Staining. More sensitive TUNEL staining was used to evaluate the cell apoptosis. Following fixation in 4% paraformaldehyde for 1 h at room temperature, the cells were permeabilized with 0.1% TritonX-100 for 10 min. After washed with PBS, the cells were incubated with TUNEL staining (Roche, Germany) for 1 h at 37°C in the dark, according to the manufacturer's protocol. Apoptotic alterations were observed under the inverted fluorescence microscope (Olympus, Japan).

2.7. ROS Measurement. The intracellular ROS level was measured by 2,7-dichlorofluorescin diacetate (DCFH-DA; Beyotime, China). In the presence of ROS, DCFH-DA is oxidized into the fluorescent dichlorofluorescein (DCF). After treatment, the collected cells were resuspended in DCFH-DA and incubated in the dark for 30 minutes at 37°C. The mean fluorescence intensity (MFI) of DCF was measured by flow cytometry.

2.8. Mitochondrial Membrane Potential (MMP) Assay. MMP was measured by JC-1 (Beyotime, China) according to the manufacturer's instructions. In brief, the harvested NPCs were resuspended in the mixture contained 500 μL 10% DMEM/F-12 and 500 μL JC-1 staining fluid. After incubated in the dark for 30 minutes at 37°C, the cells were washed with ice-cold staining buffer (1x) and resuspended in 500 μL staining buffer (1x). The values of MMP staining expressed as the ratio of red over green fluorescence intensities were determined by flow cytometry.

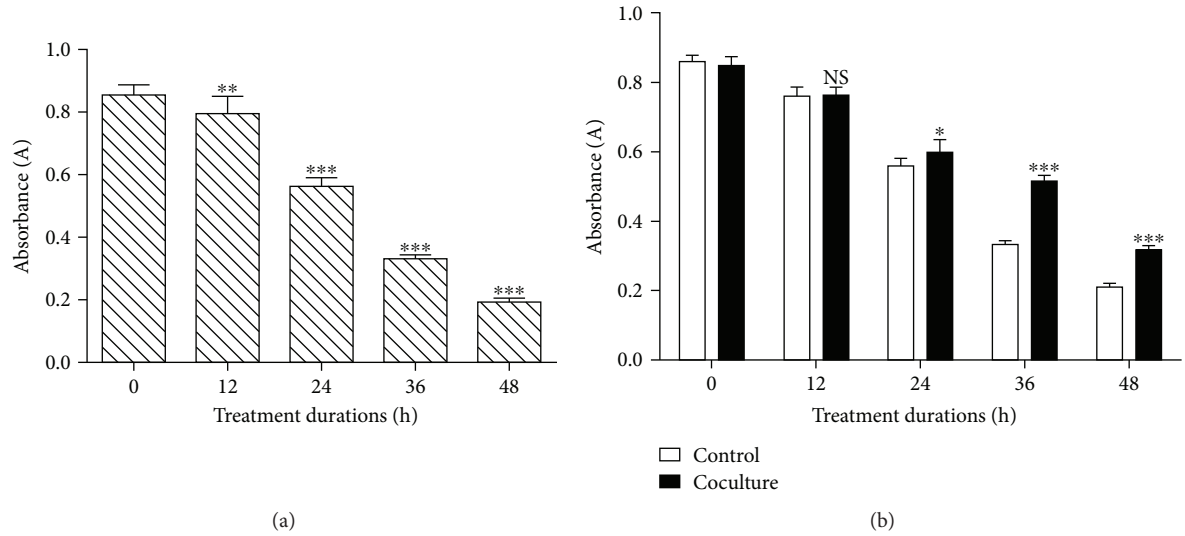

Figure 1: Cell viability of NPCs exposed to compression measuring by the CCK-8 assay. (a) NPCs were exposed to compression for 0, 12, 24, 36, or 48 h. (b) Coculture with BMSCs was applied to all-time point to verify the protective effects of BMSCs. NS means no statistical significant difference. NP cells without compression treatment as control. The data are expressed as mean ± SD from three independent experiments. ($^{*}P < 0.05$, $^{**}P < 0.01$, and $^{***}P < 0.001$ versus control).

2.9. Transmission Electron Microscopy (TEM). TEM was performed as previously described [18]. Briefly, harvested cells were washed with PBS and deionized water, respectively, and then pelleted by centrifugation. Cells were prefixed with 2.5% glutaraldehyde for 2 h and postfixed in 1% osmium tetroxide for 2 h. Then the cells were dehydrated in ethanol and infiltrated and embedded in epon 812. Ultrathin sections were stained with uranyl acetate and lead citrate and examined with a Tecnai G^2 12 TEM (FEI Company, Holland).

2.10. Western Blot Analysis. NPCs were lysed on ice using a standard buffer (Beyotime, China). Total protein was extracted by protein extraction kit (Beyotime, China) and a cell mitochondria Isolation Kit (Beyotime, China) was used to extract the mitochondria-free plasma protein for cytosolic cytochrome *c* detection. The cell lysate was centrifuged at 12,000 ×g for 10 min at 4°C. After protein transfer, the membranes were blocked by nonfat milk and then incubated overnight at 4°C with rat polyclonal antibody against cleaved caspase-3 (Abcam, 1 : 500), Bax (Abcam, 1 : 1000), Bcl-2 (Abcam, 1 : 1000), cleaved caspase-9 (Abcam, 1 : 1000), cytochrome *c* (Abcam, 1 : 1000), and *β*-actin (Abcam, 1 : 3000). After several times of washing, the membrane was incubated with secondary antibodies for 1 h at room temperature. Finally, the immunoreactive membranes were visualized via the enhanced chemiluminescence (ECL) method following the manufacturer's instructions (Amersham Biosciences, USA).

2.11. Statistical Analysis. All measurements were performed at least three times. The data were expressed as mean ± standard deviation (SD). Student's *t*-tests were used in the analysis of two-group parameters. One-way analysis of variance (ANOVA) test was used in comparisons of multiple sets of data, followed by the Tukey's post hoc test. $P < 0.05$ were considered significant.

3. Results

3.1. Coculturing with BMSCs Increased the Cell Viability of NPCs. To determine the effect of BMSCs on the viability of compression-treated NPCs, a CCK-8 assay was performed. As shown in Figure 1(a), the compression inhibited the viability of the NPCs in a time-dependent manner from 0 to 48 h (Figure 1(a), $P < 0.01$). NPCs were divided into coculture and control groups. For NPCs cocultured with BMSCs under compression stress, BMSCs significantly increased the viability of NPCs compared to the cells exposed to compression alone. From the time point 36 h, the *P* value of each group was less than 0.001 (Figure 1(b)). Therefore, the time point 36 h was used in the following experiments.

3.2. Protective Effect of BMSCs on Compression-Induced Apoptosis in NPCs. With compression treatment for 36 h, the NPCs exhibited shrunk or threadlike morphology and almost detached from the plates (Figure 2(a)). Furthermore, Hoechst 33258 staining revealed the brightly stained condensed nuclei, and the number of TUNEL-positive cells increased (Figures 2(b) and 2(c)). As expected, BMSCs could obviously attenuate the morphological changes indicative of apoptosis (Figure 2). The flow cytometry demonstrated that the apoptosis rate of the NPCs treated with compression for 36 h was significantly higher than control ($P < 0.01$). However, coculturing with BMSCs partially prevented this compression-induced apoptosis (Figures 2(d) and 2(e), $P < 0.05$). Interestingly, coculturing with BMSCs mainly reduced the percentage of apoptotic cells at the early stage (Figure 2(e), $P < 0.001$). And there was no significant

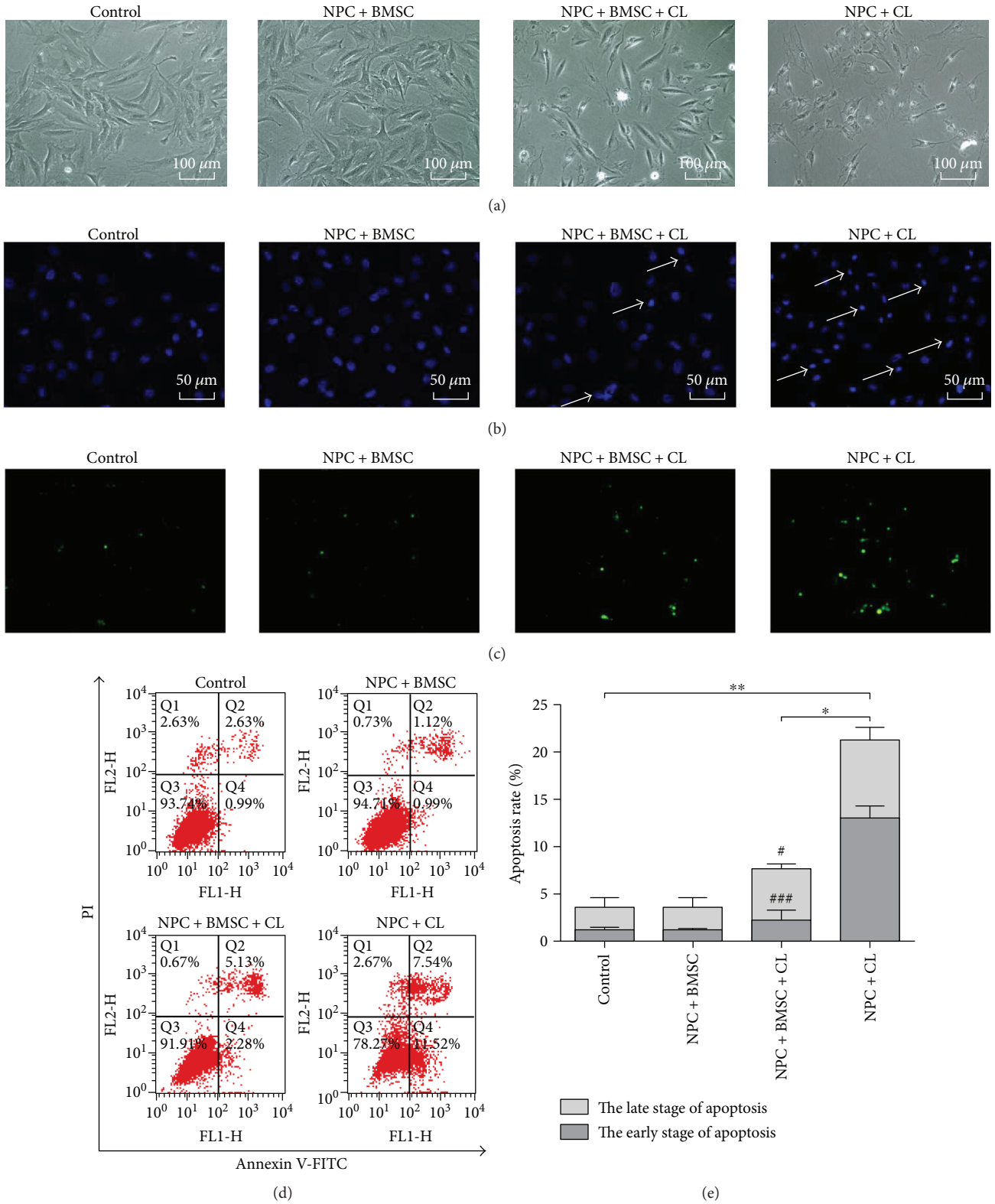

Figure 2: The antiapoptosis effect of BMSCs on NPCs exposed to compression. (a) The phase-contrast photomicrograph of NPCs. (b) Hoechst 33258 staining of NPCs. Apoptotic cells were characterized by the brightly stained condensed nuclei (indicated by arrows). (c) TUNEL staining of NPCs. (d) Representative images of cell apoptosis by flow cytometry analysis after Annexin V/PI dual staining. (e) Summary data showing the apoptosis rate in different groups. The cells at the early stage of apoptosis were stained with Annexin V+/PI−, and the cells at the late stage of apoptosis were stained with Annexin V+/PI+. CL means compression load. The data are expressed as mean ± SD from three independent experiments ($^{*}P < 0.05$ and $^{**}P < 0.01$ versus control or NPC + BMSC + CL; $^{\#}P < 0.05$ and $^{\#\#\#}P < 0.001$ versus NPC + CL).

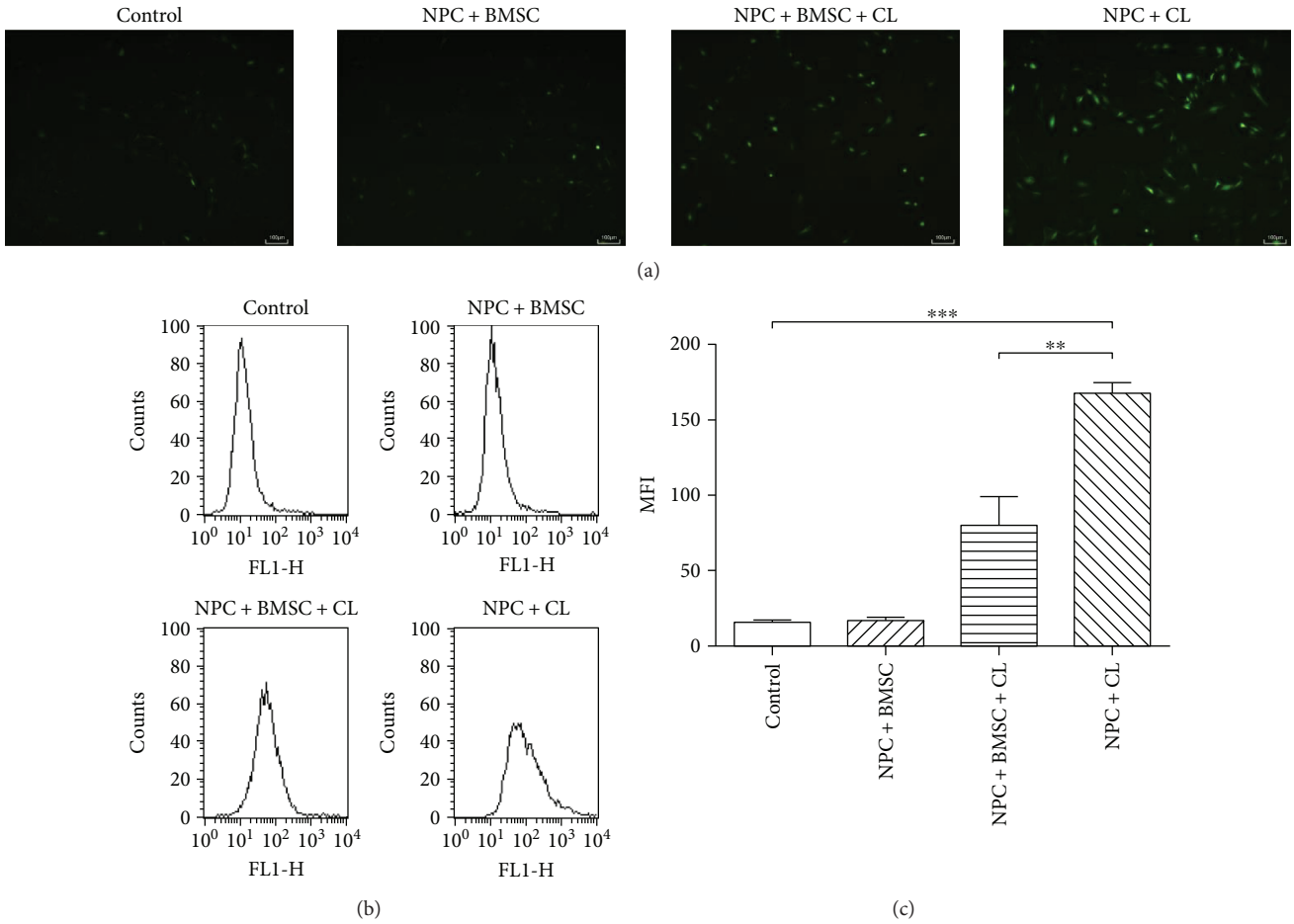

Figure 3: The effect of BMSCs on the compression-induced intracellular accumulation of ROS in NPCs. (a) Typical graphs of ROS imaged by fluorescence microscopy. (b) The intracellular ROS levels were measured by flow cytometry through DCFH-DA staining. (c) Summary data showing the mean fluorescence intensity (MFI) in different groups. CL means compression load. The data are expressed as mean ± SD from three independent experiments ($^{**}P < 0.01$ and $^{***}P < 0.001$ versus control or NPC + BMSC + CL).

difference between the control group with the cocultures not exposed to compression.

3.3. BMSCs Inhibit Compression-Induced ROS Production. Excessive ROS could impair mitochondrial function and increase the apoptosis rate of NPCs. As shown in the fluorescence images, compression treatment increased the fluorescence intensity, which indicated the production of ROS. Conversely, coculturing with BMSCs reduced the DCF fluorescence induced by compression (Figure 3(a)). Consistent with the fluorescence results, FACS analyses showed that the levels of intracellular ROS production in the NPCs treated with compression increased significantly compared to the untreated control group ($P < 0.001$), whereas coculturing with BMSCs inhibited the compression-induced increase in ROS production (Figures 3(b) and 3(c), $P < 0.01$).

3.4. BMSCs Inhibit Compression-Induced Decrease of MMP ($\Delta\psi_m$). MMP assay was applied to evaluate mitochondrial function. In the control group, the NPCs stained with JC-1 exhibited intense red fluorescence with weak green fluorescence. But on the contrary, the green fluorescence in the NPCs subjected to compression became stronger, while the red fluorescence became weaker. Coculturing with BMSCs could partly reverse the harmful change and decrease the loss of the $\Delta\psi_m$ (Figure 4(c)). Flow cytometric analysis showed that the NPCs exposed to compression exhibited a remarkable reduction of $\Delta\psi_m$ compared to controls ($P < 0.05$), which was indicated by the decrease of red/green fluorescence ratio. However, coculturing with BMSCs significantly increased the red/green fluorescence ratio and maintained the $\Delta\psi_m$ of compression-treated NPCs (Figures 4(a) and 4(b), $P < 0.001$).

3.5. Observation of the Mitochondrial Ultrastructure of NPCs by TEM. In order to intuitively observe the mitochondrial ultrastructure of NPCs with compression treatment, TEM was applied to evaluate mitochondrial integrity and state. In the control group, the mitochondrial ultrastructure was normal with well-defined cristae. But in the compression-treated NPCs, disintegrating cristae and swelling mitochondria were observed, which indicated the mitochondria were damaged. Not surprisingly, coculturing with BMSCs

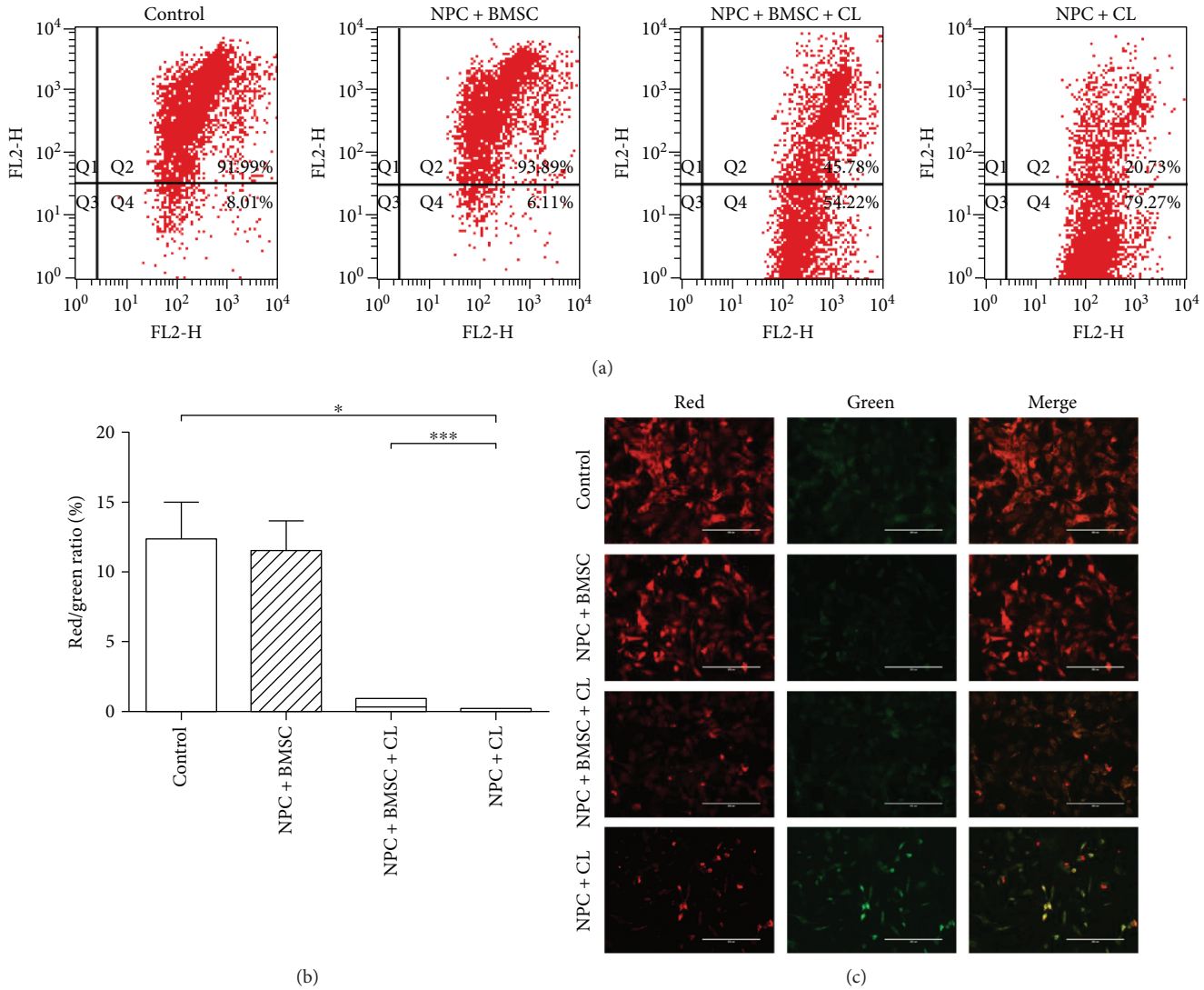

Figure 4: Coculture with BMSCs maintained the MMP of NPCs exposed to compression. (a) The MMP was analyzed by flow cytometry through JC-1 staining. (b) Summary data showing the quantitative MMP expressed as the ratio of red/green fluorescence intensity. (c) The representative fluorescence images of in situ JC-1 staining. CL means compression load. The data are expressed as mean ± SD from three independent experiments ($^{*}P < 0.05$ and $^{***}P < 0.001$ versus control or NPC + BMSC + CL).

exhibited a significant improvement in ultrastructure collapse of the mitochondria. These results suggested that coculturing with BMSCs could improve the mitochondrial state of the NPCs exposed to compression (Figure 5).

3.6. Coculturing with BMSCs Blocks Compression-Induced Activation of the Mitochondrial Pathway. The expression of the mitochondria-mediating proteins (cleaved caspase-3 and-9, cytochrome *c*, Bax, and Bcl-2) was determined by Western blotting. As shown in Figure 6, compression treatment resulted in increased cleaved caspase-3 and -9, cytosolic cytochrome *c*, and Bax and decreased Bcl-2 compared to the control group. However, coculturing with BMSCs partially reversed the changes of the protein level ($P < 0.05$). All these results indicated that BMSCs could protect NPCs from compression-induced apoptosis by inhibiting the mitochondrial or intrinsic pathway.

4. Discussion

Currently, there are limited long-lasting and effective treatments in the IVDD therapy. In recent years, many studies have demonstrated that MSCs, especially BMSC-based therapies, are promising for IVD repair [20–22]. In a short-term follow-up of disc cell therapy in vivo, Omlor et al. [23] suggested that BMSCs could keep metabolic activity in a porcine nucleotomy model after 3 days. And in other different degenerative disc models, it was reported that BMSC transplantation could improve the ECM synthesis and disc height [24–26]. These results provide some indication that BMSCs are able to adapt to the degenerative microenvironment and initiate a protective function or an anabolic response, therefore, to regenerate the disc. Apart from BMSCs, other kinds of MSCs, such as adipose-derived MSCs [27] and umbilical cord-derived MSCs [28], could also delay the IVDD.

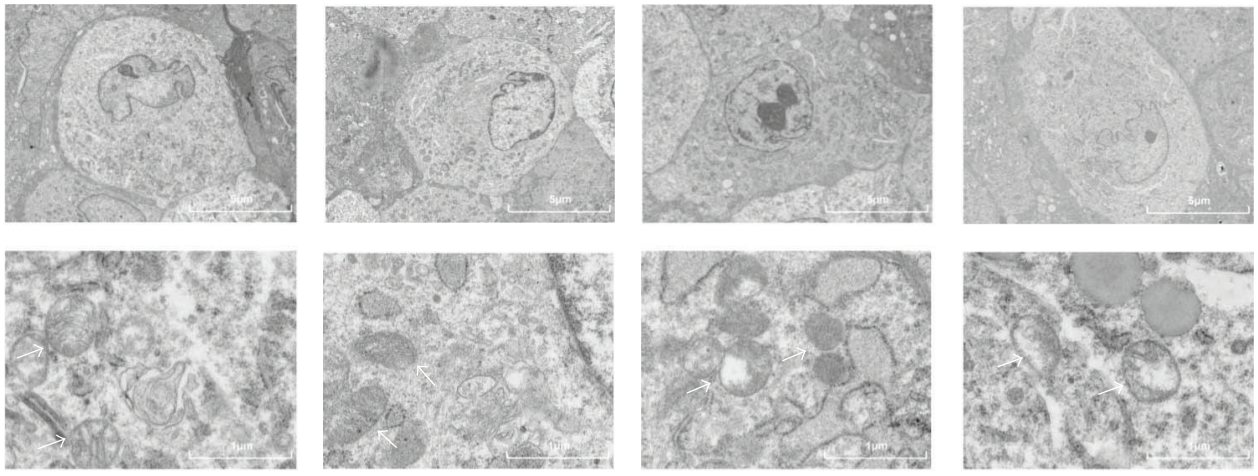

Figure 5: The mitochondrial ultrastructure of NPCs was assessed using TEM. (a) Control group and (b) NPC + BMSC group displayed normal mitochondria. (c) NPC + BMSC + CL group BMSCs improved the ultrastructure collapse of the mitochondria in NPCs with compression treatment. (d) NPC + CL group demonstrated disintegrating cristae and swelling mitochondria. CL means compression load (mitochondria were indicated by arrows).

Although MSCs showed encouraging regeneration effect for IVDD, the mechanism of which is unclear. A lot of studies suggested that the regeneration effect was achieved by the interaction between MSCs and NPCs under different conditions [29]. On one hand, coculturing of MSCs and NPCs promote the differentiation and migration of MSCs [15, 16, 30]. On the other hand, MSCs increase anabolism and decrease catabolism of NPCs and induce an anti-inflammatory effect [15, 17, 31–33]. However, there are few reports discussing the effect of MSC on the NP cell death, such as apoptosis.

In the present study, an indirect coculture system exposed to compression was established to explore the antiapoptosis effect of BMSC on NPCs and the underlying mechanism under compression condition. In our previous studies, we demonstrated that excessive compression would induce NPC apoptosis and result in IVDD [12, 18]. The results in this study were consistent with it and more importantly, we found that BMSCs could protect against compression-induced apoptosis, which was indicated by flow cytometric analysis and morphologic observation.

There are two signaling pathways of apoptosis, mitochondrial (intrinsic) and extrinsic pathways. The mitochondrial pathway had been verified to be involved in various stress-induced apoptosis of NPCs in our previous study and other studies [4, 5, 12]. Therefore, we assumed that the mitochondrial pathway was involved in the antiapoptosis effect of BMSCs on compression-treated NPCs.

ROS are formed primarily from the mitochondria and play an important role in cell signaling and homeostasis in normal physical level. But various stresses, such as compression, can enhance the production of ROS [12]. Excessive ROS can damage mitochondrial function and activate the mitochondrial apoptotic pathway, which manifests as a decrease of MMP and release of cytochrome *c* and then lead to cell apoptosis [34]. Our data showed that compression treatment could significantly increase the ROS level and decrease the MMP, and coculturing with BMSCs partially reversed the change. The protective effect was also confirmed by TEM, which intuitively exhibited the changes of mitochondrial ultrastructure in different groups. These results suggested that BMSCs could protect against compression-induced mitochondrial damage, and the mitochondrial pathway might involve in the antiapoptosis effect.

To further verify our hypothesis at a molecular level, we measured the expression of caspase-3 and -9, cytosolic cytochrome *c*, Bax, and Bcl-2. Bax is a proapoptotic protein, while Bcl-2 is an antiapoptotic protein. Both of them are two classical biomarkers for the mitochondrial pathway and belong to Bcl-2 family proteins [35–37]. In the nondegenerative human lumbar intervertebral disc, Wang et al. [38] reported that there was a high expression of Bcl-2 and a low expression of Bax. Conversely, in the degenerative IVD, Bcl-2 expression was decreased and Bax was increased. And the Bax/Bcl-2 complex dissociation led to the release of cytochrome *c*. Cytochrome *c*, along with Apaf-1 and caspase-9, forms multiprotein apoptosome, which ultimately produces cleaved caspase-9 and -3 and leads to the cell apoptosis [39]. Indeed, an increase of cleaved caspase-3 and -9, upregulation of cytosolic cytochrome *c* and Bax, and downregulation of Bcl-2 was detected in the NPCs with compression treatment compared to the control group, which was in line with our previous study [12]. More importantly, this effect was significantly attenuated by coculturing with BMSCs. Clearly, our findings confirmed that the compression-induced NPC apoptosis was mediated via the mitochondrial apoptotic pathway (Supplementary Figure S1), and the mitochondrial apoptotic pathway was involved in the antiapoptosis effect of BMSCs.

Certainly, there were some limitations of the study. First, the antiapoptosis effect of BMSCs on NPCs was performed in vitro and based on the rat cells. So, further studies with human cells and animal studies need to be carried out. Second, the results in the present study suggested that the

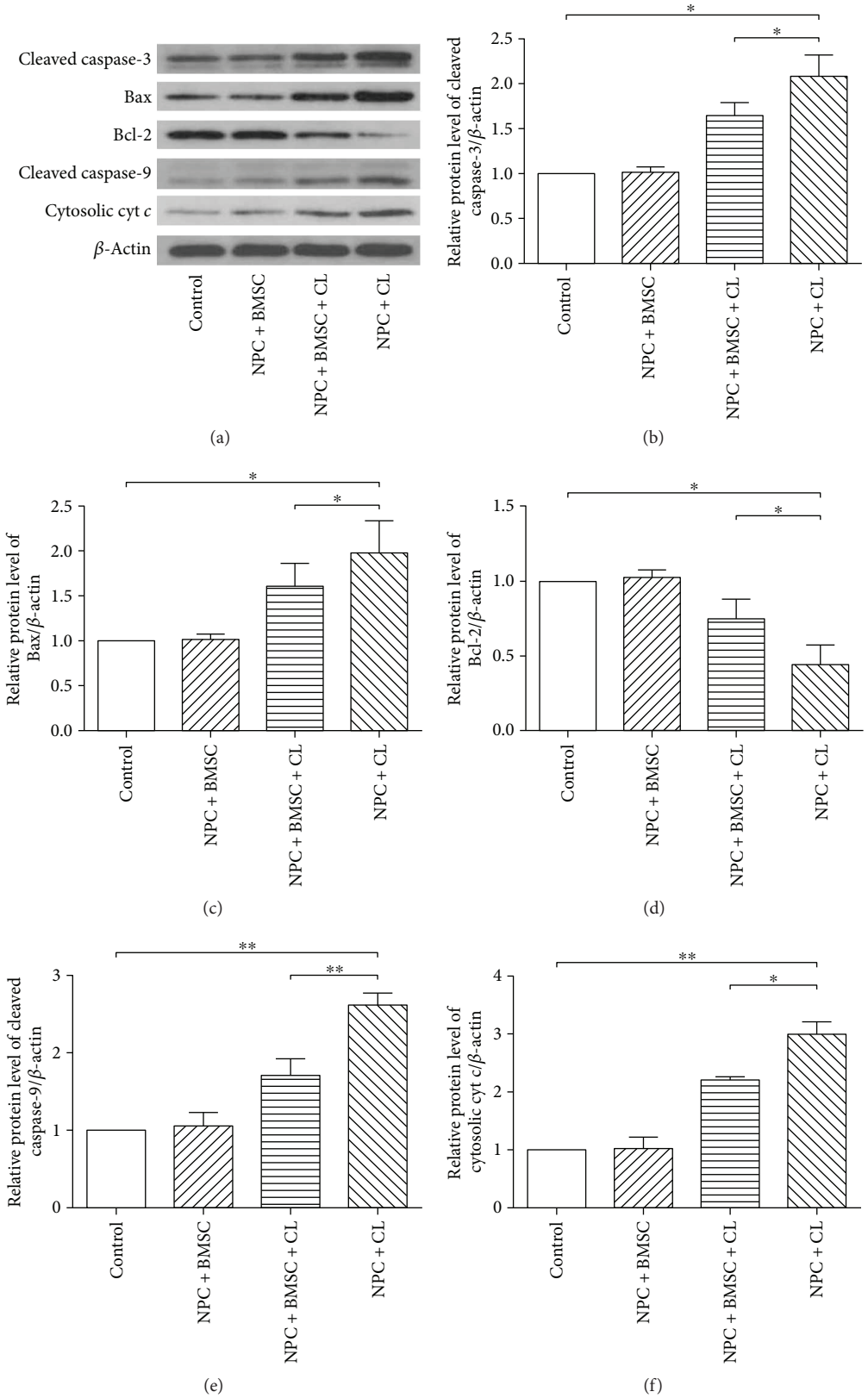

Figure 6: The protein expression of cleaved caspase-3, Bax, Bcl-2, cleaved caspase-9, and cytosolic cytochrome *c* (cytosolic cyt *c*) determined by Western blotting. (a) The typical Western blot bands of cleaved caspase-3, Bax, Bcl-2, cleaved caspase-9, and cytosolic cytochrome *c* (cytosolic cyt *c*). (b), (c), (d), (e), (f) Summary data showing protein levels of cleaved caspase-3, Bax, Bcl-2, cleaved caspase-9, and cytosolic cytochrome *c* (cytosolic cyt *c*). CL means compression load. The data are expressed as mean ± SD from three independent experiments ($^{*}P < 0.05$ and $^{**}P < 0.01$ versus control or NPC + BMSC + CL).

compression loading could induce NPC apoptosis through the mitochondrial apoptotic pathway. However, how NPCs sensed compression loading and converted it to apoptotic signals remained unclear. It was reported that transmembrane calcium ion channels, receptor tyrosine kinases, and integrins were the major mechanosensors [8]. Therefore, further studies to identify the mechanosensors are needed (Supplementary Figure S1). Finally, although the results in the present study demonstrated that BMSCs could protect against compression-induced apoptosis of NPCs by inhibiting the mitochondrial pathway, the precise mechanism of the antiapoptosis effect was not fully understood. The use of 0.4 μm pore-size transwell inserts ensured that only secreted factors were easily passed. It indicated that the BMSCs suppressed the apoptosis of NPCs, at least in part, through the paracrine mechanism. It was reported that some mediators (including growth factors, cytokines, chemokines, anti-inflammatory factors, and exosomes) played an essential role in the interaction between MSCs and IVD cells [40–43]. So, what specific secreted factor that plays a major role in the antiapoptosis effect remains to be explored (Supplementary Figure S1).

In conclusion, findings from our study demonstrated the antiapoptosis effect of BMSC on NPCs exposed to compression in vitro. In addition, our data suggested that the mitochondrial apoptotic pathway was involved in the antiapoptosis effect. These results of the present study clarify the underlying molecular mechanism of the antiapoptosis effect and enhance the understanding of the regenerative effect of MSCs.

Conflicts of Interest

The authors declare no conflicts of interest.

Authors' Contributions

Zengwu Shao designed the experiment and wrote the manuscript. Sheng Chen, Lei Zhao, Deyao Shi, Donghua Huang, and Fashuai Wu performed the experiments. Sheng Chen and Xiangyu Deng analyzed the experimental data. Hang Liang revised the manuscript. All authors reviewed the manuscript.

Acknowledgments

This work was supported by the National Natural Science Foundation of China (Grant nos. 81572203 and 91649204) and the National Key Research and Development Program of China (Grant no. 2016YFC1100100).

Supplementary Materials

The schematic diagram of the mechanism and signaling pathway of the antiapoptosis effect of BMSCs on NPCs under compression. Compression loadings enhanced the production of ROS, decreased mitochondrial membrane potential, suppressed the expression of Bcl-2, and increased the expression of Bax. And the Bax/Bcl-2 complex dissociation led to the release of cytochrome *c*. Cytochrome *c*, along with Apaf-1 and caspase-9, formed multiprotein apoptosome, which ultimately produced cleaved caspase-9 and 3 and led to the cell apoptosis. These effects were significantly attenuated by coculturing with BMSCs. The potential mechanosensors of NPCs and paracrine factors secreted by BMSCs remain to be explored. *(Supplementary Materials)*

References

[1] Y. R. Rampersaud, A. Bidos, C. Fanti, and A. V. Perruccio, "The need for multidimensional stratification of chronic low back pain (LBP)," *Spine*, vol. 42, no. 22, pp. E1318–E1325, 2017.

[2] D. Hoy, C. Bain, G. Williams et al., "A systematic review of the global prevalence of low back pain," *Arthritis & Rheumatism*, vol. 64, no. 6, pp. 2028–2037, 2012.

[3] W. Tong, Z. Lu, L. Qin et al., "Cell therapy for the degenerating intervertebral disc," *Translational Research*, vol. 181, pp. 49–58, 2017.

[4] L. Yang, Z. Rong, M. Zeng et al., "Pyrroloquinoline quinone protects nucleus pulposus cells from hydrogen peroxide-induced apoptosis by inhibiting the mitochondria-mediated pathway," *European Spine Journal*, vol. 24, no. 8, pp. 1702–1710, 2015.

[5] J. Shen, S. Xu, H. Zhou et al., "IL-1β induces apoptosis and autophagy via mitochondria pathway in human degenerative nucleus pulposus cells," *Scientific Reports*, vol. 7, article 41067, 2017.

[6] W. Jiang, X. Zhang, J. Hao et al., "SIRT1 protects against apoptosis by promoting autophagy in degenerative human disc nucleus pulposus cells," *Scientific Reports*, vol. 4, no. 1, 2015.

[7] D. Chen, D. Xia, Z. Pan et al., "Metformin protects against apoptosis and senescence in nucleus pulposus cells and ameliorates disc degeneration *in vivo*," *Cell Death & Disease*, vol. 7, no. 10, article e2441, 2016.

[8] C. Neidlinger-Wilke, F. Galbusera, H. Pratsinis et al., "Mechanical loading of the intervertebral disc: from the macroscopic to the cellular level," *European Spine Journal*, vol. 23, Supplement 3, pp. 333–343, 2014.

[9] R. D. Bowles and L. A. Setton, "Biomaterials for intervertebral disc regeneration and repair," *Biomaterials*, vol. 129, pp. 54–67, 2017.

[10] C. L. Le Maitre, A. J. Freemont, and J. A. Hoyland, "Expression of cartilage-derived morphogenetic protein in human intervertebral discs and its effect on matrix synthesis in degenerate human nucleus pulposus cells," *Arthritis Research & Therapy*, vol. 11, no. 5, article R137, 2009.

[11] Z. Sun, B. Luo, Z. H. Liu et al., "Adipose-derived stromal cells protect intervertebral disc cells in compression: implications for stem cell regenerative disc therapy," *International Journal of Biological Sciences*, vol. 11, no. 2, pp. 133–143, 2015.

[12] F. Ding, Z. W. Shao, S. H. Yang, Q. Wu, F. Gao, and L. M. Xiong, "Role of mitochondrial pathway in compression-induced apoptosis of nucleus pulposus cells," *Apoptosis*, vol. 17, no. 6, pp. 579–590, 2012.

[13] U. G. Longo, N. Papapietro, S. Petrillo, E. Franceschetti, N. Maffulli, and V. Denaro, "Mesenchymal stem cell for prevention and management of intervertebral disc degeneration," *Stem Cells International*, vol. 2012, Article ID 921053, 7 pages, 2012.

[14] D. Oehme, T. Goldschlager, P. Ghosh, J. V. Rosenfeld, and G. Jenkin, "Cell-based therapies used to treat lumbar

degenerative disc disease: a systematic review of animal studies and human clinical trials," *Stem Cells International*, vol. 2015, Article ID 946031, 16 pages, 2015.

[15] Z. Sun, Z. H. Liu, X. H. Zhao et al., "Impact of direct cell co-cultures on human adipose-derived stromal cells and nucleus pulposus cells," *Journal of Orthopaedic Research*, vol. 31, no. 11, pp. 1804–1813, 2013.

[16] A. A. Allon, K. Butcher, R. A. Schneider, and J. C. Lotz, "Structured coculture of mesenchymal stem cells and disc cells enhances differentiation and proliferation," *Cells, Tissues, Organs*, vol. 196, no. 2, pp. 99–106, 2012.

[17] S. H. Yang, C. C. Wu, T. T. Shih, Y. H. Sun, and F. H. Lin, "In vitro study on interaction between human nucleus pulposus cells and mesenchymal stem cells through paracrine stimulation," *Spine*, vol. 33, no. 18, pp. 1951–1957, 2008.

[18] K. G. Ma, Z. W. Shao, S. H. Yang et al., "Autophagy is activated in compression-induced cell degeneration and is mediated by reactive oxygen species in nucleus pulposus cells exposed to compression," *Osteoarthritis and Cartilage*, vol. 21, no. 12, pp. 2030–2038, 2013.

[19] D. Kong, J. Zhu, Q. Liu et al., "Mesenchymal stem cells protect neurons against hypoxic-ischemic injury via inhibiting parthanatos, necroptosis, and apoptosis, but not autophagy," *Cellular and Molecular Neurobiology*, vol. 37, no. 2, pp. 303–313, 2017.

[20] Y. Huang, V. Y. L. Leung, W. W. Lu, and K. D. Luk, "The effects of microenvironment in mesenchymal stem cell–based regeneration of intervertebral disc," *The Spine Journal*, vol. 13, no. 3, pp. 352–362, 2013.

[21] V. Y. L. Leung, D. M. K. Aladin, F. Lv et al., "Mesenchymal stem cells reduce intervertebral disc fibrosis and facilitate repair," *Stem Cells*, vol. 32, no. 8, pp. 2164–2177, 2014.

[22] Y. Zhao, Z. Jia, S. Huang et al., "Age-related changes in nucleus pulposus mesenchymal stem cells: an in vitro study in rats," *Stem Cells International*, vol. 2017, Article ID 6761572, 13 pages, 2017.

[23] G. W. Omlor, J. Fischer, K. Kleinschmitt et al., "Short-term follow-up of disc cell therapy in a porcine nucleotomy model with an albumin-hyaluronan hydrogel: in vivo and in vitro results of metabolic disc cell activity and implant distribution," *European Spine Journal*, vol. 23, no. 9, pp. 1837–1847, 2014.

[24] F. Yang, V. Y. Leung, K. D. Luk, D. Chan, and K. M. Cheung, "Mesenchymal stem cells arrest intervertebral disc degeneration through chondrocytic differentiation and stimulation of endogenous cells," *Molecular Therapy*, vol. 17, no. 11, pp. 1959–1966, 2009.

[25] H. Yang, J. Wu, J. Liu et al., "Transplanted mesenchymal stem cells with pure fibrinous gelatin-transforming growth factor-β1 decrease rabbit intervertebral disc degeneration," *The Spine Journal*, vol. 10, no. 9, pp. 802–810, 2010.

[26] Y. Zhang, S. Drapeau, S. A. Howard, E. J. M. A. Thonar, and D. G. Anderson, "Transplantation of goat bone marrow stromal cells to the degenerating intervertebral disc in a goat disc injury model," *Spine*, vol. 36, no. 5, pp. 372–377, 2011.

[27] G. Marfia, R. Campanella, S. E. Navone et al., "Potential use of human adipose mesenchymal stromal cells for intervertebral disc regeneration: a preliminary study on biglycan-deficient murine model of chronic disc degeneration," *Arthritis Research & Therapy*, vol. 16, no. 5, p. 457, 2014.

[28] X. Pang, H. Yang, and B. Peng, "Human umbilical cord mesenchymal stem cell transplantation for the treatment of chronic discogenic low back pain," *Pain Physician*, vol. 17, no. 4, pp. E525–E530, 2014.

[29] S. M. Richardson, G. Kalamegam, P. N. Pushparaj et al., "Mesenchymal stem cells in regenerative medicine: focus on articular cartilage and intervertebral disc regeneration," *Methods*, vol. 99, pp. 69–80, 2016.

[30] X. Hu, Y. Zhou, X. Zheng et al., "Differentiation of menstrual blood-derived stem cells toward nucleus pulposus-like cells in a coculture system with nucleus pulposus cells," *Spine*, vol. 39, no. 9, pp. 754–760, 2014.

[31] A. Ouyang, A. E. Cerchiari, X. Tang et al., "Effects of cell type and configuration on anabolic and catabolic activity in 3D co-culture of mesenchymal stem cells and nucleus pulposus cells," *Journal of Orthopaedic Research*, vol. 35, no. 1, pp. 61–73, 2016.

[32] C. Cao, J. Zou, X. Liu et al., "Bone marrow mesenchymal stem cells slow intervertebral disc degeneration through the NF-κB pathway," *The Spine Journal*, vol. 15, no. 3, pp. 530–538, 2015.

[33] H. Yang, C. Cao, C. Wu et al., "TGF-βl suppresses inflammation in cell therapy for intervertebral disc degeneration," *Scientific Reports*, vol. 5, no. 1, article 13254, 2015.

[34] C. X. Zhang, T. Wang, J. F. Ma, Y. Liu, Z. G. Zhou, and D. C. Wang, "Protective effect of CDDO-ethyl amide against high-glucose-induced oxidative injury via the Nrf2/HO-1 pathway," *The Spine Journal*, vol. 17, no. 7, pp. 1017–1025, 2017.

[35] J. H. Chen, C. H. Yang, Y. S. Wang, J. G. Lee, C. H. Cheng, and C. C. Chou, "Acrylamide-induced mitochondria collapse and apoptosis in human astrocytoma cells," *Food and Chemical Toxicology*, vol. 51, pp. 446–452, 2013.

[36] K. W. Kim, K. Y. Ha, J. S. Lee, K. W. Rhyu, H. S. An, and Y. K. Woo, "The apoptotic effects of oxidative stress and antiapoptotic effects of caspase inhibitors on rat notochordal cells," *Spine*, vol. 32, no. 22, pp. 2443–2448, 2007.

[37] K. C. Nguyen, W. G. Willmore, and A. F. Tayabali, "Cadmium telluride quantum dots cause oxidative stress leading to extrinsic and intrinsic apoptosis in hepatocellular carcinoma HepG2 cells," *Toxicology*, vol. 306, pp. 114–123, 2013.

[38] H. Wang, H. Liu, Z. M. Zheng et al., "Role of death receptor, mitochondrial and endoplasmic reticulum pathways in different stages of degenerative human lumbar disc," *Apoptosis*, vol. 16, no. 10, pp. 990–1003, 2011.

[39] K. Sinha, J. Das, P. B. Pal, and P. C. Sil, "Oxidative stress: the mitochondria-dependent and mitochondria-independent pathways of apoptosis," *Archives of Toxicology*, vol. 87, no. 7, pp. 1157–1180, 2013.

[40] D. Sakai and S. Grad, "Advancing the cellular and molecular therapy for intervertebral disc disease," *Advanced Drug Delivery Reviews*, vol. 84, pp. 159–171, 2015.

[41] G. Fontana, E. See, and A. Pandit, "Current trends in biologics delivery to restore intervertebral disc anabolism," *Advanced Drug Delivery Reviews*, vol. 84, pp. 146–158, 2015.

[42] K. Lu, H. Y. Li, K. Yang et al., "Exosomes as potential alternatives to stem cell therapy for intervertebral disc degeneration: in-vitro study on exosomes in interaction of nucleus pulposus cells and bone marrow mesenchymal stem cells," *Stem Cell Research & Therapy*, vol. 8, no. 1, p. 108, 2017.

[43] X. Cheng, G. Zhang, L. Zhang et al., "Mesenchymal stem cells deliver exogenous miR-21 *via* exosomes to inhibit nucleus pulposus cell apoptosis and reduce intervertebral disc degeneration," *Journal of Cellular and Molecular Medicine*, 2017.

Hindawi
Stem Cells International
Volume 2017, Article ID 6921703, 10 pages
https://doi.org/10.1155/2017/6921703

Research Article

The Flavonoid Glabridin Induces OCT4 to Enhance Osteogenetic Potential in Mesenchymal Stem Cells

June Seok Heo,[1,2] Seung Gwan Lee,[3] and Hyun Ok Kim[2,4]

[1]*Department of Integrated Biomedical and Life Sciences, College of Health Science, Korea University, Seoul 02841, Republic of Korea*
[2]*Cell Therapy Center, Severance Hospital, Seoul 03722, Republic of Korea*
[3]*Department of Health and Environmental Science, College of Health Science, Korea University, Seoul 02841, Republic of Korea*
[4]*Department of Laboratory Medicine, Yonsei University College of Medicine, Seoul 03722, Republic of Korea*

Correspondence should be addressed to Seung Gwan Lee; seunggwan@korea.ac.kr and Hyun Ok Kim; hyunok1019@yuhs.ac

Received 8 June 2017; Revised 27 September 2017; Accepted 3 October 2017; Published 14 November 2017

Academic Editor: Farid Menaa

Mesenchymal stem cells (MSCs) are a promising tool for studying intractable diseases. Unfortunately, MSCs can easily undergo cellular senescence during *in vitro* expansion by losing stemness. The aim of this study was to improve the stemness and differentiation of MSCs by using glabridin, a natural flavonoid. Assessments of cell viability, cell proliferation, β-galactosidase activity, differentiation, and gene expression by reverse transcription PCR were subsequently performed in the absence or presence of glabridin. Glabridin enhanced the self-renewal capacity of MSCs, as indicated by the upregulation of the *OCT4* gene. In addition, it resulted in an increase in the osteogenic differentiation potential by inducing the expression of osteogenesis-related genes such as *DLX5* and *RUNX2*. We confirmed that glabridin improved the osteogenesis of MSCs with a significant elevation in the expression of *OSTEOCALCIN* and *OSTEOPONTIN* genes. Taken together, these results suggest that glabridin enhances osteogenic differentiation of MSCs with induction of the *OCT4* gene; thus, glabridin could be useful for stem cell-based therapies.

1. Introduction

Mesenchymal stem cells (MSCs) derived from various tissues are very promising sources for cellular therapies and regenerative medicine, since they are easily accessible and differentiate into a variety of cell types, including osteoblasts, chondrocytes, and adipocytes [1, 2]. MSCs have been applied to cell-based therapies due to their numerous advantages including anti-inflammatory and immunomodulatory effects [3, 4]. However, despite the high expansion potential of MSCs, when cultured *in vitro*, they easily undergo proliferation arrest prior to significant telomere shortening due to intrinsic and/or extrinsic environmental factors [5, 6]. It is known that oxidative stress—due to an imbalance between the production of free radicals and the ability of the body to detoxify their harmful effects—is one of the main factors that induce senescence [7]. Senescence represents an arrested state in which cells remain viable but not stimulated to proliferate by serum or passage in culture. Cellular senescence of MSCs reduces functionality, which might impair their regenerative potential [8]. Therefore, MSCs need to be expanded for clinical application through *in vitro* long-term cultivation without early growth stop or cellular senescence.

Glabridin is an isoflavan compound found in the root extract of licorice [9]. A number of studies have reported that glabridin exhibits protective functions against oxidative stresses and cytotoxicity [10, 11]. In addition, it has been reported to inhibit cancer stem cell-like properties of human breast cancer cells, suggesting that it could enhance the effectiveness of breast cancer therapy [12]. Recently, it was also shown that glabridin attenuates oxidative damage and cellular dysfunction and upregulates osteoblast differentiation genes in osteoblastic cells [13]. These findings suggest the interesting possibility that glabridin could have positive effects on MSC culture *in vitro*. Although there is some evidence that glabridin protects cells from oxidative stress, no study has investigated whether glabridin can prevent MSC senescence. We therefore hypothesized that glabridin would

Table 1: Primer sequences used for RT-PCR.

Gene	Primer sequence (5′–3′)	Annealing temperature (°C)	Product size (bp)
GAPDH	Forward: GTGGTCTCCTCTGACTTCAACA Reverse: CTCTTCCTCTTGTGCTCTTGCT	62	210
OCT4	Forward: GACAACAATGAGAACCTTCAGGAGA Reverse: TTCTGGCGCCGGTTACAGAACCA	62	218
SOX2	Forward: AACCAAGACGCTCATGAAGAAG Reverse: GCGAGTAGGACATGCTGTAGGT	62	341
cMYC	Forward: TCGGATTCTCTGCTCTCCTC Reverse: CGCCTCTTGACATTCTCCTC	62	413
KLF4	Forward: ATTCTCTCCAATTCGCTGACCC Reverse: TTCAGCACGAACTTGCCCAT	62	376
NANOG	Forward: ATAGCAATGGTGTGACGCAG Reverse: GATTGTTCCAGGATTGGGTG	62	219
P53	Forward: TCGACATAGTGTGGTGGTGC Reverse: TTGGACTTCAGGTGGCTGGA	58	480
LIN28	Forward: GCTCCGTGTCCAACCAGCAG Reverse: TTTCCTTTTGGCCGCCTCTC	58	376
P16	Forward: CGAATAGTTACGGTCGGAGG Reverse: GCATGGTTACTGCCTCTGGT	62	309
DLX5	Forward: ACCATCCGTCTCAGGAATCG Reverse: ACCTTCTCTGTAATGCGGCC	60	384
RUNX2	Forward: TTGCAGCCATAAGAGGGTAG Reverse: GTCACTTTCTTGGAGCAGGA	58	470
PPARG	Forward: TCTCTCCGTAATGGAAGACC Reverse: GCATTATGAGACATCCCCAC	55	474
C/EBPA	Forward: CCAAGAAGTCGGTGGACAAGAA Reverse: TCATTGTCACTGGTCAGCTCCA	62	145
BMP7	Forward: CCAACGTCATCCTGAAGAAATAC Reverse: GCTTGTAGGATCTTGTTCATTGG	60	271
SOX9	Forward: GGTTGTTGGAGCTTTCCTCA Reverse: TAGCCTCCCTCACTCCAAGA	61	400
P21	Forward: GCGATGGAACTTCGACTTTG Reverse: CGTTTTCGACCCTGAGAGAGTC	60	285
OSTEOCALCIN	Forward: CGCAGCCACCGAGACACCAT Reverse: GGGCAAGGGCAAGGGGAAGA	62	405
OSTEOPONTIN	Forward: GAGACCCTTCCAAGTAAGTCCA Reverse: GATGTCCTCGTCTGTAGCATCA	62	354
COMP	Forward: GAAGAACGACGACCAAAAGGAC Reverse: GTCACAAGCATCTCCCACAAAG	62	232
TYPE I COLLAGEN	Forward: CACAGAGGTTTCAGTGGTTTGG Reverse: GCACCAGTAGCACCATCATTTC	62	191
AP2	Forward: AAGAAGTAGGAGTGGGCTTTGC Reverse: CCACCACCAGTTTATCATCCTC	62	381
LPL	Forward: AGAGAGGACTTGGAGATGTGGA Reverse: GGAAGACTTTGTAGGGCATCTG	62	264

preserve MSC functionality and would be beneficial for MSC culture *in vitro*.

The aim of this study was to examine the effects of glabridin on MSC *in vitro* culture. Treatment of MSCs with glabridin provided a favorable environment that improved stemness through upregulation of the *OCT4* gene, which is involved in pluripotency. To investigate the effects of glabridin on the differentiation potential of MSCs, we examined genes for osteogenic factors (*DLX5* and *RUNX2*), chondrogenic factors (*BMP7* and *SOX9*), and adipogenic factors (*PPARG* and *C/EBPA*). We found that the treatment of MSCs with glabridin led to osteoblast differentiation with the upregulation of osteoblast markers such as *OSTEOCALCIN* and *OSTEOPONTIN*. To our knowledge, this is the first study to indicate that glabridin is a beneficial factor that induces the *OCT4* gene and improves osteogenic

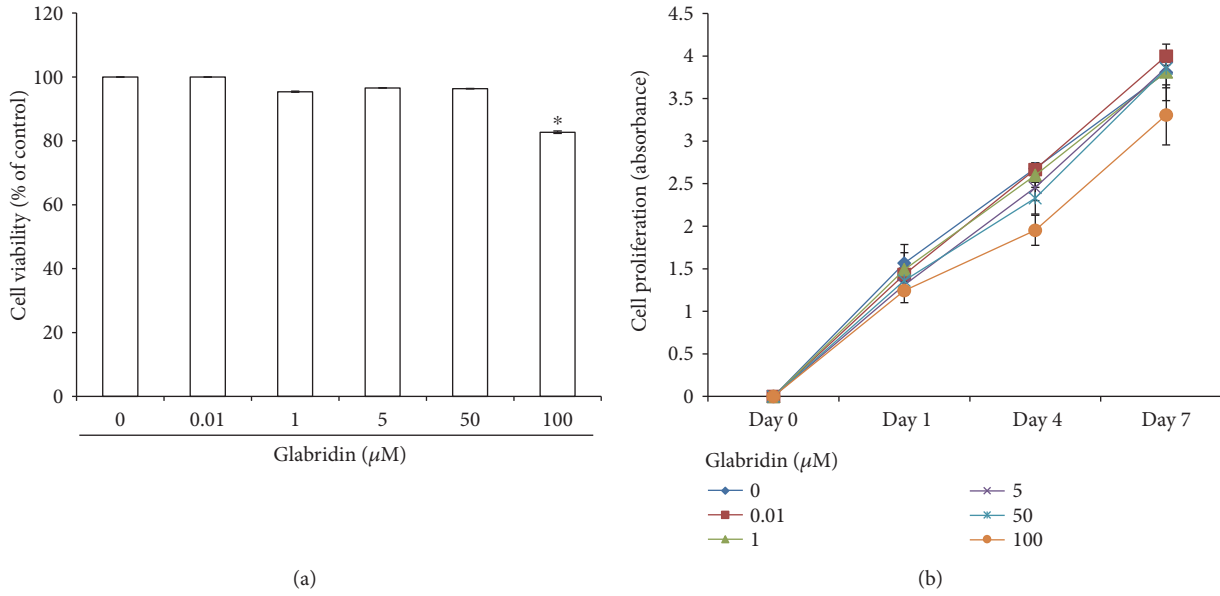

FIGURE 1: (a) Effect of glabridin on cell viability in bone marrow-derived mesenchymal stem cells (MSCs). Cell viability of MSCs treated with an increasing concentration of glabridin was determined by a CCK-8 assay. The data are expressed as the mean ± SD of three independent experiments. $^*P < 0.05$ versus untreated control. (b) Growth rates of cultured MSCs. Cells were cultivated with an increasing concentration of glabridin for 7 days. Proliferation activity was measured using a CCK-8 kit containing WST-8. The data are expressed as the mean ± SD of three independent experiments.

differentiation of MSCs during culture *in vitro*. These findings will be useful for preparing highly functional MSCs for cell-based clinical applications.

2. Materials and Methods

2.1. Cell Culture. The bone marrow was collected from healthy donors after obtaining written informed consent. This study was approved by the Institutional Review Boards of Severance Hospital of Yonsei University Health System, Seoul, Korea. As previously described, mononuclear cells were isolated by Ficoll-Hypaque density gradient centrifugation (Pharmacia Biotech, Uppsala, Sweden), and the MSCs were cultured using the plastic adherence method [14]. The cells were maintained in DMEM Low Glucose supplemented with 10% fetal bovine serum (FBS) and 1% penicillin/streptomycin (P/S) at 37°C with 5% CO_2 (all from Invitrogen, Carlsbad, CA, USA). The medium was changed every 3 or 4 days. The cells were subcultured using 0.05% trypsin/EDTA (Invitrogen) when they reached approximately 80–90% confluence. Glabridin (0.01–100 μM) was purchased from Sigma-Aldrich (St. Louis, MO, USA).

2.2. Cell Viability Test. The cells were seeded into 12-well plates (Corning Inc., Corning, NY, USA) at a density of 4×10^4 cells/well for assessment of cell viability. The next day, cells were treated with glabridin (0.01–100 μM), directly added to the medium, for 24 h. The viability of the cells was analyzed using a CCK-8 kit (Dojindo Co., Kumamoto, Japan), which measures cell metabolic activity, according to the manufacturer's instructions [15]. Briefly, 50 μM of the CCK-8 solution was added to each well of the culture plate at the end of the culture period. After 4 h of incubation, absorbance was measured at 450 nm. Cells incubated without glabridin were used as a control.

2.3. Cell Proliferation Assay. Cells were plated at a density of 2×10^4/well in 12-well plates (Corning) for analysis of cell growth. When the cells were replated, glabridin (0.01–100 μM) was added to each well of the culture plate. A proliferation assay was performed using a CCK-8 kit. CCK-8 contains WST-8 [2-(2-methoxy-4-nitrophenyl)-3-(4-nitrophenyl)-5-(2,4-dissulfophenyl)-2H-tetrazolium, monosodium salt], which produces a water-soluble formazan dye upon reduction in the presence of an electron carrier. CCK-8, being nonradioactive, allows sensitive colorimetric assays for the determination of the number of viable cells during cell proliferation. Cultures were maintained for 7 days and then analyzed for cell growth on days 1, 4, and 7 according to the manufacturer's instructions. Cells incubated with the culture medium alone were used as a control. The absorbance of the cells was normalized to their respective day 0 absorbance.

2.4. Reverse Transcription PCR (RT-PCR). Total RNA was isolated using TRIzol reagent (Invitrogen). Standard reverse transcription was performed using transcriptase II (Invitrogen). RT-PCR was performed using PCR primers (Bioneer, Daejeon, Korea) under the conditions listed in Table 1. Glyceraldehyde 3-phosphate dehydrogenase (*GAPDH*) level was used as an internal control. The signal intensity of the product was normalized to its respective *GAPDH* signal intensity.

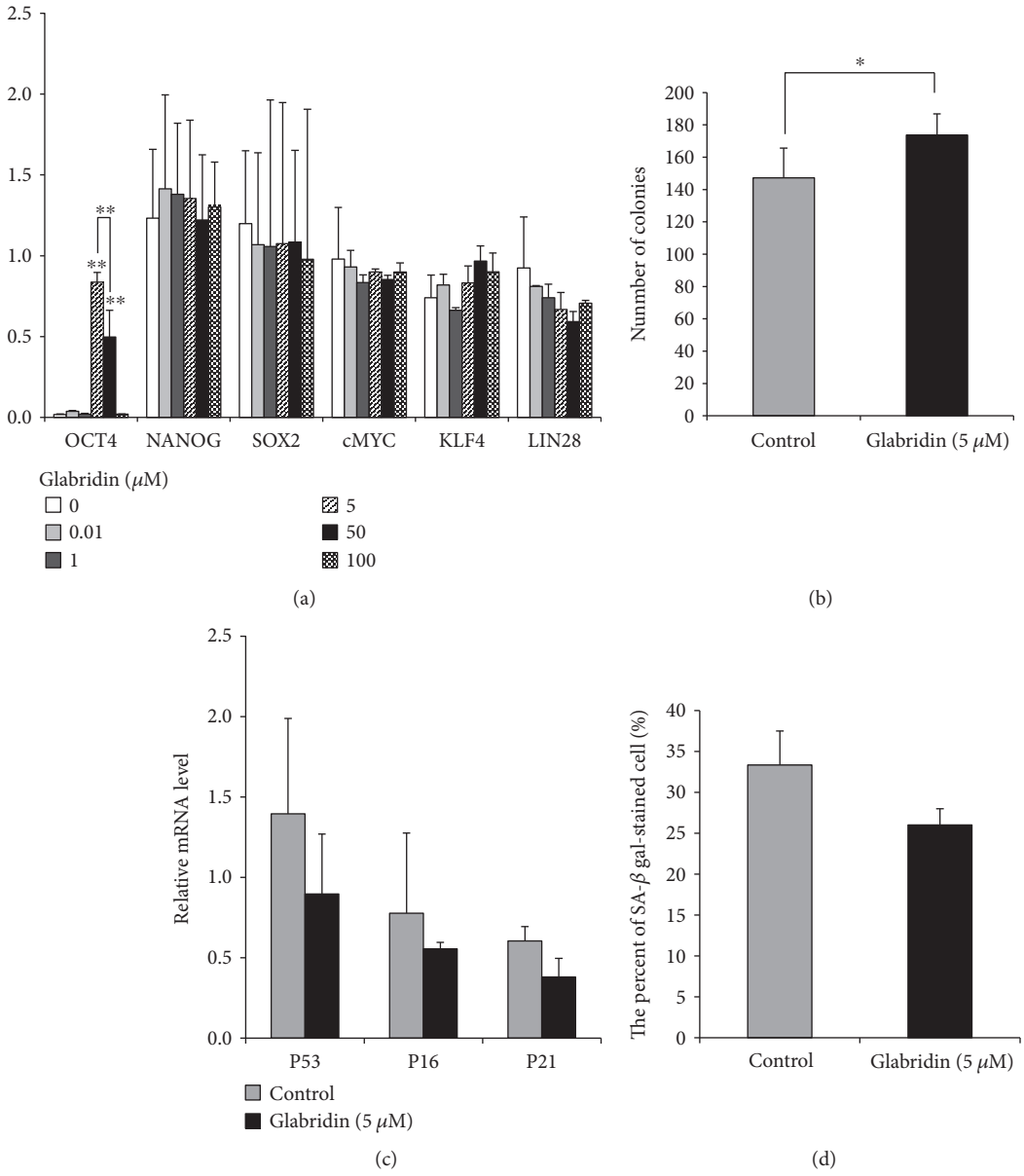

Figure 2: Effect of glabridin on stemness and senescence in MSCs. (a) Stemness marker expression in MSCs treated with an increasing concentration of glabridin. (b) Stemness was evaluated by a CFU-F assay. The number of colonies (>50 cells) was counted. (c) *P53*, *P16*, and *P21* mRNA expression levels were analyzed using reverse transcription PCR (RT-PCR). (d) Senescence-associated (SA) β-gal assay. The number of β-gal-positive cells was counted. The data are expressed as the mean ± SD of three experiments. $^{*}P < 0.05$ and $^{**}P < 0.01$ versus untreated control.

2.5. Colony Forming-Unit-Fibroblast (CFU-F) Assay. For assessment of self-renewal properties, a CFU-F assay was performed. Briefly, 1×10^3 cells were plated in 100 mm dishes (Corning), and the cells were cultured for 14 days. Following incubation for 14 days, the cells were washed with phosphate-buffered saline (PBS; Invitrogen). Then, the cells were stained with 0.5% crystal violet (Sigma-Aldrich) for 5 min at room temperature, and stained colonies were counted.

2.6. β-Galactosidase Staining. Senescent cells show an increase in cell size and the senescence-associated expression of β-galactosidase activity. A senescence detection kit (BioVision Inc., CA, USA) was used to histochemically detect β-galactosidase activity in cultured cells, according to the manufacturer's instructions. Briefly, cultured cells were washed with PBS and fixed with 4% paraformaldehyde at room temperature. After washing with PBS, cells were incubated with β-galactosidase staining solution for 24 h at 37°C. The number of β-galactosidase-stained cells was counted under a light microscope (Olympus-IX71; Olympus, Tokyo, Japan).

2.7. Differentiation Assay. To induce MSC differentiation into osteoblasts, chondrocytes, and adipocytes, cells were cultured in osteogenic induction medium, chondrogenic

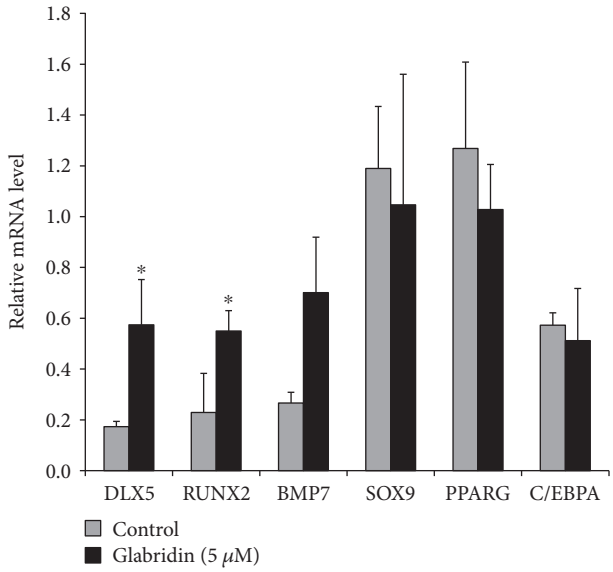

Figure 3: Gene expression in MSCs following glabridin treatment. RT-PCR analysis of osteogenic, chondrogenic, and adipogenic markers was performed in control and glabridin-treated MSCs. Relative mRNA expression levels of trilineage-associated genes in the control and glabridin-treated MSCs. Expression levels relative to *GAPDH* are shown. The data are expressed as the mean ± SD of three experiments. $^{*}P < 0.05$ versus untreated control.

induction medium, or adipogenic induction medium for 3 weeks (Cambrex, Lonza, MD, USA), respectively. The medium was changed every 3 or 4 days, and the cells for chondrogenic differentiation were treated with 10 ng/ml transforming growth factor (TGF)-β3 (Cambrex) whenever the medium was replaced. The induced cells were stained with von Kossa to confirm osteogenesis, safranin O to confirm chondrogenesis, and oil red O to confirm adipogenesis. Images of the stained cells were taken using a phase microscope (Olympus-IX-71). To measure the calcium content in osteogenesis, the Calcium LiquiColor kit (Stanbio Laboratory, Boerne, USA) was used according to a previously described method [16]. Briefly, the cells were washed with PBS and treated with 0.5 N HCl. After shaking for 3 h by using an orbital shaker, the supernatant was transferred to a new tube for analysis. Ortho-cresolphthalein complexone (OCPC) was added to the sample, and absorbance was determined at 550 nm. For quantitative analysis of adipogenesis, absorbance was measured at 500 nm after destaining with isopropanol for 30 min according to a previously reported method [16]. To quantitatively evaluate chondrogenesis, the absorbance of sulfated glycosaminoglycan was measured at 656 nm by using the Blyscan assay kit (Biocolor Ltd., County Antrim, UK). Briefly, the supernatant was transferred to a new tube and each sample was mixed with 1,9-dimethylmethylene blue (DMMB) dye, which is used to measure sulfated glycosaminoglycan (sGAG) content, according to the manufacturer's instructions and a previous report [17].

2.8. Statistical Analysis. Quantitative data are expressed as the means ± standard deviation (SD). Statistical comparisons were performed by a Student's *t*-test and one-way analysis of variance (ANOVA) with post hoc Bonferroni corrections. The differences were considered statistically significant at $P < 0.05$. Statistical analyses were performed using SPSS software (SPSS Inc., Chicago, IL, USA).

3. Results

3.1. Effect of Glabridin on the Viability and Proliferation of MSCs. To investigate the effect of glabridin on MSC survival, cells were cultured with increasing concentrations (0.01–100 μM) of glabridin for 24 h and then cell viability was measured using a CCK-8 assay. Glabridin at concentrations of 0.01–50 μM had no effect on cell survival, whereas incubation with 100 μM glabridin decreased the cell viability of MSCs (Figure 1(a)). These results show that 100 μM glabridin itself was cytotoxic to MSCs.

To evaluate the effect of glabridin on MSC proliferation, MSCs were cultured for 7 days to determine whether glabridin stimulates MSC growth, and then cell proliferation was determined using the CCK-8 assay. A decrease in cell growth was detected in MSCs cultured with 100 μM glabridin, while the cells cultured with 0.01–50 μM glabridin exhibited proliferation properties similar to those of the control cells (Figure 1(b)). These results show that glabridin did not facilitate the growth rates of the MSCs.

3.2. Effect of Glabridin on MSC Stemness. In order to identify the self-renewal capacity of MSCs, we analyzed the expression levels of stemness markers in the MSCs cultured with 0.01–100 μM glabridin. *NANOG*, *SOX2*, *cMYC*, *KLF4*, and *LIN28* were similarly expressed with all concentrations of glabridin (Figure 2(a)). Interestingly, the *OCT4* gene—involved in the self-renewal of undifferentiated stem cells—was markedly detected in MSCs cultured with 5 μM glabridin (Figure 2(a)). Therefore, we chose this concentration of glabridin (5 μM) for all subsequent cell experiments. The CFU-F assay was used to investigate whether *OCT4* expression with glabridin promotes the self-renewal capacity of MSCs. Glabridin significantly enhanced the self-renewal capacity of the treated cells compared with that of the control cells (Figure 2(b)). In addition, to confirm whether glabridin affected the cell cycle, the mRNA expression levels of *P53*, $P16^{INK4a}$, and $P21^{Cip1}$ in MSCs treated with glabridin were measured. The expression levels of *P53*, $P16^{INK4a}$, and $P21^{Cip1}$ of MSCs treated with glabridin were decreased compared to those in control cells (Figure 2(c)). We next examined whether glabridin prevented MSC senescence. MSCs treated with glabridin showed a decrease in the percentage of β-galactosidase-stained cells compared to control cells although there was no significance (Figure 2(d)). Together, these results suggest that glabridin augments the self-renewal capacity with upregulation of the *OCT4* gene.

3.3. Changes of Differentiation Potential in MSCs by Glabridin. We subsequently examined the osteogenesis-, chondrogenesis-, and adipogenesis-related gene expression levels in the MSCs after glabridin treatment. *DLX5* and *RUNX2* genes, which are involved in osteogenesis, were

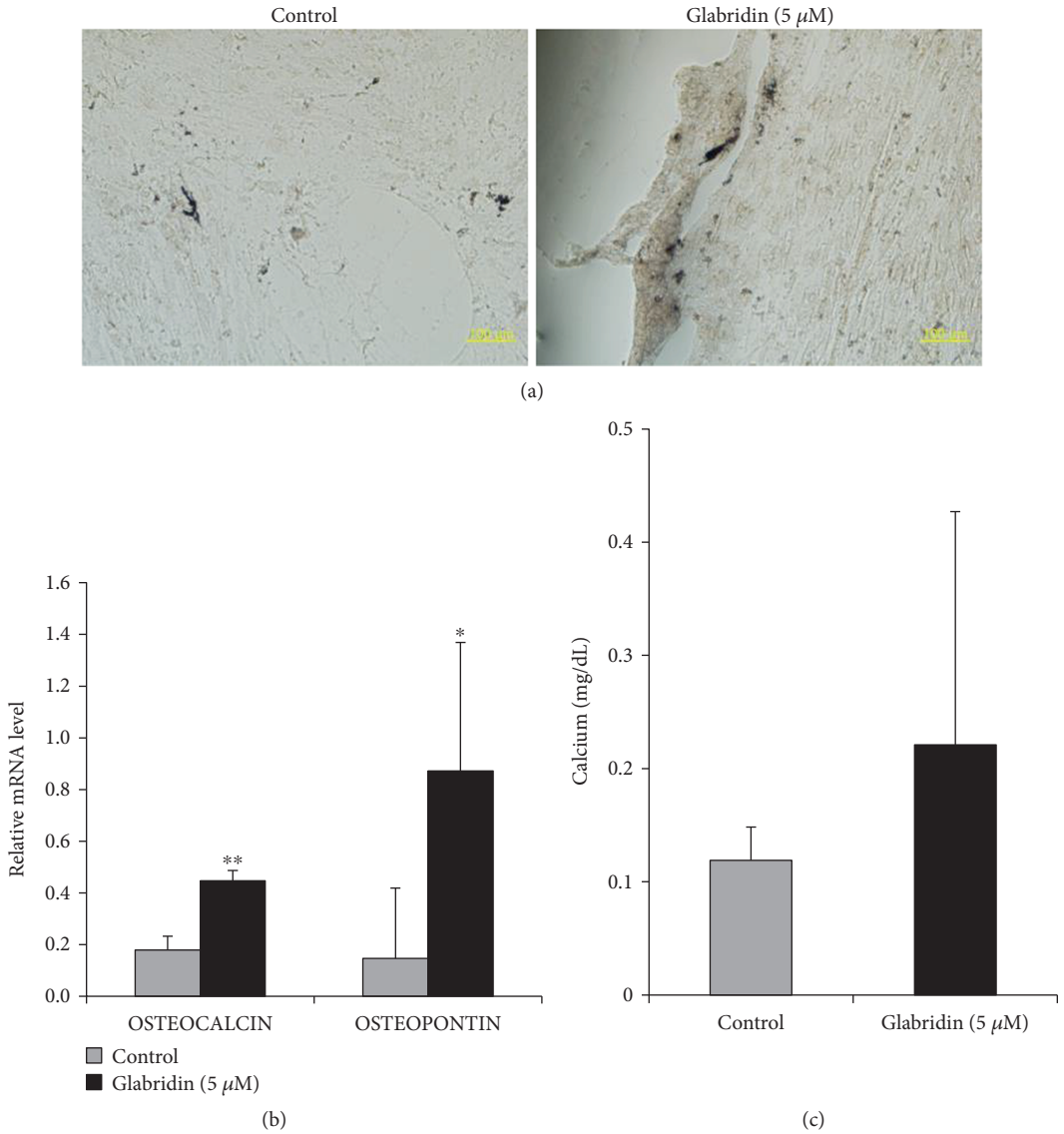

Figure 4: Effect of glabridin on osteogenesis in MSCs. (a) Osteogenic differentiation was evaluated by von Kossa staining (magnification: 200x). (b) Osteogenic potential was analyzed by *OSTEOCALCIN* and *OSTEOPONTIN* gene expression using RT-PCR. (c) Differentiation of MSCs into osteoblasts was determined by calcium quantification. The data are expressed as the mean ± SD of three experiments. $^{*}P < 0.05$ and $^{**}P < 0.01$ versus untreated control.

markedly upregulated by glabridin (Figure 3). With respect to chondrogenesis, the *BMP7* gene was upregulated, whereas the expression of *SOX9* gene was similar to MSCs treated with glabridin (Figure 3). The adipogenesis-related *C/EBPA* gene was similarly expressed in glabridin-treated MSCs compared to that in control cells, while the expression level of the *PPARG* gene decreased with glabridin treatment (Figure 3). These results indicate that glabridin strongly affects the osteogenic potential of MSCs.

3.4. Glabridin Enhances Osteogenesis of MSCs. To evaluate the differentiation capacity of MSCs, cells were induced by glabridin to form osteoblasts, chondrocytes, and adipocytes. MSCs treated with glabridin showed higher amounts of von Kossa staining, which detects calcium-containing mineralized nodules, compared to control cells (Figure 4(a)), and the expression of *OSTEOCALCIN* and *OSTEOPONTIN* genes of osteogenic differentiation markers was upregulated in MSCs treated with glabridin (Figure 4(b)). Moreover, we confirmed that MSCs cultured with glabridin had a higher degree of calcium accumulation compared to control cells although there were no significant differences (Figure 4(c)). Chondrogenesis was assessed by safranin O staining. After chondrogenic induction, MSCs cultured with glabridin exhibited a slightly higher chondrogenic differentiation capacity (Figure 5(a)). However, the *COMP* and the *TYPE I COLLAGEN* genes of the chondrogenic differentiation markers were similarly expressed despite chondrogenic induction in both conditions (Figure 5(b)). Sulfated glycosaminoglycan content was slightly increased in MSCs grown with glabridin, irrespective of the PCR data (Figure 5(c)). There were no significant differences. In adipogenesis, glabridin slightly

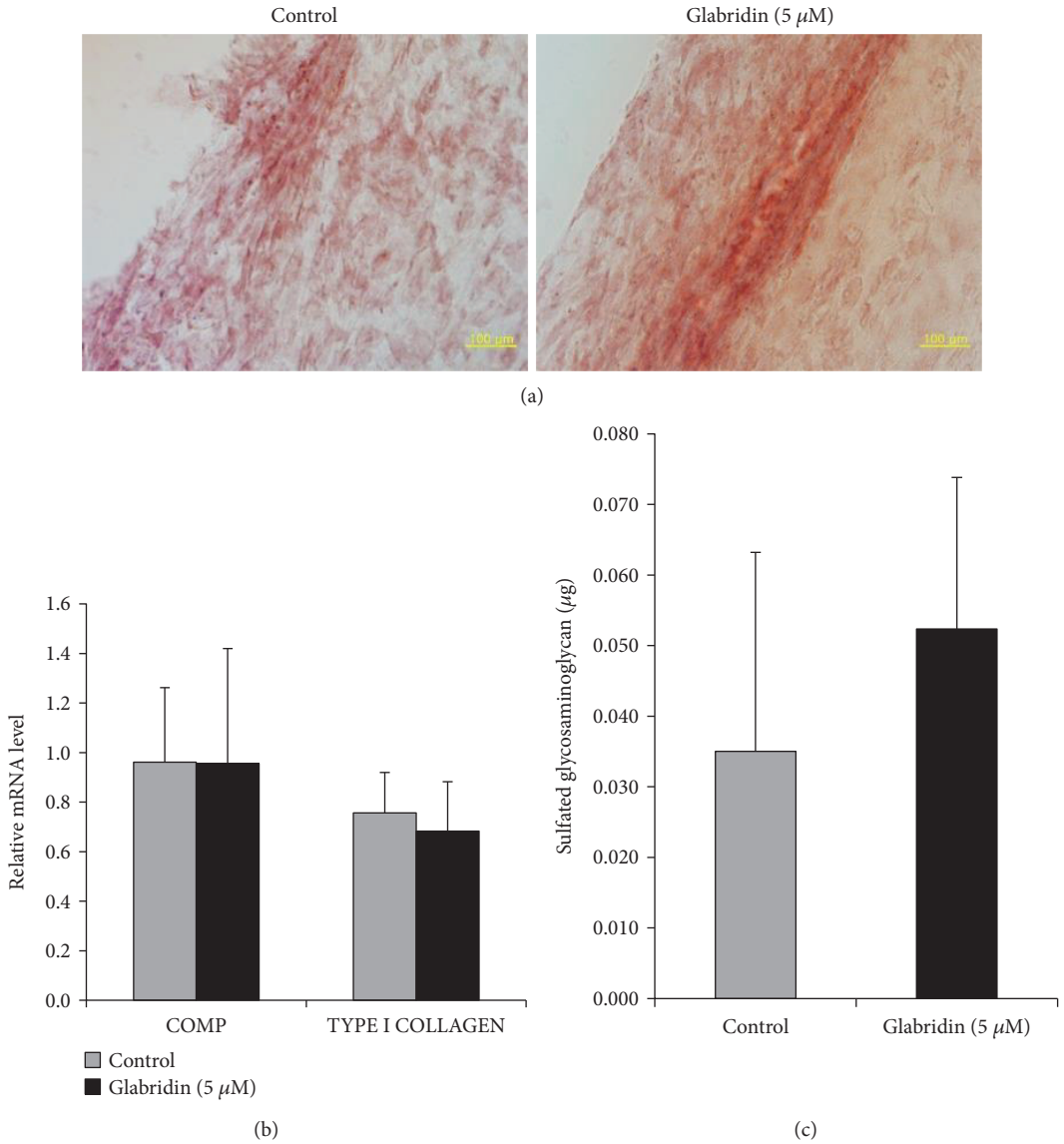

Figure 5: Effect of glabridin on chondrogenesis in MSCs. (a) Chondrogenic differentiation was evaluated by safranin O staining (magnification: 200x). (b) Chondrogenic potential was analyzed by levels of *COMP* and *TYPE I COLLAGEN* gene expression using RT-PCR. (c) Differentiation of MSCs into chondrocytes was determined by glycosaminoglycan quantification. The data are expressed as the mean ± SD of three experiments.

suppressed adipogenic differentiation as shown in Figure 6(a). In addition, the *AP2* and *LPL* genes of adipogenesis-related markers were slightly decreased in glabridin-treated cells without a significant difference (Figure 6(b)). We also confirmed that the absorbance value of lipid droplets was reduced in MSCs induced with glabridin (Figure 6(c)). Together, these results imply that glabridin prominently enhanced the osteogenic differentiation capacity of MSCs by upregulating the *OSTEOCALCIN* and *OSTEOPONTIN* genes.

4. Discussion

Of the adult stem cells, MSCs have been widely used for clinical applications because of their plastic and anti-inflammatory effects [18, 19]. Although MSCs represent a new approach to treat intractable diseases, clinical trials using these cells have been impeded by low quantities of cells and difficulty of cell culture, described as cellular or replicative senescence. MSCs can easily enter a state of growth arrest, known as senescence, despite high self-renewal capacity by internal and/or external stimuli [5]. Therefore, the culture and maintenance of MSCs without the loss of stemness are very critical for their extensive clinical use.

In general, cells are affected by multiple biochemical and biophysical factors such as the extracellular matrix (ECM) and soluble factors [20, 21]. Previously, we prevented senescence and augmented MSC growth using poly-L-lysine (PLL) of ECM proteins [22]. PLL definitely improved the proliferation capacity and functionality of MSCs. However, using PLL as a coating substrate is time-consuming because culture vessels should be incubated and dried for a long time

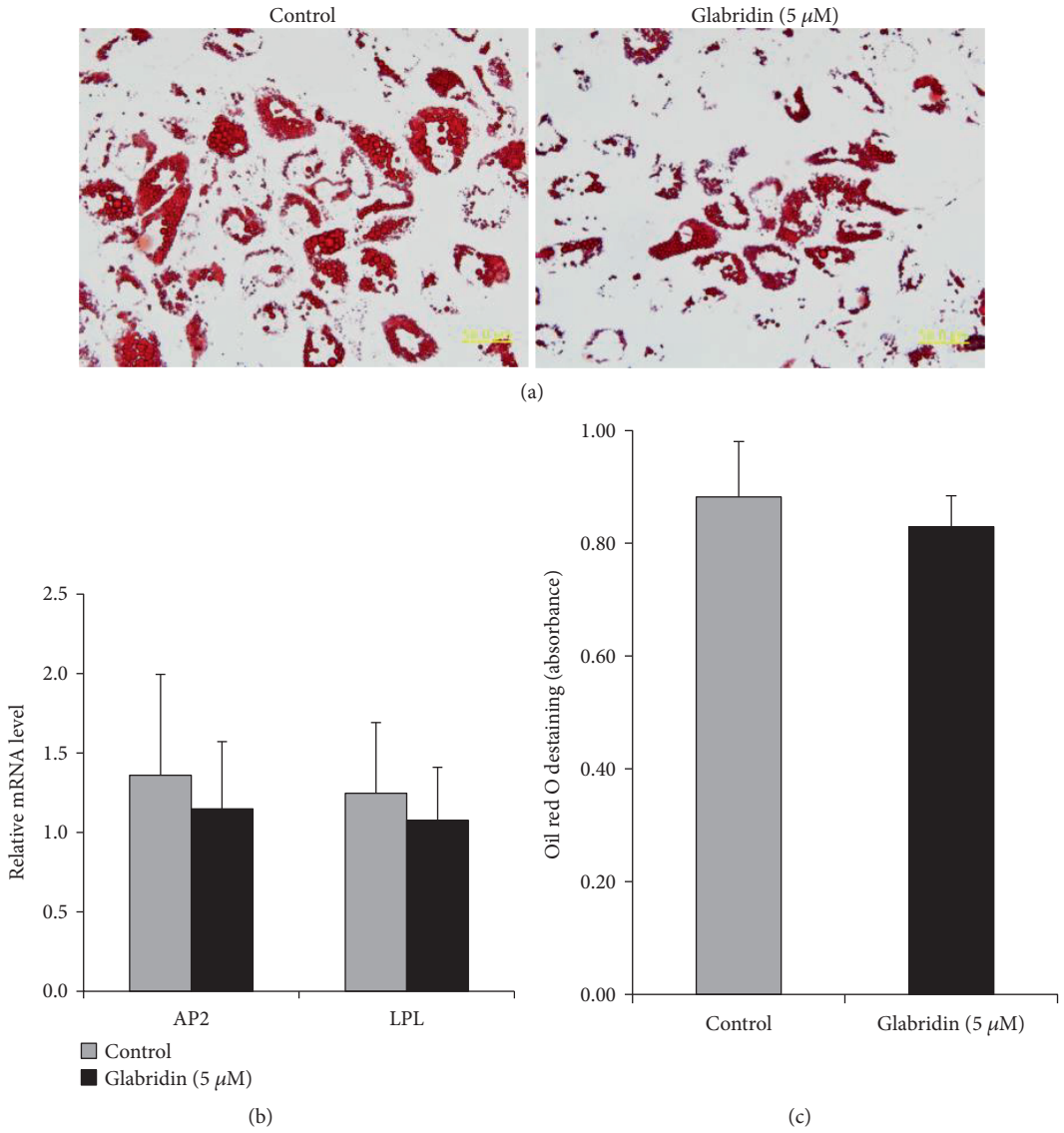

Figure 6: Effect of glabridin on adipogenesis in MSCs. (a) Adipogenic differentiation was evaluated by oil red O staining (magnification: 400x). (b) Adipogenic capacity was analyzed by *AP2* and *LPL* mRNA expression using RT-PCR. (c) Absorbance was determined after oil red O destaining for quantitative analysis. The data are expressed as the mean ± SD of three experiments.

after PLL coating. Recently, Kim et al. reported that glabridin, one of the major active flavonoids in licorice, attenuates oxidative damage and improves osteogenic differentiation function [13]. It was also reported that glabridin inhibits the cancer stem cell-like properties in hepatocellular carcinoma cells [23]. Cellular senescence is very closely related to oxidative stress [24]. In the present study, we applied glabridin, which has an antioxidant activity, to a cell culture condition. We found that glabridin did not significantly affect the viability of bone marrow-derived MSCs. In addition, glabridin did not activate cell proliferation in *in vitro* culture. We analyzed the expression levels of *OCT4*, *NANOG*, *SOX2*, *cMYC*, *KLF4*, and *LIN28* genes known as stemness markers of stem cells to investigate molecular patterns of self-renewal capacity. *NANOG*, *SOX2*, *cMYC*, *KLF4*, and *LIN28*, which are involved in pluripotency and self-renewal of stem cells, were similarly expressed in all conditions. *OCT4*, an essential transcription factor in the maintenance of pluripotency, is expressed in embryonic stem cells [25]. In addition, *OCT4* is a very important gene for the generation of induced pluripotent stem cells [26]. It is known that *OCT4*, as a specific marker of embryonic stem cells, is also expressed in MSCs [27]. However, it is hard to detect the expression of *OCT4* in MSCs because it readily disappears during culture *in vitro* [28]. Recently, Piccinato et al. showed that a high *OCT4* gene expression might be a potential hallmark and predictor of greater *in vitro* lifespan and growth potential of MSCs [29]. These results indicate that the expression level of the *OCT4* gene may be a specific factor that affects MSC senescence.

In this study, the *OCT4* gene was strongly induced in the presence of 5 μM glabridin. However, there was no dose-dependent *OCT4* expression by glabridin. Rather, MSCs treated with 100 μM glabridin did not express *OCT4*. The

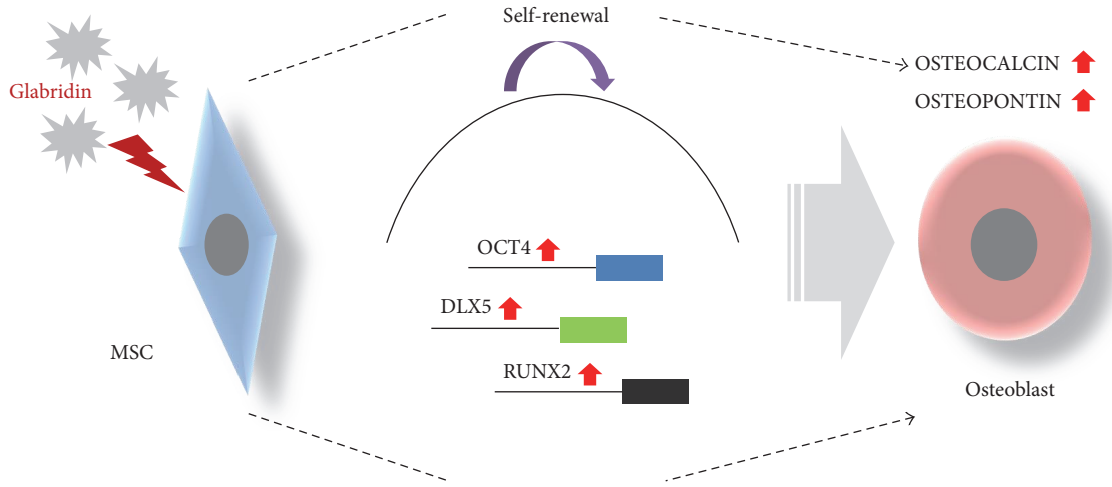

Figure 7: Schematic summary of the effect of glabridin on osteogenesis of MSCs. Our results suggest that glabridin upregulates the expression level of the *OCT4* gene associated with stemness and that of *DLX5* and *RUNX2* genes related to osteogenesis. Glabridin enhances *OCT4*-induced osteogenesis of MSCs by activating *OSTEOCALCIN* and *OSTEOPONTIN* genes for osteogenic differentiation.

expression of *OCT4* might be suppressed by a decrease in viability as shown in Figure 1. When MSCs were treated with glabridin, a significant increase in their self-renewal capacity was observed, implying that glabridin enhances CFU-F capacity by inducing the *OCT4* gene. Several studies have reported that cellular senescence is regulated by the *P53*, $P16^{INK4a}$, and $P21^{Cip1}$ pathways via the accumulation of reactive oxygen species [30–32]. We have confirmed that the *P53*, $P16^{INK4a}$, and $P21^{Cip1}$ mRNA expression levels were inhibited by glabridin although there was no significance. These results coincide with previous results, demonstrating that cellular senescence of MSCs could be suppressed via inhibition of *P53* and $P21^{Cip1}$ [33]. In addition, glabridin delayed MSC senescence as observed by β-galactosidase staining, showing that glabridin positively affects cell senescence in MSCs cultured *in vitro*. Together, these results strongly support that glabridin has antisenescence effects.

Recently, it was reported that MSC treatment with glabridin resulted in a significant elevation of alkaline phosphatase (ALP) activity, collagen content, and expression of osteoblast differentiation genes [13]. To investigate the effects of glabridin on MSC differentiation potential, trilineage (osteogenesis, chondrogenesis, adipogenesis)-related key transcription factors were analyzed by RT-PCR after treatment with glabridin as compared with control cells. When MSCs were treated with glabridin, significant increases in the gene expression of *DLX5* and *RUNX2* for osteogenesis were observed. In the differentiation assay, our results demonstrated that glabridin could significantly improve osteogenic differentiation capacity with significant upregulation of *OSTEOCALCIN* and *OSTEOPONTIN* genes of osteogenesis markers. Regarding chondrogenesis, sulfated glycosaminoglycan contents were also elevated by glabridin, but glabridin had no effects on the chondrogenic differentiation marker genes. Moreover, glabridin slightly attenuated adipogenic differentiation capacity with changes in the expression levels of genes associated with adipogenesis. These results correspond to a previous result, demonstrating that overexpression of *DLX5*, a key factor for osteogenesis, inhibited the expression of adipogenic marker genes [34]. In the present results, enhancement of osteogenesis inhibited adipogenesis of human MSCs, due to the reverse relationship between osteogenic and adipogenic differentiation.

In summary, we have shown that glabridin improved osteogenic differentiation capacity of MSCs by inducing the expression of the *OCT4* gene of the pluripotency factors and augmenting *DLX5* and *RUNX2* gene expression for osteogenesis as shown in Figure 7. We thus conclude that glabridin could be used in the MSC culture system *in vitro*. Furthermore, MSC culture using glabridin will contribute greatly to regenerative medicine and cell-based therapies including bone diseases.

Conflicts of Interest

The authors declare no conflicts of interest. The authors have no commercial, proprietary, or financial interest in the products or companies described in this article.

References

[1] P. Bianco, M. Riminucci, S. Gronthos, and P. G. Robey, "Bone marrow stromal stem cells: nature, biology, and potential applications," *Stem Cells*, vol. 19, no. 3, pp. 180–192, 2001.

[2] G. Chamberlain, J. Fox, B. Ashton, and J. Middleton, "Concise review: mesenchymal stem cells: their phenotype, differentiation capacity, immunological features, and potential for homing," *Stem Cells*, vol. 25, no. 11, pp. 2739–2749, 2007.

[3] A. I. Caplan and J. E. Dennis, "Mesenchymal stem cells as trophic mediators," *Journal of Cellular Biochemistry*, vol. 98, no. 5, pp. 1076–1084, 2006.

[4] P. H. Lee, J. E. Lee, H. S. Kim et al., "A randomized trial of mesenchymal stem cells in multiple system atrophy," *Annals of Neurology*, vol. 72, no. 1, pp. 32–40, 2012.

[5] K. Itahana, J. Campisi, and G. P. Dimri, "Mechanisms of cellular senescence in human and mouse cells," *Biogerontology*, vol. 5, no. 1, pp. 1–10, 2004.

[6] J. S. Lee, M. O. Lee, B. H. Moon, S. H. Shim, A. J. Fornace Jr., and H. J. Cha, "Senescent growth arrest in mesenchymal stem cells is bypassed by Wip1-mediated downregulation of intrinsic stress signaling pathways," *Stem Cells*, vol. 27, no. 8, pp. 1963–1975, 2009.

[7] S. Loft, P. Hogh Danielsen, L. Mikkelsen, L. Risom, L. Forchhammer, and P. Moller, "Biomarkers of oxidative damage to DNA and repair," *Biochemical Society Transactions*, vol. 36, no. 5, pp. 1071–1076, 2008.

[8] M. M. Bonab, K. Alimoghaddam, F. Talebian, S. H. Ghaffari, A. Ghavamzadeh, and B. Nikbin, "Aging of mesenchymal stem cell in vitro," *BMC Cell Biology*, vol. 7, p. 14, 2006.

[9] Y. W. Chin, H. A. Jung, Y. Liu et al., "Anti-oxidant constituents of the roots and stolons of licorice (Glycyrrhiza glabra)," *Journal of Agricultural and Food Chemistry*, vol. 55, no. 12, pp. 4691–4697, 2007.

[10] E. M. Choi, "Glabridin protects osteoblastic MC3T3-E1 cells against antimycin A induced cytotoxicity," *Chemico-Biological Interactions*, vol. 193, no. 1, pp. 71–78, 2011.

[11] H. Haraguchi, N. Yoshida, H. Ishikawa, Y. Tamura, K. Mizutani, and T. Kinoshita, "Protection of mitochondrial functions against oxidative stresses by isoflavans from *Glycyrrhiza glabra*," *Journal of Pharmacy and Pharmacology*, vol. 52, no. 2, pp. 219–223, 2000.

[12] F. Jiang, Y. Li, J. Mu et al., "Glabridin inhibits cancer stem cell-like properties of human breast cancer cells: an epigenetic regulation of miR-148a/SMAd2 signaling," *Molecular Carcinogenesis*, vol. 55, no. 5, pp. 929–940, 2016.

[13] H. S. Kim, K. S. Suh, A. Ko et al., "The flavonoid glabridin attenuates 2-deoxy-D-ribose-induced oxidative damage and cellular dysfunction in MC3T3-E1 osteoblastic cells," *International Journal of Molecular Medicine*, vol. 31, no. 1, pp. 243–251, 2013.

[14] H. S. Sohn, J. S. Heo, H. S. Kim, Y. Choi, and H. O. Kim, "Duration of *in vitro* storage affects the key stem cell features of human bone marrow-derived mesenchymal stromal cells for clinical transplantation," *Cytotherapy*, vol. 15, no. 4, pp. 460–466, 2013.

[15] K. S. Suh, S. Chon, S. Oh et al., "Prooxidative effects of green tea polyphenol (−)-epigallocatechin-3-gallate on the HIT-T15 pancreatic beta cell line," *Cell Biology and Toxicology*, vol. 26, no. 3, pp. 189–199, 2010.

[16] Y. H. Kim, D. S. Yoon, H. O. Kim, and J. W. Lee, "Characterization of different subpopulations from bone marrow-derived mesenchymal stromal cells by alkaline phosphatase expression," *Stem Cells and Development*, vol. 21, no. 16, pp. 2958–2968, 2012.

[17] L. X. Tay, C. K. Lim, A. Mansor, and T. Kamarul, "Differential protein expression between chondrogenic differentiated MSCs, undifferentiated MSCs and adult chondrocytes derived from *Oryctolagus cuniculus in vitro*," *International Journal of Medical Sciences*, vol. 11, no. 1, pp. 24–33, 2014.

[18] G. H. Cui, Y. Y. Wang, C. J. Li, C. H. Shi, and W. S. Wang, "Efficacy of mesenchymal stem cells in treating patients with osteoarthritis of the knee: a meta-analysis," *Experimental and Therapeutic Medicine*, vol. 12, no. 5, pp. 3390–3400, 2016.

[19] E. Sykova, P. Rychmach, I. Drahoradova et al., "Transplantation of mesenchymal stromal cells in patients with amyotrophic lateral sclerosis: results of phase I/IIa clinical trial," *Cell Transplantation*, vol. 26, no. 4, pp. 647–658, 2016.

[20] Y. Xu, X. Zhu, H. S. Hahm et al., "Revealing a core signaling regulatory mechanism for pluripotent stem cell survival and self-renewal by small molecules," *Proceedings of the National Academy of Sciences of the Unites States of America*, vol. 107, no. 18, pp. 8129–8134, 2010.

[21] J. You, D. S. Shin, D. Patel, Y. Gao, and A. Revzin, "Multilayered heparin hydrogel microwells for cultivation of primary hepatocytes," *Advanced Healthcare Materials*, vol. 3, no. 1, pp. 126–132, 2014.

[22] J. S. Heo, H. O. Kim, S. Y. Song, D. H. Lew, Y. Choi, and S. Kim, "Poly-L-lysine prevents senescence and augments growth in culturing mesenchymal stem cells *ex vivo*," *BioMed Research International*, vol. 2016, Article ID 8196078, 13 pages, 2016.

[23] F. Jiang, J. Mu, X. Wang et al., "The repressive effect of miR-148a on TGF beta-SMADs signal pathway is involved in the glabridin-induced inhibition of the cancer stem cells-like properties in hepatocellular carcinoma cells," *PLoS One*, vol. 9, no. 5, article e96698, 2014.

[24] V. Turinetto, E. Vitale, and C. Giachino, "Senescence in human mesenchymal stem cells: functional changes and implications in stem cell-based therapy," *International Journal of Molecular Sciences*, vol. 17, no. 7, 2016.

[25] D. J. Rodda, J. L. Chew, L. H. Lim et al., "Transcriptional regulation of *Nanog* by OCT4 and SOX2," *Journal of Biological Chemistry*, vol. 280, no. 26, pp. 24731–24737, 2005.

[26] K. Takahashi, K. Tanabe, M. Ohnuki et al., "Induction of pluripotent stem cells from adult human fibroblasts by defined factors," *Cell*, vol. 131, no. 5, pp. 861–872, 2007.

[27] J. M. Lee, J. Jung, H. J. Lee et al., "Comparison of immunomodulatory effects of placenta mesenchymal stem cells with bone marrow and adipose mesenchymal stem cells," *International Immunopharmacology*, vol. 13, no. 2, pp. 219–224, 2012.

[28] T. M. Liu, Y. N. Wu, X. M. Guo, J. H. Hui, E. H. Lee, and B. Lim, "Effects of ectopic Nanog and Oct4 overexpression on mesenchymal stem cells," *Stem Cells and Development*, vol. 18, no. 7, pp. 1013–1021, 2009.

[29] C. A. Piccinato, A. L. Sertie, N. Torres, M. Ferretti, and E. Antonioli, "High *OCT4* and low $p16^{INK4A}$ expressions determine *in vitro* lifespan of mesenchymal stem cells," *Stem Cells International*, vol. 2015, Article ID 369828, 11 pages, 2015.

[30] U. Herbig, W. A. Jobling, B. P. Chen, D. J. Chen, and J. M. Sedivy, "Telomere shortening triggers senescence of human cells through a pathway involving ATM, p53, and $p21^{CIP1}$, but not $p16^{INK4a}$," *Molecular Cell*, vol. 14, no. 4, pp. 501–513, 2004.

[31] K. Ksiazek, "A comprehensive review on mesenchymal stem cell growth and senescence," *Rejuvenation Research*, vol. 12, no. 2, pp. 105–116, 2009.

[32] Z. Tothova, R. Kollipara, B. J. Huntly et al., "FoxOs are critical mediators of hematopoietic stem cell resistance to physiologic oxidative stress," *Cell*, vol. 128, no. 2, pp. 325–339, 2007.

[33] T. Ito, R. Sawada, Y. Fujiwara, Y. Seyama, and T. Tsuchiya, "FGF-2 suppresses cellular senescence of human mesenchymal stem cells by down-regulation of TGF-β2," *Biochemical and Biophysical Research Communications*, vol. 359, no. 1, pp. 108–114, 2007.

[34] H. L. Lee, K. M. Woo, H. M. Ryoo, and J. H. Baek, "Distal-less homeobox 5 inhibits adipogenic differentiation through the down-regulation of peroxisome proliferator-activated receptor γ expression," *Journal of Cellular Physiology*, vol. 228, no. 1, pp. 87–98, 2013.